Energy & Environmental Science

ROYAL SOCIETY OF CHEMISTRY

REVIEW

View Article Online
View Journal | View Issue

Cite this: *Energy Environ. Sci.*, 2025, **18**, 5025

Polymeric membranes in carbon capture, utilization, and storage: current trends and future directions in decarbonization of industrial flue gas and climate change mitigation

Arash Mollahosseini, *[ab] Mostafa Nikkhah Dafchahi,[c] Saeed Khoshhal Salestan, [de] Jia Wei Chew, [d] Mohammad Mozafari,[f] Masoud Soroush,[fg] Sabahudin Hrapovic,[h] Usha D. Hemraz,[i] Ronaldo Giro,[j] Mathias B. Steiner,[j] Young-Hye La,[k] Seyed Fatemeh Seyedpour Taji,[e] Khalid Azyat,[a] Muhammad Amirul Islam,[a] Sajjad Kavyani,[l] Xinyu Wang,[ae] Jae-Young Cho*[ae] and Mohtada Sadrzadeh *[e]

The urgency to mitigate global warming and climate change has catalyzed advancements in decarbonization technologies, with membrane separation emerging as a key area of interest. Noted for its compact design, high separation efficiency, scalability, and versatility, membrane technologies offer promising solutions for carbon capture, utilization, and storage (CCUS). In particular, polymeric membranes are attractive due to their cost-effectiveness, ease of fabrication, and mechanical flexibility. This review examines the latest developments in polymeric membranes for CCUS, emphasizing material properties, durability, stability, and process optimization. A thorough analysis of membrane-based separation processes is provided, covering various feedstocks and capturing mechanisms, including pre-combustion, post-combustion, oxy-fuel combustion, and chemical looping, with steam methane reforming processes as an integral part of major emission-intensive industries producing products such as petrochemicals and fertilizers together with non-green hydrogen. The review also explores complementary CCUS processes—absorption–stripping, adsorption, cryogenic, and biological technologies—and details the challenges faced by gas separation membranes, such as permeability-selectivity tradeoff, plasticization, and physical aging. The role of computational approaches, particularly artificial intelligence, in driving innovations through polymer and membrane modifier design is also highlighted. By addressing process simulation, design challenges, carbon utilization, economic feasibility, and technology readiness levels, this comprehensive review offers valuable insights into the current state and future potential of membrane-assisted decarbonization for CCUS applications.

Received 13th November 2024,
Accepted 21st March 2025

DOI: 10.1039/d4ee05328a

rsc.li/ees

Broader context

Carbon-neutral technologies are vital to protecting the environment and preserving planetary health. Carbon capture, utilization and storage (CCUS) technologies are the major focal points of scientific and industrial efforts to combat climate change. Membrane separation technologies are perfect candidates for CCUS applications in the energy, cement, and chemical industries. These technologies could be applied to the existing infrastructures with minimum environmental footprint. The advancement in polymeric membranes for CCUS has led to low-cost and efficient separation units with higher efficiency. A holistic overview of the technologies is offered to highlight global warming challenges and membrane's contributions to collaborative ecosystems.

[a] *Quantum and Nanotechnologies Research Centre, National Research Council Canada, 11421 Saskatchewan Drive, Edmonton, AB T6G 2M9, Canada. E-mail: arash.mollahosseini@gmail.com*
[b] *Physical Sciences Department, MacEwan University, Edmonton, AB T5H 0K9, Canada*
[c] *Department of Chemical and Biological Engineering, University of Saskatchewan, 57 Campus Drive, Saskatoon, SK S7N 5A9, Canada*
[d] *Chemical Engineering, Chalmers University of Technology, 412 96, Gothenburg, Sweden*
[e] *Department of Mechanical Engineering, 10-241 Donadeo Innovation Center for Engineering, University of Alberta, Edmonton, AB T6G 1H9, Canada*
[f] *Department of Chemical and Biological Engineering, Drexel University, Philadelphia, PA 19104, USA*
[g] *Department of Material Science and Engineering, Drexel University, Philadelphia, PA 19104, USA*
[h] *Aquatic and Crop Resource Development, National Research Council of Canada, 6100 Royalmount Avenue, Montreal, H4P 2R2, Quebec, Canada*
[i] *Human Health Therapeutics, National Research Council of Canada, 6100 Royalmount Avenue, Montreal, Quebec, H4P 2R2, Canada*
[j] *IBM Research, Av. República do Chile, 330, CEP 20031-170, Rio de Janeiro, Brazil*
[k] *IBM Almaden Research Center, 650 Harry Rd, San Jose, California 95120, USA*
[l] *Department of Chemical and Materials Engineering, University of Alberta, Edmonton, Alberta, T6G 1H9, Canada*

1. Introduction

To limit global annual temperature rise to 1.5 to 2 °C, greenhouse gas (GHG) emissions must be reduced by 2025, with a net-zero plan executed by 2070.[1] Decarbonization strategies have been central in combating global warming over the past two decades, involving modifications to existing processes and adopting low-carbon technologies.[2] While most decarbonization efforts focus on the transportation and energy sectors, there is also growing interest in developing new fuels and energy sources.[3] However, the ongoing reliance on GHG-intensive industries is crucial for economic growth, as fossil fuel consumption and economic development are deeply connected.[4] To address the environmental impacts of using fossil fuels, increasing attention has been given to improving process efficiency and minimizing emissions.[5] Despite these efforts, GHG emissions are projected to grow at 1% annually until 2040, with CO_2 emissions in the energy sector expected to increase from 36 billion metric tons in 2020 to 43.2 billion metric tons by 2040.[6]

Given these projections, various mitigation strategies are urgently needed to prevent severe environmental changes. Some of the proposed pathways include enhancing energy efficiency, shifting to low-carbon or zero-carbon energy sources, and employing carbon capture utilization and storage (CCUS).[6–8] CCUS is vital for separating CO_2 from industrial and energy-related sources, transporting it for storage or utilization, and permanently removing it from the atmosphere.[9] The primary CO_2 sources are fossil fuel power plants, and industrial sectors like iron, steel, cement, and chemical production. Other sectors, including agriculture, livestock, and land-use changes, also contribute to rising GHG levels.[10,11] Removing CO_2 directly from its primary stationary sources has been identified as the most effective method for emission reduction, steering researchers toward CCUS processes.

CCUS mainly involves separating CO_2 from exhaust or turbine streams in industrial and urban sectors, followed by storage. While the future role of CCUS technologies in achieving net-zero emissions remains uncertain, their application is necessary for current industrial sectors.[12,13] Existing CCUS technologies, such as physical/chemical absorption, adsorption, bioremediation, and cryogenic separation, are energy-intensive and can increase the energy demand of power plants by 10–40%.[14,15] Therefore, there is a pressing need for energy-efficient CO_2 separation methods. Membrane separation has emerged as a promising candidate due to its energy-conserving nature and high separation efficiency.[16–18]

This literature review aims to (i) provide an overview of current CCUS scenarios, (ii) introduce various membrane-based materials for carbon capture, utilization, and storage, (iii) offer an overview of the products with more commercialization chances, (iv) discuss the technology readiness level (TRL) of membranes and compare it with the other CCUS technologies and take a look at impact assessment studies, (v) review the most recent efforts focused on the process simulation, computational, machine learning and artificial intelligence-related research for membrane-based gas separation processes, (vi) and compare the cost-effectiveness of these membrane-based solutions with existing conventional technologies. Many previous reviews focus on either the traditional CCUS technologies or specific aspects of membrane separation, such as material types or separation mechanisms.[19–28] However, this review takes a broader approach by first examining the characteristics of various CO_2-rich streams. Understanding the diversity and specific properties of these streams allows for a stronger foundation when discussing both conventional and advanced CCUS scenarios, addressing their distinct requirements and operational challenges. In addition to offering detailed insights into membrane materials, separation mechanisms, and performance metrics in CCUS applications, the review extends beyond traditional technologies, such as absorption–stripping, adsorption, cryogenic separation, and bioprocesses, by exploring membrane-based hybrid methods. This broader perspective enables a more complete analysis of how these emerging membrane technologies can integrate with existing systems to enhance efficiency and sustainability. It also addresses recent advancements in membrane technology, including modifications and applications, thereby filling a gap in the literature where these technological nuances are often overlooked.

The paper also differentiates itself from prior studies by discussing computational efforts, artificial intelligence, and machine learning for membrane design and optimization. Focusing on the economic feasibility and technology readiness levels (TRLs), it provides a pragmatic perspective on the future implementation of membrane-based CCUS. Ultimately, this review consolidates current techno-economic insights while offering a comprehensive roadmap for the future development of membrane-based CCUS technologies. It distinguishes itself from previous studies by adopting a holistic approach, addressing the entire spectrum of CCUS processes, from material science and separation mechanisms to economic feasibility and advanced computational methods. By integrating these diverse aspects into one framework, this review provides a more unified perspective on the potential and challenges of membrane-based CCUS, setting it apart from more narrowly focused works.

2. Emission-producing industries and their effluents

Understanding the target stream is essential before exploring various CCUS methods. Flue gas, also known as exhaust or stack gas, is the outlet stream of the combustion process, carrying the products of the fuel and air reaction. The composition of these streams can vary significantly depending on factors such as the pollution source, the nature of the plant, and operational conditions.[29] Power plants generate flue gas that contains dust particles, sulfur oxides, and nitrogen oxides. Standard power plant emissions typically need to meet the following conditions: Impure carbon particles (soot) < 10 mg m^{-3}, $SO_2 < 35$ mg m^{-3}, $NO_x < 50$ mg m^{-3}.[30] World Health Organization (WHO), established Air Quality Guidelines (AQG, version 2021) with 24-hour concentration limit of $SO_2 < 40$ μg m^{-3}, $NO_2 < 25$ μg m^{-3}, fine particle matters with diameter equal or less than 2.5 μm ($PM_{2.5}$) < 15 μg m^{-3}, (PM_{10}) < 45 μg m^{-3}, and CO < 4 μg m^{-3}.[31] WHO does not recognize CO_2 as a direct air pollutant for outdoor environments.

Industries could create CO_2 as a side product in a reaction or through combustion. Major producers are power plants (through furnaces, turbines, boilers), cement industry (through precalciners), refineries (through process heaters, catalytic cracker), iron and steel production industries (through blast furnaces, oxygen furnaces), petrochemical production (through steam cracking process), fertilizer production (through reforming processes for ammonia production, urea production), and alcohol production (through fermentation).[32] Indirect generation of CO_2 must also be considered through supply chain, feedstock and utility production, *etc*.[33] The contribution of each industry to CO_2 emissions varies by region due to differences in social and industrial activity profiles. As an example, the two major emission producers in the world, US is mainly producing CO_2 (more than 50% of overall emission production) through consumption of coal and natural gas in power plants,[32] while China creating CO_2 through the manufacturing industries.[34]

Pre-treating flue gas before the CCUS process can enhance CCUS efficiency and improve the maintenance of downstream equipment.[35] When dealing with fuel sources such as municipal waste incineration, coal, sludge from water treatment plants, other products used as fuel in the cement plants, and biogas, the exhaust may contain other components, including hydrogen chloride, hydrogen fluoride, and heavy metal derivatives. The flue gas composition also depends on the air stream's characteristics fed into the combustor and the air/fuel ratio, as air pollutants can impact combustion efficiency and the exhaust stream quality. Combustion conditions are another crucial factor; for instance, a typical oxygen and hydrocarbon-fueled combustor converts most sulfur content to sulfur dioxide. However, high temperatures and excess oxygen favor the formation of sulfur trioxide. Conversely, low oxygen content in the combustion reaction can result in fuel derivatives in the exhaust.[36]

The sensitivity of each CCUS process needs to be considered in the design parameters, making it essential to understand the differences between various sources. Different filter materials and separation mechanisms react uniquely to contaminants and impurities during membrane separation. For example, moisture has a counterintuitive effect: while it can facilitate CO_2 transport through amine-containing membrane materials, excessive water vapor may form a water film on the membrane, hindering the process.[37] Table 1 compares flue gas composition from various sources, while Table 2 illustrates the typical output composition after the CCUS process.

Components in the CO_2-rich stream can significantly alter its thermophysical properties. These changes may include a higher critical point pressure, increased likelihood of a two-phase stream within certain pressure and temperature ranges, and variations in density and compressibility. Additionally, transport properties that affect heat, mass, and momentum transfer can also change, impacting the stream's behavior.[40–42]

3. The CCUS perspective in different scenarios

CCUS technologies can be adopted for various scenarios, including pre-combustion, post-combustion, oxy-fuel combustion, and chemical looping combustion.[14,43–45] Among the most common technologies for fuel processing, hydrogen production, and fertilizer manufacturing are steam methane reforming (SMR) and auto thermal reforming (ATR), which produce CO_2 as a byproduct. Removing CO_2 from SMR and ATR discharges may

Table 1 Different emission's components, concentrations, and characteristics[35,36,38,39]

Source	CO_2 (vol%)	N_2[a1] (vol%)	O_2 (vol%)	H_2O (vol%)	Ar (vol%)	CH_4 (vol%)	SO_2 (ppm)	NO_x (ppm)	H_2S (ppm)
Natural gas combined cycle	7	66	14	6	1	N/A	N/A	10–300	N/A
Integrated gasification combined cycle	3	76	12	14	1	N/A	10–200	10–100	N/A
Coal-based power plants	11	76	6	6	1	N/A	300–5000	500–800	N/A
Municipal waste incineration power plant	6–12	Balance	7–14	10–18	1	N/A	200–1500	200–500	N/A
Cement industry resources	19	59	7	13	1	N/A	5–1200	100–1500	N/A
Household resources	34–38	0–5	0–1	6	N/A	50–60	N/A	N/A	100–900
Agriculture resources	19–33	0–1	Less than 0.5	6	N/A	60–75	N/A	N/A	3000–10 000
Agrifood resources	26	N/A	N/A	6	N/A	68	N/A	N/A	400
Refinery	12.3	71.8	4.4	10.3	1.2	N/A	N/A	N/A	N/A
Iron and steel industry (basic oxygen furnace)	34.5	60.4	N/A	4.5	0.6	N/A	N/A	N/A	N/A
Iron and steel industry (blast furnace)	21.5	46.5	3.7	4.2	0.6	N/A	N/A	N/A	N/A

[a] CO: 23.45%.

Table 2 Impurities in the CO_2 after each CCUS process[40]

CCUS process	Impurities
CO_2 captured from natural gas sweetening	CH_4, amines, H_2O
CO_2 captured from heavy oil production and upgrading	H_2S, N_2, O_2, CO, H_2O, H_2, COS, Ar, SO_x, NO_x
CO_2 captured from power plants using post-combustion capture	N_2, amines, H_2O, O_2, NH_3, SO_x, NO_x
CO_2 captured from power plants using oxy-combustion capture	N_2, O_2, SO_2, H_2S, Ar
CO_2 captured from power plants using pre-combustion capture	H_2, CO, N_2, H_2S, CH_4

lessen the load and optimize the product's ultimate cost.[46–49] It can also be used to directly remove CO_2 from the air rather than targeting specific emission streams. The selection of the appropriate CCUS scenario and the related processes depends on several factors. These include the operational characteristics of the plant generating emissions, the economic feasibility and efficiency of the CCUS process, and the environmental regulations that dictate the permissible levels of emissions. Each scenario offers distinct advantages and challenges, with the choice largely driven by the specific needs and conditions of the industrial application.

3.1. Pre-combustion

During fuel preparation for power generation, such as in coal gasification plants or integrated gasification power plants (IGCC), hydrocarbons react with water and oxygen, forming CO, CO_2, and hydrogen. Subsequently, the water-gas shift (WGS) reaction converts CO into CO_2, reducing its content in the syngas. This syngas is then utilized for power generation, but the high concentration of CO_2 can adversely impact combustion efficiency. Therefore, removing excess CO_2 is essential to optimize overall process efficiency. This CO_2 removal step is also referred to as hydrogen or fuel purification, commonly known as upgrading. Fig. 1 illustrates the pre-combustion CO_2 removal scenario in power generation, where the separation element is represented using a membrane unit, reflecting the focus of this review on membrane-based separation technologies.

Removing CO_2 before using the fuel is crucial, particularly in natural gas purification after extraction from wells. This process reduces the burden on downstream operations, minimizes pipeline corrosion, and enhances extraction efficiency when the separated CO_2 stream is reinjected into the wells. Furthermore, CO_2 removal increases the energy content of natural gas, ensuring compliance with market and regulatory standards. It also optimizes the performance of gas processing equipment and significantly boosts the economic value of the gas. A schematic of this process is shown in Fig. 2, highlighting its role in improving overall system efficiency.

3.2. Post-combustion

Post-combustion strategies focus on removing CO_2 from exhaust streams after combustion, where hydrocarbon fuel is mixed with air. In conventional combustion streams at ambient pressure, CO_2 concentrations range between 3–15%.[50,51] The main challenge in these processes arises from the low concentration of CO_2 and the high temperature of the outlet stream, both of which complicate the sizing and design of separation systems. Low concentrations drive up separation costs, leading to an 8 to 12% decrease in process efficiency.[52,53] Despite these challenges, a key advantage of post-combustion CCUS strategies is their compatibility with existing infrastructure, requiring no significant changes to upstream processes. This adaptability is one reason why post-combustion remains the only fully commercialized CCUS strategy to date.[54] Fig. 3 provides a schematic representation of this scenario.

3.3. Oxy-fuel combustion

Oxy-fuel combustion refers to using pure oxygen for combustion instead of air. This process increases the CO_2 concentration in the exhaust to over 80% and reduces NO_x emissions by eliminating nitrogen from the combustion process. This higher concentration of CO_2 makes it easier to capture and remove from the flue gas compared to post-combustion CCUS methods.[55,56] Conventional furnaces, where 79% N_2 enables steady propagation because of CO_2's lower thermal diffusivity, stronger radiation, dissociation, and cooling effects. Stable oxy-fuel flames usually include up to 70% CO_2 in the CO_2/O_2 combination since higher concentrations lead to instability.[57,58] Oxy-fuel combustion has a

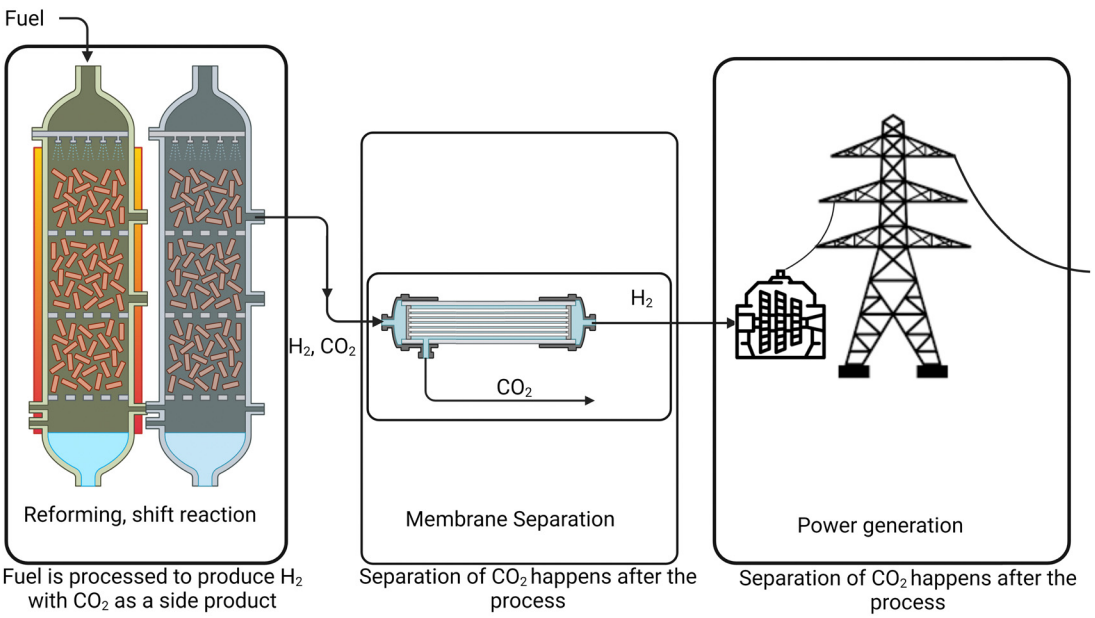

Fig. 1 Schematic of pre-combustion CO_2 removal after reforming and water-gas shift reaction.

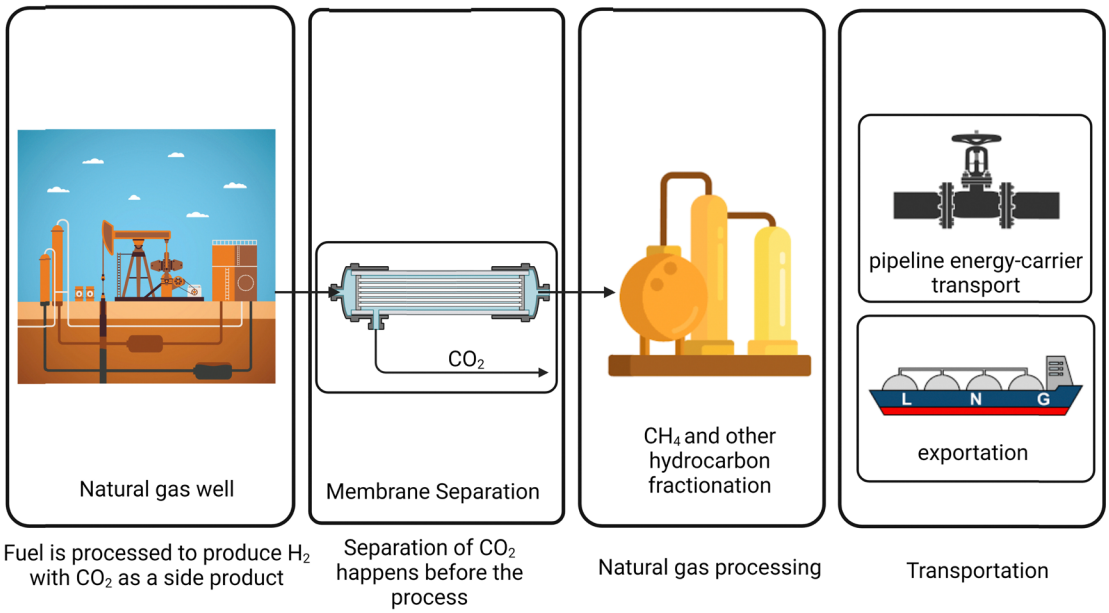

Fig. 2 Schematic of pre-combustion CO_2 removal from natural gas before conversion, consumption or exportation.

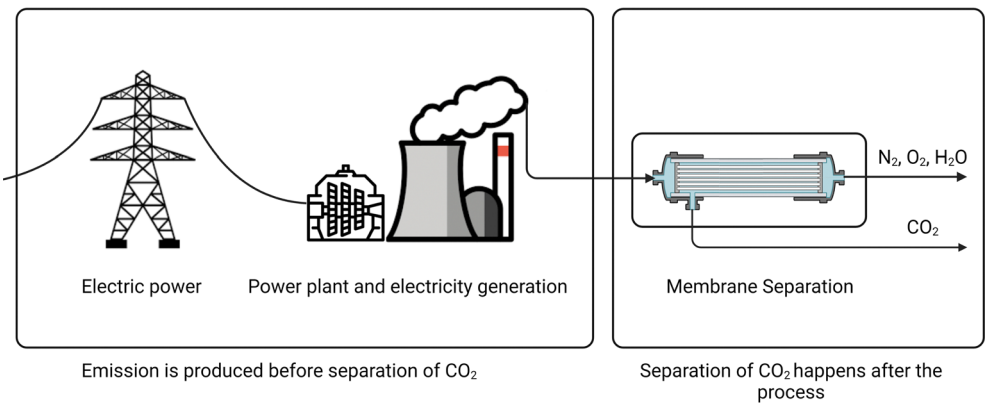

Fig. 3 Schematic of post-combustion CO_2 removal from the flue gas after emission production in different industries.

few challenges to overcome, including high temperature (close to 3500 °C), and instability of the flame due to the pure O_2 usage instead of air.

Recirculating the flue gas (in wet or dry state) back to the burner is a common practice to help regulate the flame temperature during combustion, allowing the process to stay within the metallurgical constraints.[59] Wet flue gas could trigger corrosion and erosion. Dry flue gas recirculation is therefore advised, in which flue gas is recycled downstream of the operation of gas cleanup units, including moisture condensers, particulate filters, and flue gas desulfurization units.[60]

Techno-economic evaluations identify oxy-fuel combustion as one of the most cost-effective and energy-efficient CCUS solutions available.[61–63] However, the requirement for pure oxygen, which is usually produced *via* energy-intensive cryogenic processes, represents a significant drawback. The oxygen supply process can lead to an approximate 10% reduction in power plant efficiency, although this impact varies depending on the plant's baseline characteristics.[64] These challenges, particularly the high energy demand for oxygen production, continue to pose significant obstacles to the large-scale implementation of oxy-fuel combustion.[65]

3.4. Chemical looping combustion

Chemical looping combustion (CLC) is a relatively new process to which CCUS strategies can be applied. It divides the combustion process into two reactors. In the first reactor (air reactor), an oxygen carrier, typically a metal such as nickel, iron, or copper[66,67]) reacts with air to oxidize the metal. The metal oxide is then transferred to a second reactor (fuel reactor) where it reacts with a hydrocarbon fuel, producing pure CO_2 while reducing the metal oxide back to its metallic form. The metal is then cycled back to the air reactor for reuse.[68]

Since the idea's inception in 1983, CLC has gained attention for its potential in carbon capture, leading to significant developments, including a 1 MWth pilot plant established in Germany in 2015.[66,69] Research efforts are currently focused on improving various aspects of the process, such as enhancing the performance and

durability of the oxygen carriers[70–72] and refining process integration and intensification techniques to optimize efficiency.[73–75] CLC shows promise for increasing CCUS efficiency while lowering energy penalties compared to traditional methods.

3.5. Direct air capture

Direct air capture (DAC) focuses on removing CO_2 directly from the atmosphere, distinguishing itself among CCUS technologies by targeting non-stationary and widely distributed emission sources, which collectively contribute nearly 50% of human-made CO_2 emissions. Originally proposed by Lackner in the 1990s as a method to combat climate change, DAC has gained considerable attention from researchers focused on improving its efficiency and reducing costs.[76] Unlike traditional CCUS methods that concentrate on emissions from specific stationary sources, DAC relies on adsorption and absorption processes to capture CO_2 from the air. However, one of its key challenges lies in the costly regeneration of sorbents, which limits the technology's economic viability. Additional concerns include DAC's high energy and material demands and complexities surrounding proper CO_2 storage. Despite its promising potential, these issues continue to raise doubts about DAC's large-scale implementation.[76,77] Table 3 provides a comparison of different CCUS strategies. The ocean absorbs approximately 27% of atmospheric CO_2, converting it into carbonate and bicarbonate ions while maintaining climate equilibrium. The rising atmospheric CO_2 concentration, alongside the decreasing ocean pH, suggests a weakened capacity of the ocean as a natural carbon sink, prompting interest in direct air capture from the ocean (DOC).[78] DOC, a less-explored subdivision of DAC, reverses the acidity of the ocean water with the controlled impact on the environment and sea life. Using alternative renewable energies and novel technologies with low emissions to produce alkaline solutions for pH adjustment has been a major topic of focus for academic and technology development teams.[79] Utilization of DOC technologies will likely require the development of advanced solvents and adsorbent materials with improved capture capacity, selectivity, and lower regeneration costs.

4. Current processes and technologies for CCUS

Several processes have been developed for carbon capture, utilization, and storage (CCUS), spanning a range from laboratory-scale research efforts to more commercialized applications. Each process exhibits unique characteristics in terms of scale, application scope, retrofit potential, and cost-effectiveness. Fig. 4 provides a general classification of these available processes, highlighting key distinctions across different approaches. In this subsection, an in-depth overview of these CCUS processes is presented to provide a comprehensive understanding of the current technological landscape and its implications.

4.1. Absorption–stripping

The only fully commercialized CCUS technology is absorption. Fig. 5 shows a typical amine-based absorption–stripping flow

Table 3 Comparison of pros and cons for different CCUS scenarios[76,80–82]

CCUS scenario	Removal efficiency (vol% CO_2)	CO_2 separation cost (USD per tone CO_2)	Energy consumption (GJ per tone CO_2)	Pros	Cons
Pre-combustion[a]	90	34 to 63	3.35	Proper for high concentration and partial pressure of CO_2, easy separation, suitable for most of the existing plants, developed/matured technology	Temperature and efficiency complications in case of H_2-rich streams, high Capex and Opex, Applicable new IGCCs only
Post-combustion	90	46 to 74	4.14	Matured process and already in use	Low CO_2 removal efficiency in low CO_2 concentrations High parasitic power requirement
Oxyfuel combustion	Higher than 90	52	4.05	Proper for high CO_2 levels, applicable to current plants through retrofitting and repowering	High cost of oxygen supply, energy-intensive,
Chemical looping	96 to 99	Less than 59.20	0.95	Works with low-cost oxygen-carrying metals, proper for high CO_2 levels,	Immature and under development
Direct air capture[b]	85 to 93	140 to 340	5.25	Proper for non-stationary sources	Low CO_2 partial pressures in the air make the process cost and energy-deficient

[a] The scenario covers technologies in autothermal reforming (ATR) and steam methane reforming (SMR).[46,48] [b] The scenario covers direct ocean capture (DOC).[83]

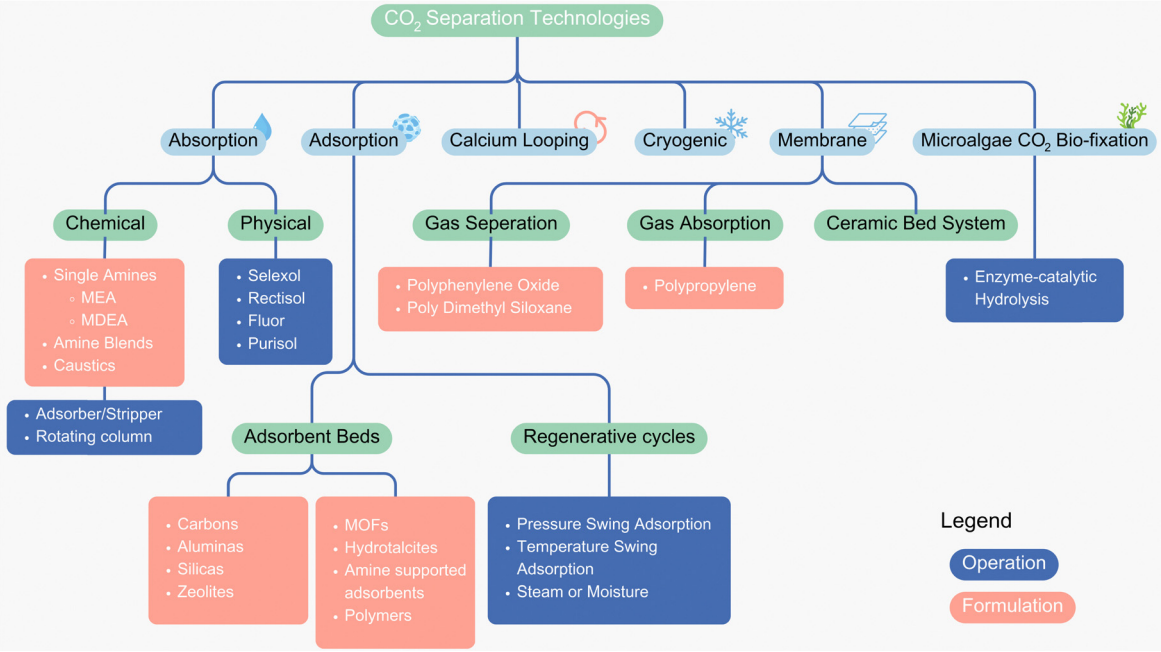

Fig. 4 Classification of different CCUS technologies.[14,45]

sheet for post-combustion carbon capture. In this process, CO_2-laden flue gas enters a separator to remove trapped particles before passing through an absorption column, where it comes into contact a lean amine solution, absorbing the CO_2. The resulting "rich" amine solution is heated *via* a heat exchanger before entering a stripper column, where steam removes the CO_2. The CO_2-laden vapor is condensed at the top of the column, and recycled vapor returns as reflux. The lean amine is then reheated in the heat exchanger and recirculated back to the absorption column. A significant drawback of this process is the high energy demand for regenerating the rich amine, which can account for up to 50% of the annual process costs, significantly increasing overall plant expenses.[84,85]

The selection of solvent is a crucial and continually evolving element in the CO_2 absorption process. An ideal solvent should have high CO_2 solubility, low energy requirements for regeneration, and fast reaction kinetics with CO_2.[86] Amines, particularly monoethanolamine (MEA), are the most recognized and cost-effective solvents, with other common options including diethanolamine (DEA), methyl diethanolamine (MDEA), and triethanolamine (TEA).[85] Inorganic solvents, such as potassium carbonate and sodium carbonate mixed with ammonia, are also used, with potassium carbonate being the most popular. Inorganic solvents offer advantages like greater stability, reduced environmental impact, and lower energy demands for regeneration compared to primary and secondary amines.[87] However, amines are preferred in coal-fired flue gas applications due to their superior CO_2 selectivity.[88]

Ongoing research focuses on improving the efficiency of these absorbents by focusing on enhancing kinetics, solubility, energy efficiency, and key operational characteristics like foaming, viscosity, surface tension, and thermal stability, all while reducing environmental impact. Numerous studies have examined the properties of amine-based solutions for CCUS, including vapor–liquid equilibrium (VLE) data that are critical for process optimization.[89–96]

Post-combustion adsorption processes are often preferred over alternative technologies for several reasons: (i) they have a long history of practical use, providing extensive industry experience in handling and maintenance; (ii) they typically require minimal modifications to existing infrastructure; and (iii) maintenance of the CCUS system can be performed without disrupting upstream operations.[14]

In addition to solvent selection, the absorption–stripping process can be optimized through several advanced techniques and process integrations. Methods such as absorber intercooling, multi-solvent feeding, employing a semi-lean solvent stream in the stripper, and solvent splitting in the rich phase have shown potential to enhance efficiency.[97] These modifications are aimed at addressing the main challenges of reducing energy penalties and achieving capture costs below $20 per ton of CO_2.[98] Another promising strategy is increasing CO_2 concentration in the flue gas, which typically ranges from 3% to 15%, depending on the source. Utilizing membrane-based technologies for initial CO_2 concentration can significantly improve the overall CCUS process efficiency.[99,100]

Despite their widespread use, absorption–desorption methods for CO_2 capture present several challenges, including high energy requirements for solvent regeneration and producing harmful byproducts from oxidative degradation. Other issues, such as equilibrium limitations, amine degradation, and equipment corrosion due to the aqueous phase, further complicate the process.[101] Continued research is focused on refining solvent performance and advancing process improvements to

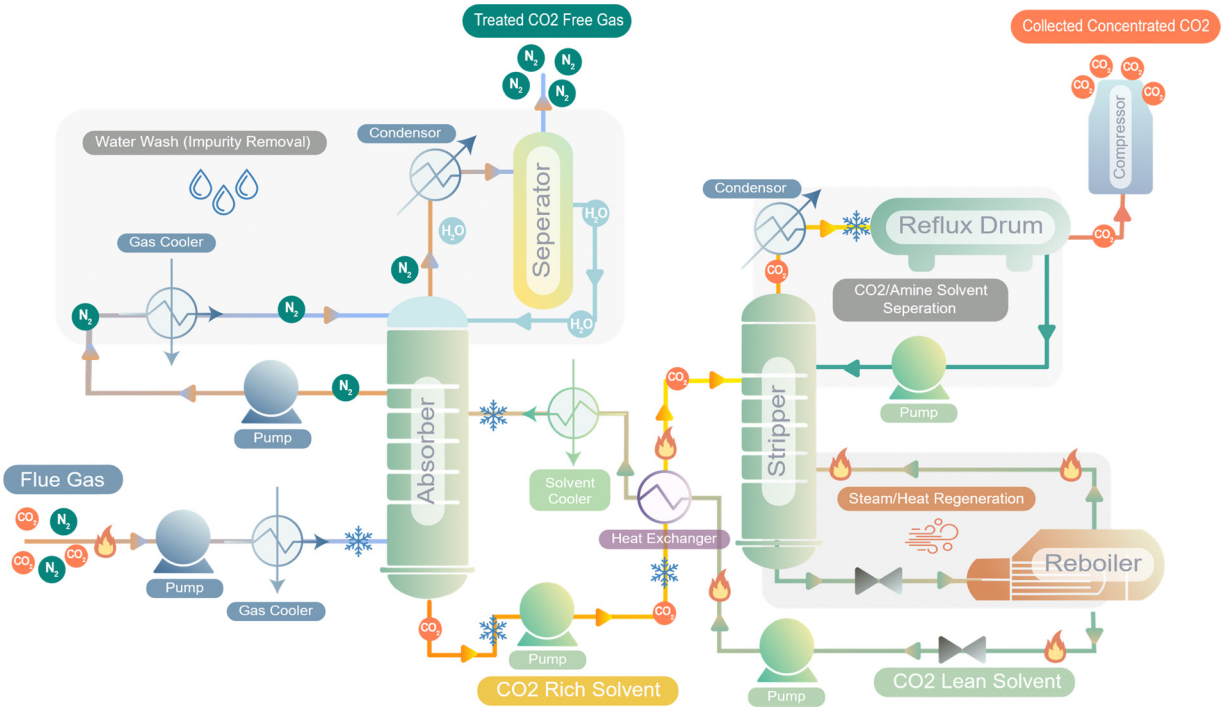

Fig. 5 Typical post-combustion carbon capture process flow sheet.[54]

address these challenges. Comprehensive reviews of recent developments in absorption-based post-combustion CCUS technologies can be found in the literature.[87,97,102–105]

4.2. Adsorption

Adsorption-based CCUS technologies take advantage of CO_2's stronger binding affinity for certain adsorbents compared to other flue gas components.[106] Physical adsorption uses van der Waals forces to bind CO_2 molecules to the adsorbent's surface, offering an easier regeneration process than absorption, which requires chemical bonds. The ease of regenerating adsorbents, either thermally or by pressure modulation, significantly reduces the energy consumption in the CCUS process, making adsorption a more energy-efficient option.

Key performance metrics for adsorption-based CCUS technologies include adsorbent durability, CO_2 selectivity, adsorption capacity, and the stability of the adsorbent after multiple adsorption/desorption cycles.[107] In the temperature swing adsorption (TSA), the adsorbent is regenerated by increasing the adsorption bed's temperature, often using hot gas or steam. In contrast, pressure swing adsorption (PSA) and vacuum swing adsorption (VSA) use pressurized flue gas to adsorb CO_2, followed by a reduction in column pressure to release the captured CO_2.

While PSA and VSA are more energy-efficient under certain operational conditions,[14] TSA may be a more practical solution for large-scale applications, as flue gases are often at atmospheric pressure, making it costly to compress high volumes of gas continuously.[84] Therefore, TSA might provide a more feasible option in scenarios where cost control is critical despite its energy demands.[108]

4.3. Cryogenic technologies

Cryogenic CCUS involves separating CO_2 from a gas stream by cooling it to the point where CO_2 transitions to a liquid or solid phase, making it easier to extract. This phase-change-based technique relies on the differences in the boiling points or desublimation characteristics of the stream components. Fig. 6 categorizes the various cryogenic CCUS technologies, and Fig. 7 illustrates the decarbonization process of flue gas using cryogenic methods.

When cryogenic separation is based on boiling point differences, it is classified as conventional vapor–liquid separation, commonly used in natural gas purification to liquefy and remove CO_2. However, significant drawbacks include the high energy requirements for high-pressure equipment and the risk of solid formation leading to blockages. Additionally, water content in the gas stream must be meticulously removed to prevent ice formation, which can disrupt pressure profiles.[109] The solidification of CO_2 can be further avoided by the Ryan/Holmes extractive technology, which uses a heavier hydrocarbon for enhanced solubility of the liquified CO_2, as well as a few other parameters that facilitate the separation process.[110] The separation parameters, *i.e.*, recovery ratio and purity of the streams, are adjusted by tuning operational pressure and temperature and using flash separation units and stripping columns, which eliminate $O_2/N_2/Ar$ components (gases with lower boiling points).[111,112]

Cryogenic processes, while energy-intensive, offer high CO_2 purity without toxic chemicals and can be applied to streams with varying CO_2 concentrations. The unconventional cryogenic process, which uses CO_2 desublimation (solid–vapor equilibrium), may reduce

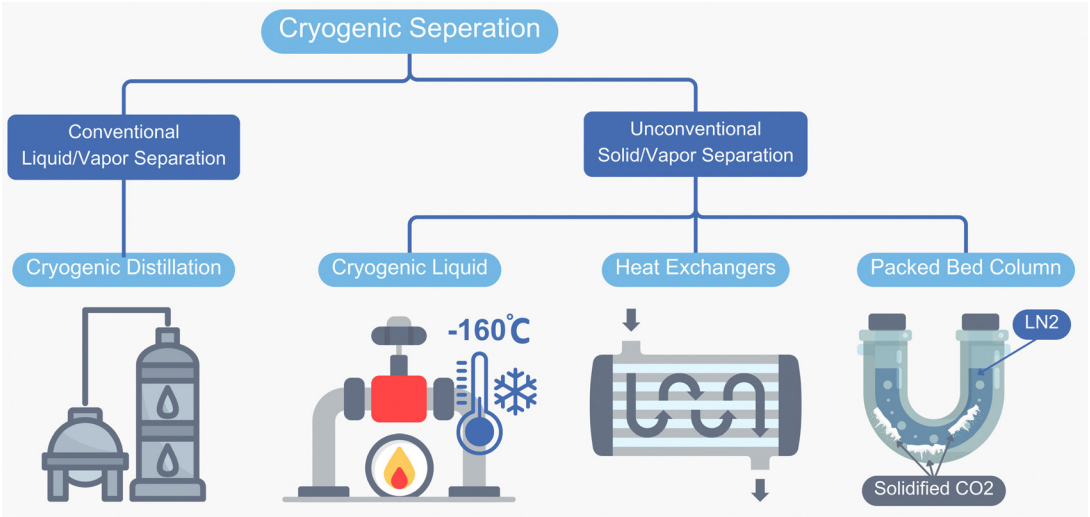

Fig. 6 Cryogenic CCUS processes classification.

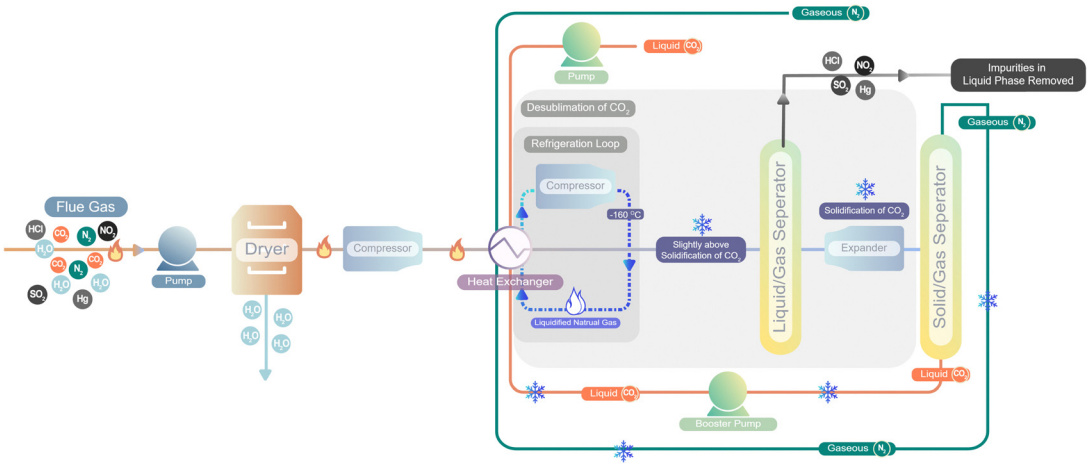

Fig. 7 Cryogenic process for flue gas decarbonization.

energy intensity at higher CO_2 concentrations.[113] Available technologies include:

(i) Normal pressure cooling process of the flue gas, requiring temperatures below −100 °C.

(ii) Direct multistep compression above the critical pressure (about 73 atm), where liquefied CO_2 can be stored in the seabed—though highly energy-intensive.

(iii) Hybrid approaches, where pressurized streams are cooled to liquefy CO_2 or pressurized liquid CO_2 is solidified through throttling and temperature-pressure adjustments.

These methods must avoid air or nitrogen dilution to improve energy efficiency and could benefit from cold energy recovery.[35,114,115]

4.4. Biological processes

Biological carbon mitigation processes leverage bioreactions within living organisms to naturally consume CO_2. Through photosynthesis, solar energy drives the conversion of CO_2 into organic carbon, a process known as bio-sequestration. Practices such as agroforestry, cropland extension, and pasture development are examples of biological carbon mitigation, though their overall impact on atmospheric CO_2 removal is considered minimal. Nonetheless, these practices persist as interim measures until more practical, large-scale solutions are developed.[116]

One promising approach in biological carbon mitigation is the bioconversion of CO_2 using microalgae bioreactors, which offer high photosynthetic efficiency (3% to 8%) and robust biomass productivity.[117] Flue gases rich in CO_2 provide an ideal environment for algal cultivation,[118] with the potential for economic advantages in biorefineries.[119] However, pollutants like SO_x and NO_x in flue gases can acidify the culture medium, limiting the growth of certain algal species. To mitigate these challenges, technical solutions such as feed stream pretreatment and selecting suitable algae (thermotolerant, pH-tolerant, with enhanced photosynthetic efficiency) have been proposed.[118,120] Additionally, using enzymes can enhance CO_2 consumption,

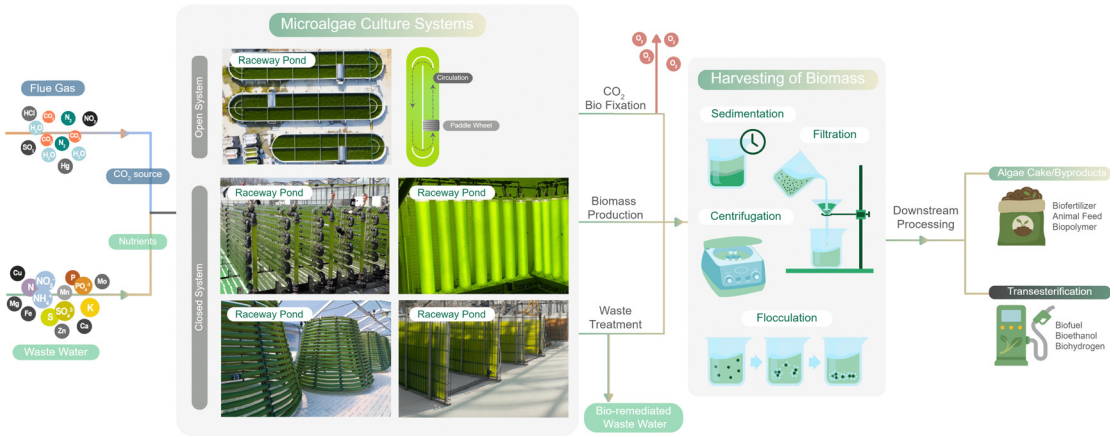

Fig. 8 Photoreactors for microalgae culture to reduce carbon emission.[122]

Table 4 Comparison of different CO_2 separation processes with the focus on energy consumption

Technology	Energy consumption	Key challenges	Advantages	Ref.
Absorption–stripping	3–6.5 GJ per ton CO_2	High energy for solvent regeneration, corrosion, solvent degradation	Mature and widely used, high CO_2 selectivity	123 and 124
Adsorption (TSA)	3.5–5.6 GJ per ton CO_2	High heating requirement, slower cycle times	Lower energy demand than absorption, reusable adsorbents	125 and 126
Adsorption (PSA/VSA)	0.4–4 GJ per ton CO_2 Lower than TSA, varies with pressure	Pressure dependency, moderate scalability	More energy-efficient than TSA, fast cycle times	127 and 128
Cryogenic separation	2.3–4.4 GJ per ton CO_2	Extreme cooling needed, risk of ice/solid CO_2, formation	High CO_2 purity, no chemical waste	129
Biological processes (Microalgae)	Low, dependent on sunlight & reactor conditions	Slow process, requires large space and sunlight	Sustainable, can integrate with biofuel production	130 and 131
Membrane separation	1 GJ per ton CO_2	Not commercialized	Retrofittable for different industries, lower capital and operation costs	132

enabling more sustainable reactors that utilize environmentally friendly solvents.[121] Fig. 8 illustrates various bioreactor systems for CO_2 bio-sequestration. Table 4 also compares the technologies reviewed in Section 4.

5. Membrane-based CCUS technologies

The concept of gas separation membranes was initially proposed in 1866.[133] Asymmetric membranes were practically put in use into the 1960s by Loeb and Sourirajan's pioneering work.[134,135] Membrane separation techniques rely on differences in diffusivity, solubility, absorption, and adsorption properties of gases across various materials.[136] Membranes are particularly effective for CO_2 separation due to the significant size difference between CO_2 and other gases in flue gas mixtures.[137] The advantages of membrane technology in CCUS applications include avoiding phase changes in gas streams, scalability, adaptability to both post-combustion and pre-combustion techniques, and the potential for process intensification. Additionally, membranes are low-maintenance, occupy a small footprint, and can function under harsh conditions depending on the material.[138] For example, a membrane unit designed for a 600 MW power plant was estimated to require only 0.004 km^2 area, significantly less than amine-based units.[139]

The driving force for transport through the membrane is the chemical potential difference, which can manifest as pressure, concentration, temperature, or electrical gradient, depending on the specific process.[140] In the gas separation process, the driving force is the transmembrane pressure. Gas molecules vary in size, represented by their kinetic diameter, along with other characteristics, such as activation energy and shape factors, which influence the separation process. Table 5 summarizes the molecular characteristics relevant to pre- and post-combustion processes.

Depending on the gas stream composition and the membrane characteristics, the transport mechanism may involve Knudsen diffusion, molecular sieving, solution diffusion, or a combination of these. In porous membranes, molecular sieving (with pore sizes between 0.5 to 2 nm) and Knudsen diffusion (with pore sizes from 5 to 10 nm) are the dominant mechanisms.[142] Molecular sieving occurs when the membrane pore size is nearly equivalent to the size of the gas molecules, allowing smaller molecules to pass while blocking larger ones. In Knudsen diffusion, the permeation rate is proportional to the velocity of the gas molecules and inversely proportional to the square root of their molecular weight, provided the pore size is smaller than the gas molecules' mean free path.[143]

Table 5 Characteristics of gas molecules in various membrane-based CCUS and decarbonization processes[141]

Molecule	Kinetic diameter (A)	Polarizability (A^3)	Dipole moment (D)	Quadrupole moment (D A)
H_2O	2.65	1.50	1.85	2.30
H_2	2.89	0.78	0	0.66
CO_2	3.30	2.50	0	4.30
O_2	3.46	1.58	0	0.039
NO	3.49	1.70	0.15	N/A
H_2S	3.60	3.78	0.97	N/A
N_2	3.64	1.71	0	1.54
CO	3.76	1.95	0.11	2.50
CH_4	3.80	2.44	0	0.02

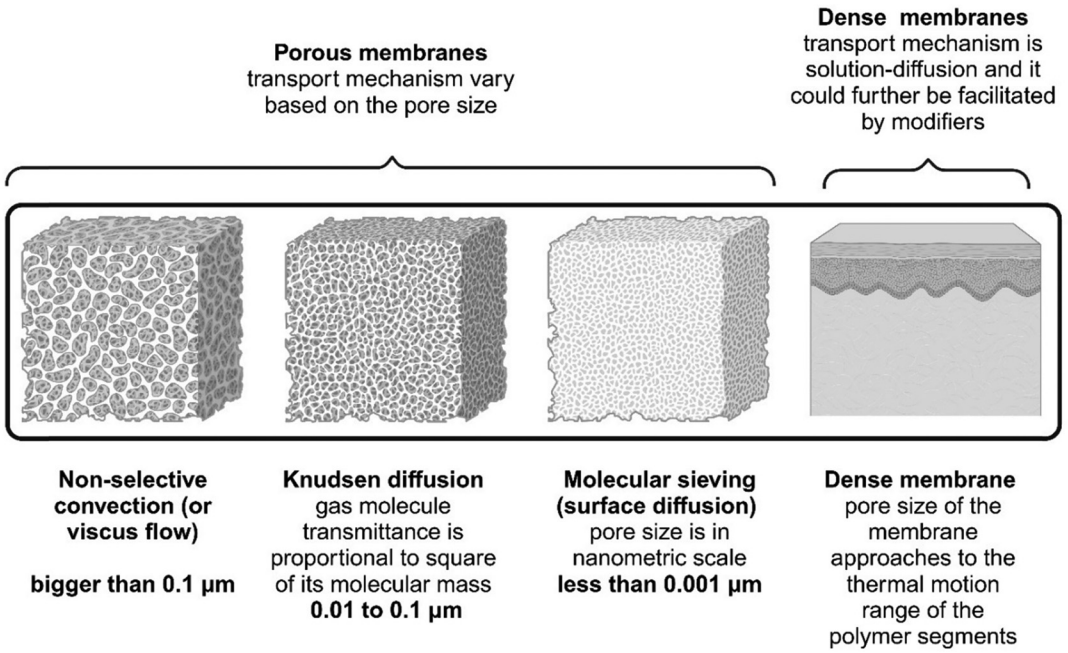

Fig. 9 Membrane's pore size and attributed transport mechanisms.

On the other hand, dense membranes separate gases through solution diffusion, where target gas molecules adsorb onto the membrane surface, diffuse through the membrane, and then desorb on the opposite side. Catalytic reactions can further facilitate this process, particularly in hydrogen purification using palladium membranes.[144,145] Fig. 9 illustrates the pore size ranges and corresponding transport mechanisms.

5.1. CCUS membranes from the material point of view

Gas separation membranes can be categorized into four main types: inorganic (ceramic), organic (polymeric), metallic, and hybrid membranes (also known as mixed matrix membranes, which contain both organic and inorganic components). Ceramic membranes, which emerged in the 1960s for applications such as gas separation and beer extraction, are particularly well-suited for use in harsh operating conditions due to their durability and thermal stability.[146,147] Common ceramic membrane materials include alumina, zirconia, silicon nitride, and perovskites like calcium titanium oxide. These materials are prized for their robustness in extreme conditions. For example, dense perovskite-based ceramic membranes are well-suited for high-temperature oxygen separation in integrated gasification combined cycle (IGCC) plants equipped with CCUS technologies.[148,149] Therefore, despite their high production costs, ceramic membranes remain a viable option for pre-combustion CCUS applications.[149] Ceramic membranes are generally three times as expensive as polymeric filters,[150] with ceramic materials costing around \$500–\$2000 per m^2 compared to \$50–\$400 per m^2 for polymeric membranes.[150–155] These cost differences push many industries toward using polymeric membranes, with additional benefits such as defect-free large-scale production further encouraging this trend.[156]

On the other hand, polymeric membranes offer a lower-cost alternative to ceramic ones. Various polymeric materials, such as cellulose-based polymers, polysulfone (PSF), polyether sulfone (PES), polyimide (PI), polyamide (PA), and polybenzimidazole (PBS), have been introduced for gas separation. While easier to fabricate, polymeric membranes have limited resistance to mechanical, thermal, and chemical stress. For example, high-temperature resistant polymers like PBS may struggle under extreme conditions, such as those found in IGCC plants,

Table 6 Polymeric and ceramic membranes for gas separation[141,158]

	Membrane material	Working criteria	Target gas	Details
Organic	Porous polymers (standalone and composite, rubbery/glassy)	Molecular sieving/ solution-diffusion	CO_2 or H_2	Low resistance to temperature and harsh operating conditions, low production cost
Inorganic	Dense metal (Palladium, Palladium composites)	Solution-diffusion	H_2	Highly selective to H_2 Moderate to high resistance to temperature Sensitive to impurities
	Dense ceramic (Molten carbonates, composite metal-ceramics, composite metal–metal)	Solution-diffusion/ chemical reaction	CO_2 or H_2	Moderate to high-temperature resistance, excellent corrosion resistance (towards organic solvents and a wide pH range), suitable for cleaning and steam
	Porous ceramics (mesoporous 2–50 nm) or microporous (less than 2 nm): amine-functionalized silica, zeolites, metal–organic frameworks	Molecular sieving/ diffusion	CO_2 or H_2	sterilization, and long lifetime. Brittle (requires careful handling), typically disc or tubular shaped with a low surface area/volume ratio and high investment cost.

which can reach pressures of 20 bar and temperatures between 700–900 °C.[136,157] Table 6 offers a classification of gas separation membranes based on their materials.

Another way to classify membranes is based on their symmetry. Porous ceramic membranes are typically asymmetric, consisting of one or more mesoporous sub-layers or intermediate layers, topped with a dense (microporous) selective layer. Membranes made entirely of the same material across all layers are classified as ''integral''.[159] If different materials are used for the various layers (*e.g.*, combinations of ceramics and organics), they are referred to as composite membranes.

5.2. Separation mechanism in CCUS membranes

As mentioned earlier, the separation performance of the membrane is assessed by several factors, among which selectivity and permeability are more important. Gas selectivity itself depends on two key mechanisms: diffusivity selectivity and solubility selectivity. Diffusivity selectivity occurs when the membrane discriminates gases based on molecular size, often referred to as size sieving, where smaller molecules permeate faster than larger ones. On the other hand, solubility selectivity is driven by the ability of certain gases to dissolve more readily in the membrane's polymer matrix, favoring the transport of more condensable gases, like CO_2, over less condensable ones, such as N_2 or O_2. Both mechanisms can operate concurrently, with the relative dominance depending on the specific membrane material and the feed gas composition. Membrane materials are tailored to enhance either or both selectivity types to achieve the desired separation performance in CCUS applications. Advances in material science, including mixed matrix membranes, aim to optimize these factors, providing a balance between permeability and selectivity to improve process efficiency. This section explores the CCUS membrane-based process, focusing on how these two factors influence separation efficiency.

5.2.1. Diffusivity-selectivity. Polymeric membranes are limited by the Robeson upper bound, which establishes an inverse relationship between permeability and selectivity. Essentially, as permeability increases, the membrane's ability to selectively control which gas components pass through diminishes. Increasing the pore size of the membrane can boost permeability, allowing more gas to pass through, but this comes at the cost of reduced selectivity. This permeability-selectivity trade-off, defined by the upper bound, illustrates the inherent challenge in membrane design: achieving a balance where both high permeability and high selectivity are optimized. The relationship between gas selectivity and permeability in polymeric membranes can be expressed as follows:[160]

$$\alpha_{ij} = \beta_{ij} P_i^{-\lambda ij} \quad (1)$$

$$\lambda_{ij} = \left(\frac{d_j}{d_i}\right)^2 - 1 \quad (2)$$

where λ_{ij} is the slope of the selectivity *vs.* permeability logarithmic curve, β_{ij} is the front factor, which is a function of gas solubility, the slope of the curve, the average spacing between polymeric chains, and the stiffness of the chain. In these equations, d_j is the kinetic diameter of the larger gas molecule and d_j is the kinetic diameter of the smaller gas molecule.

Glassy polymer-based membranes exhibit a higher Robeson upper bound compared to rubbery membranes due to the increased gas solubility in their nonequilibrium excess volume.[161,162] Glassy polymers, which are rigid below their glass transition temperature (T_g), tend to show better selectivity and mechanical strength. On the other hand, when the temperature exceeds T_g, polymers become flexible and rubbery, leading to significant changes in density, specific heat, dielectric coefficient, conductivity, and transport properties.[163]

Over the past few decades, glassy polymer-based membranes have gained attention due to their superior mechanical strength, reproducibility, and adaptability across a variety of applications.[164]

5.2.2. Solubility-selectivity. The different affinity of the chemical structures to the membrane materials results in different intermolecular interactions, ranging from weak van der Waals forces to stronger electrostatic or hydrogen bonding interactions. These interactions significantly impact selectivity, as they can either enhance or hinder the permeation of certain molecules. In gas separation, diffusivity–selectivity typically favors smaller, lighter molecules, as they can move more easily through the membrane's free volume. However, the membrane must maintain sufficient free volume to ensure that the diffusivity ratio between the two species is close to one, maximizing selectivity.[165]

In contrast, solubility-selectivity favors larger, more soluble molecules, which may penetrate more easily due to their chemical affinity for the membrane material. For example,

CO_2, with its significantly higher quadrupole moment compared to other common flue gas components, exhibits better solubility in membranes functionalized with polar groups.[166]

Gas solubility is influenced by several factors, including the gas' characteristics, operating conditions, and the membrane material properties. Compressible gases like CO_2, especially those with high polarity, tend to have greater solubility at higher pressures, and stronger interactions with the membrane's polar functional groups can further enhance this solubility. In polymeric membranes, gas sorption generally occurs in two distinct phases.

5.2.3. Reactive diffusivity (facilitated transport). When functional groups within the membrane structure are capable of reacting with CO_2, the facilitated transport mechanism significantly enhances both the permeability and selectivity of the membrane. In facilitated transport membranes (FTMs), normal diffusion is still active alongside reactive diffusion. The total CO_2 flux, as described by Cussler's model,[167] is expressed as a combination of Fickian diffusion and reactive diffusion, leading to the equation:

$$J_{CO_2} = \text{Fickian diffusion} + \text{Reactive diffusion} = \frac{P_{CO_2}}{l}\Delta p_{CO_2} + \frac{P_{\text{Carrier-}CO_2}}{l}\Delta p_{\text{carrier-}CO_2} \quad (3)$$

However, the complex reaction mechanisms within FTMs complicate direct flux calculation using this equation due to factors such as: (i) CO_2 partial pressure being dependent on both physisorption and chemisorption, and (ii) mass transfer resistance caused by interfacial adsorption/desorption, which is independent of membrane thickness. As a result, CO_2 transport properties in FTMs are often measured similarly to solution-diffusion membranes. Still, caution is needed when interpreting CO_2 permeability data, as high permeability in thick films doesn't always translate to high permeance in thin-film composite membranes.[168]

Although the Robeson upper bound was initially developed for homogeneous polymeric membranes, it continues to serve as a baseline for evaluating improvements in membrane selectivity and permeability.[169] Advances in materials, such as mixed matrix membranes (MMM), carbon molecular sieves (CMS), polymers with intrinsic microporosity (PIM), and thermally rearranged polymers (TR), have led to breakthroughs beyond the Robeson bound, particularly through approaches focusing on solubility-selectivity.[170–173]

5.3. Performance measurement

The performance of the gas separation membrane is commonly evaluated using constant pressure/variable volume (CP/VV), or the isobaric method, as depicted schematically in Fig. 10(a). Membrane performance is assessed through several key factors: solubility, diffusivity, permeability, and selectivity. The diffusion of a single gas through a porous membrane can be described by Fick's first law:

$$J = -D \times \frac{dC}{dx} \quad (4)$$

where J is the gas flux, D is the diffusion coefficient, and $\frac{dC}{dx}$ is the concentration gradient across the membrane. Diffusivity, as

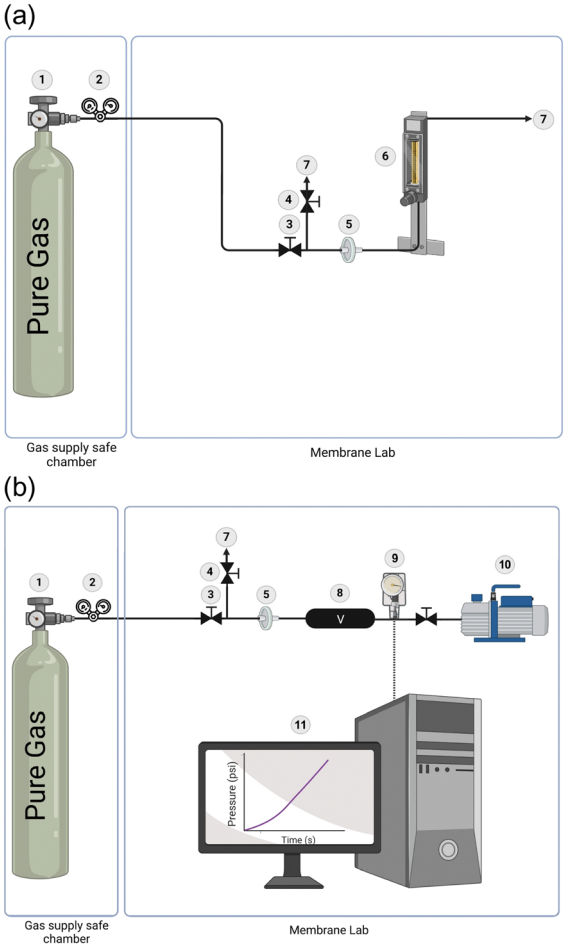

Fig. 10 Schematic illustration of: (a) constant pressure variable volume (CP/VV), and (b) constant volume variable pressure (CV/VP) setup for permeability study of gas separation membranes; (1) gas cylinder, (2) regulator, (3) startup valve, (4) bleeding valve, (5) membrane cell, (6) bubble flow meter which can be replaced by any gas flow meter, and (7) vent, (8) chamber with known constant volume, (9) pressure logger or pressure transducer, (10) vacuum pump, and (11) data collection computer.

a kinetic parameter, reflects the ability of gas molecules to move through the membrane. The steady-state flux of a single gas can be expressed as:

$$J = -D \times \frac{C_0 - C_l}{l} \quad (5)$$

where C_0 and C_l are the gas concentrations on the feed and permeate sides, and l is the membrane thickness. At low gas concentrations, Henry's law can correlate the pressure (p) and gas concentration (C):

$$C = S \times p \quad (6)$$

where S is the solubility constant or sorption constant. Using this concentration relationship in eqn (5), the flux can be rewritten as:

$$J = D \times S \times \frac{p_0 - p_l}{l} = P \times \frac{p_0 - p_l}{l} \quad (7)$$

where P is the permeability, defined as the product of solubility and diffusivity:

$$P = S \times D \tag{8}$$

Permeability can also be calculated by:

$$P_i = \frac{Q_i l}{A \Delta p_i} \tag{9}$$

where Q_i is the gas flow rate, A is the membrane effective area, and ΔP_i is the partial pressure difference of the component i across the membrane. Permeability is commonly expressed in Barrer $\left(1\ \text{Barrer} = 10^{-10}\frac{\text{cm}^3_{\text{STP}} \times \text{cm}}{\text{cm}^2 \times \text{s} \times \text{cmHg}}10\right)$.

Another important metric is permeance, expressed in gas permeation unit $\left(1\ \text{GPU} = 10^{-6}\frac{\text{cm}^3_{\text{STP}}}{\text{cm}^2 \times \text{s} \times \text{cmHg}}\right)$:[174]

$$\text{Permeance} = \frac{Q_i}{A \Delta p_i} \tag{10}$$

Selectivity is the membrane's ability to differentiate gases, defined for a binary mixture as the ratio of their permeabilities:

$$\alpha_{AB} = \frac{P_A}{P_B} = \left(\frac{S_A}{S_B}\right) \times \left(\frac{D_A}{D_B}\right) \tag{11}$$

where $\frac{S_A}{S_B}$ is the solubility selectivity and $\frac{D_A}{D_B}$ is the diffusivity selectivity.[175] A more recent approach to assessing membrane performance focuses on four aspects of CO_2 separation:

$$\text{PER}_{CO_2} = \frac{(P_{\text{mod}} - P_{\text{neat}})}{P_{\text{neat}}} \tag{12}$$

$$\text{SeER}_{CO_2} = \frac{(\alpha_{\text{mod}} - \alpha_{\text{neat}})}{\alpha_{\text{neat}}} \tag{13}$$

$$\text{DER}_{CO_2} = \frac{(D_{\text{mod}} - D_{\text{neat}})}{D_{\text{neat}}} \tag{14}$$

$$\text{SoER}_{CO_2} = \frac{(S_{\text{mod}} - S_{\text{neat}})}{S_{\text{neat}}} \tag{15}$$

where PER is the permeability enhancement ratio, SeER is the selectivity enhancement ratio, DER is the diffusivity enhancement ratio, SoER is the solubility enhancement ratio, X_{mod} is the characteristics of the membrane in a modified state, and X_{neat} is the same characteristics of the unmodified membrane.

To optimize a membrane-based gas separation process, both selectivity and permeability must be considered. The choice between diffusivity selectivity and solubility selectivity depends on the gas composition and the desired separation. When separating gases with similar molecular structures (*e.g.*, N_2 and O_2), diffusivity plays a larger role, while solubility-based separation is more critical for gases with different chemical properties, including polarity, charge, *etc.* (*e.g.*, CO_2 and CH_4).[176] Additionally, the concept of fractional free volume (FFV) can explain membrane permeability:[177]

$$\text{FFV} = \frac{V - V_0}{V} = \frac{V - V_{\text{VDW}}}{V} \tag{16}$$

where V is the total volume of the membrane, and V_0 is the occupied volume of polymeric chains, typically 1.3 times the van der Waals volume (V_{VDW}), as defined by Bondi methods.[178–180] V_{VDW} is the theoretical molecular volume in a packed structure such as a polymer chain. However, there is a minimum feasible packing density for the molecules. Consequently, each molecule requires more volume in comparison with its V_{VDW}. 1.3 V_{VDW} is considered commonly, based on the packing density of the molecular crystal structure at 0 K). The concept of FFV does not have a precise definition, yet it is useful for chain mobility and permeability clarifications.[172] Developing methodologies and chemical approaches that can result in high FFV with sufficient interconnectivity leads to a microporous membrane with perfect solubility and sorption capacity (similar to porous materials with significant surface area).[172]

The constant volume/variable pressure (CV/VP), also known as the time-lag or isochoric method, is a widely used technique for determining diffusion coefficients and assessing permeability in steady-state single or mixed gas streams due to its independence from specific gas types.[181,182] Fig. 10(b) illustrates the process. In this method, the gas permeates through the membrane and is collected in a downstream reservoir with a constant volume. A pressure transducer or sensor records the pressure in the storage tank over time, corresponding to the permeation test. The permeability of the membrane is calculated using the following equation:[183]

$$P = \frac{273.15 \times 10^{10} VL}{760 A T \left[\frac{P_0 \times 76}{14.7}\right]}\left(\frac{\text{d}p}{\text{d}t}\right) \tag{17}$$

where P is the gas permeability in Barrer (1 Barrer = 10^{-10} cm^3(STP) cm cm^{-2} cmHg^{-1} s^{-1}), P_0 is the feed pressure (psia), T is the operational temperature (K), and V is the constant volume vessel (cm^3). A is the membrane effective surface area (cm^2), L is the membrane thickness (cm), and $\frac{\text{d}p}{\text{d}t}$ is the pressure change over time (mmHg s^{-1}). The method can accurately evaluate the transport properties of the membranes within different humidity percentages.[184] CV/VP is the simplified version of the time-lag method, which is used to measure the diffusivity gasses through the membrane.

The time-lag parameter is calculated when the gas permeates from the constant pressure feed side into the constant volume permeate reservoir. Diffusivity coefficient, D is calculated using:[185]

$$D = \frac{l^2}{6\theta} \tag{18}$$

where D is the diffusion coefficient of the gas, θ represents the time-lag (the slope of the pressure *vs.* time in the steady-state region), and l is the membrane thickness.

By measuring permeability from eqn (8), the solubility parameter can be derived using eqn (5). Typically, these performance measurements (CP/VV and CV/VP) are used for single gas permeability and ideal selectivity. However, a more realistic approach involves mixed gas feeds, adjusting the upstream gas concentrations using mass flow meters, and measuring the permeate composition with gas chromatography. This setup provides insight into the real selectivity of the membrane, accounting for the effects of gas mixtures on membrane performance. Selectivity, or the selectivity factor, is calculated using:[186]

$$\alpha'_{A,B} = \frac{\frac{y_A}{y_B}}{\frac{x_A}{x_B}} \quad (19)$$

where A and B are the gas components, y is the molar fraction in the permeate, and x is the molar fraction in the feed stream.

Operating conditions like temperature and pressure significantly influence gas solubility and diffusivity. The van't Hoff–Arrhenius model and dual-mode sorption model (considering both Henry's law and Langmuir modes) describe these relationships.[187,188] Given that gas sorption enthalpy is typically negative, an increase in temperature reduces gas solubility in the polymer matrix. However, this effect depends on the specific gas–polymer interactions. Likewise, pressure effects on solubility and diffusivity vary based on the gas type, pressure range, and membrane porosity. Further details on these correlations are discussed in the literature.[188–190]

5.4. Membrane design for gas separation: sublayers, intermediate layers, and selective coatings

Flat sheet gas separation thin-film composite membranes typically consist of a support layer for mechanical strength. Separation occurs *via* a top selective layer, employing either sieving (size exclusion) or selective solution of specific components. Occasionally, an intermediate or gutter layer between the support and selective layers adjusts pore structures and controls diffusion. Each layer will be discussed separately.

5.4.1. Sublayer. A successful gas separation membrane needs high permeance to reduce the required surface area and capital costs, while maintaining high selectivity for efficient purification. A composite membrane structure with a support layer of approximately 50 μm and a selective layer of less than 1 μm provides a good balance between mechanical strength and filtration performance.[191] The support layer is typically a microfiltration (MF) or ultrafiltration (UF) membrane, which acts as a sublayer for the tighter, selective thin film. Phase separation is a common method for sublayer fabrication, enabling scalability for industrial applications. Various techniques such as temperature-induced phase separation (TIPS), non-solvent-induced phase separation (NIPS), and vapor-induced phase separation (VIPS) are used to fabricate the sublayer, each resulting in different pore structures and properties.[192] Stretching with heat pretreatment in extrusion-based membranes is also suggested for the sublayer preparation.[193] Factors like casting solution composition, coagulation bath parameters, and processing conditions play a key role in controlling characteristics like pore size, porosity, surface roughness, and charge.

On the lab scale, membranes are fabricated using a machine-driven or a handheld casting applicator. The wet film is then (immediately or after a measured time) moved to an immersion non-solvent coagulation bath to complete the phase inversion process. For large-scale production, roll-to-roll methods have been explored, allowing controlled sublayer thickness and smooth surface properties. Consumption rates of raw materials and solvents largely depend on the production methods. However, as an estimate, preparation of a single asymmetric porous sublayer by NIPS method requires approximately 50 g m^{-2}.[193] The process includes a casting system with adjustable gap and tension for controlling the thickness of the wet film, as well as a coagulation bath with a controlled dose of chemicals and unwinding and rewinding rollers. A schematic of this process is shown in Fig. 11.[194,195] After production, flat sheets are commonly converted into spiral wound modules for pilot testing.[196–198]

Sublayers are typically made of various polymeric materials selected for their chemical, thermal, and mechanical properties. The most common materials used for these sublayers include polysulfone (PSF), polyethersulfone (PES), polyacrylonitrile (PAN), polypropylene (PP), polyvinylidene fluoride (PVDF), polytetrafluoroethylene (PTFE), and cellulose acetate (CA).[193] Each material offers specific benefits depending on the application. For example, PSF and PES are widely used due to their excellent thermal resistance and chemical stability, particularly when fabricated using the phase inversion method. PES is often preferred over PSF for sublayers because it has a higher hydrophilicity, which enhances adhesion to the selective layer during interfacial polymerization.[199,200]

The selection of sublayer material is essential for balancing properties like permeability, mechanical strength, and adhesion. Porosity and pore size are controlled through the addition of hydrophilic additives such as polyvinyl pyrrolidone (PVP) and polyethylene glycol (PEG) in the casting solution,[17,201,202] which improve membrane performance by influencing the structure and properties of the support layer.

In the case of sublayers acting purely as mechanical supports, their selectivity should be close to 1, meaning they contribute minimally to gas separation.[194] However, the pore size and distribution in the sublayer can impact the overall membrane performance. Larger pores in the sublayer, even with identical top layer thickness, may slightly increase permeability, necessitating careful design to ensure an even, smooth surface that allows for uniform coating of the selective layer. Fig. 12 offers a comparison of PES sublayer's pore size effect on the gas transport and separation performance of CO_2 separation composite membrane.[194] Thus, a sublayer membrane needs to be designed and tailormade based on the specific thin film top layer, feed gas, and operating conditions. Reducing surface roughness by adjusting fabrication parameters, along with achieving an even distribution of pores, can enhance the formation of a uniform selective layer.

5.4.2. Intermediate layer. An intermediate layer, known as the "gutter" layer, prevents the selective layer solution from penetrating the pores of the underlying membrane, ensuring a smooth, defect-free surface for effective gas separation.[203] The

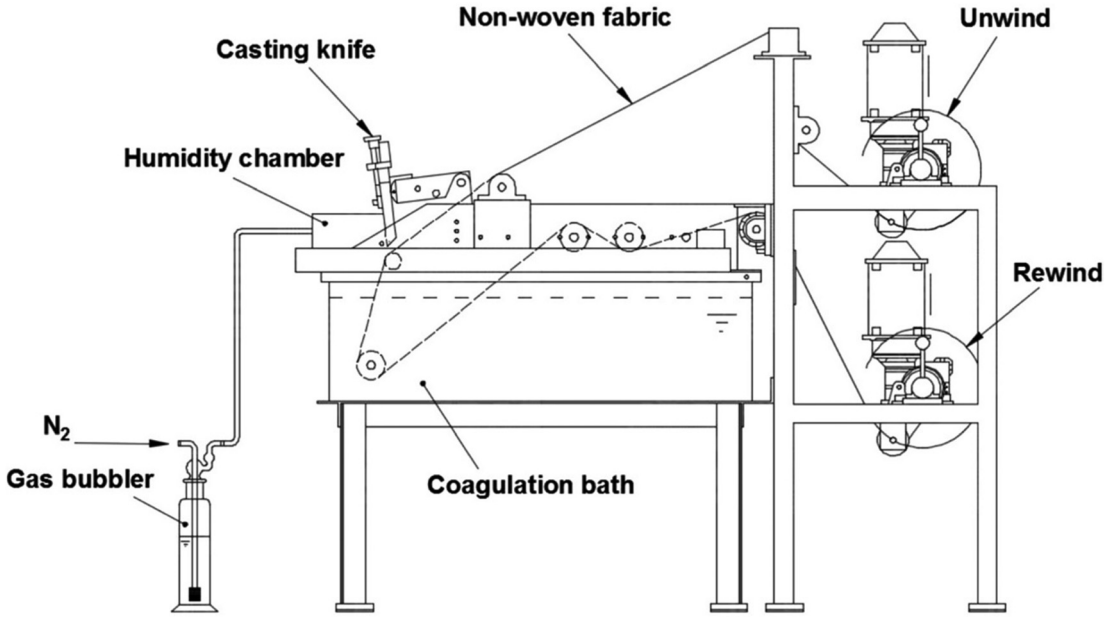

Fig. 11 Schematic for pilot production of gas separation membrane sublayer (reproduced from ref. 194 and 195 with permission from Elsevier, copyright 2025).

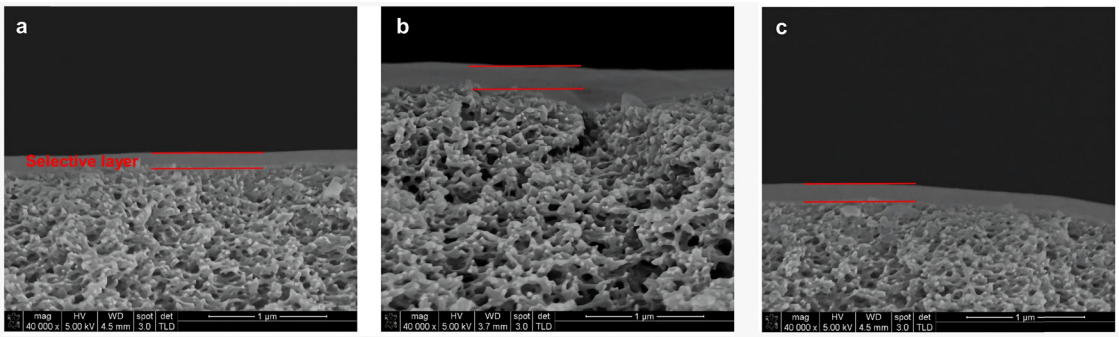

Transport performances of the composite membranes with different PES substrates

PES average pore size (nm)	PES surface porosity (%)	Selective layer thickness (nm)	CO_2 permeance (GPU)	CO_2/N_2 selectivity
42.2	11.3	145	654	154
69	17.0	160	780	135
77.5	17.8	155	764	113

Fig. 12 Increasing PES sublayer pore size with the same PVA selective layer thickness (a) thin film composite with PES average porosity of 42.2 nm, (b) thin film composite with PES average porosity of 69 nm, and (c) thin film composite with PES average porosity of 77.5 nm from ref. 194 with permission from Elsevier, copyright 2025).

main function of this layer is to reduce surface roughness, promoting a more uniform coating of the selective top layer, which is critical for optimal membrane performance.[193] To ensure excellent gas permeance, the materials used for the gutter layer must exhibit high gas permeability, superior film-forming characteristics, a smooth surface, and strong compatibility with both the sublayer and the selective layer.[204,205] Evidence of permeability improvement alongside retaining or improving the CO_2/N_2 selectivity of Pebax, polyvinyl amine (PVAm), and poly(butylene terephthalate) (PBT) membranes has been reported after using a gutter layer.[206–209]

The permeability of the gutter layer should ideally be five to ten times higher than that of the selective layer to minimize any loss in selectivity, ensuring effective mass transfer.[210] Materials

like AF2400, a Teflon-based material, offer high gas permeance and don't require additional cross-linking, making them useful for forming homogeneous films. However, AF2400 is hydrophobic, necessitating the use of a more hydrophilic material in some cases.

Two commonly used materials for gutter layers are polydimethylsiloxane (PDMS) and poly(1-trimethylsilyl-1-propyne) (PTMSP). While PTMSP demonstrates higher CO_2 permeability, it suffers from a substantial decrease in permeability (up to 80%) over time.[191,193] In contrast, PDMS, which exhibits only a 5% permeability decline over similar periods, is a more durable and effective option for CO_2 capture membranes. PDMS can be coated using techniques like dip coating or casting, and the casting solution is typically prepared using a standard ratio of PDMS, crosslinker, and catalyst.[211]

Nanomaterials such as covalent organic frameworks (COFs) are gaining attention as intermediate layers due to their tunable pore sizes. For example, a Pebax 1657 membrane modified with a COF intermediate layer showed a CO_2/N_2 selectivity of 28 and a permeance of 1840 GPU.[212] Metal–organic frameworks (MOFs) are also being explored, particularly plate-like two-dimensional (2D) MOFs that offer a smoother surface than traditional three-dimensional (3D) MOFs, making them more suitable as gutter layers. An ultra-thin zinc(II) tetrakis(4-carboxyphenyl)porphyrin) (ZnTCPP) MOF layer, when combined with Pebax 1657, achieved impressive performance, with CO_2/N_2 selectivity reaching 34 and a permeance of 1710 GPU,[203] while the same thin film material (with the thickness of 910 nm) on PTMSP gutter layer resulted in GPU of 1160 and CO_2/N_2 selectivity of 20.[213] Several fabrication techniques, including vacuum filtration, spin coating, dip coating, and casting, can be employed to form the gutter layer, depending on the desired membrane characteristics.[203,211,212] The choice of method and material significantly influences the overall membrane performance and its ability to achieve efficient gas separation. Fig. 13 illustrates the practical applications of polymer- and nanomaterial-based gutter layers in enhancing decarbonization efficiency in gas separation membranes.

5.4.3. Selective layer. The selective layer is the most critical component of gas separation membranes as it directly governs both the selectivity and permeability of the membrane. Its ability to differentiate between gas molecules, particularly CO_2, is vital for optimizing CCUS processes. Therefore, this

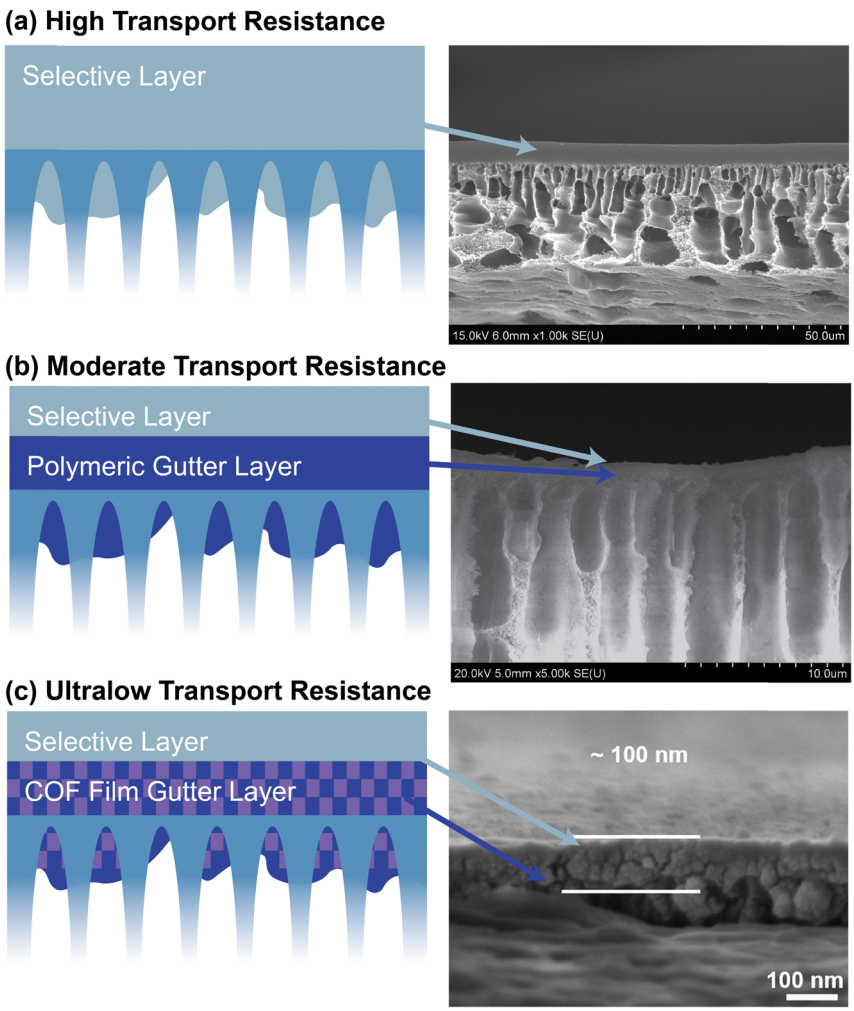

Fig. 13 Using an intermediate or gutter layer to enhance the decarbonization capacity of the polymeric thin film composite membranes[212] (with permission from Elsevier).

layer should be designed to be as CO_2-philic as possible, incorporating materials that enhance the solubility and selective transport of CO_2 over other gases.

Changing the nature of the membrane backbone chemically can shift the solubility-selectivity to diffusivity-selectivity, assuming the pore size and distribution remain constant. This creates the concept of CO_2-affinity membranes, which are constructed from materials rich in oxygen, nitrogen, or sulfur functional groups. These functional groups, including acetate, nitrile, and ether, significantly enhance CO_2 solubility.[214] Various approaches, such as monomer synthesis and impregnating base membranes with functionalized materials like MOFs and COFs, have been used to develop these membranes.[215–217]

Polymeric materials from the ethylene oxide (EO) family, including PEG and PEO, are recognized for their high CO_2 permeability due to their polar oxygen content. However, increased crystallinity in these materials reduces their permeability.[135,218,219] To address this, methods such as copolymerization with materials like polyamides (Pebax) and polyimides have been explored to reduce crystallinity and improve mechanical stability. Pebax membranes, particularly Pebax 1657 and Pebax 2533, are widely studied for CO_2 separation.[220] Pebax has been shown to benefit from adding hard segments, like polyamide, to provide mechanical strength while retaining CO_2 solubility.[220] However, neat Pebax exhibits limited permeability, prompting research into solvent effects on its microstructure and crystallinity. Modifying the casting solution composition has been shown to alter permeability and selectivity, with solvents of higher boiling points increasing crystallinity and, therefore, permeability loss.

For FTMs, functional groups that can react with CO_2 are introduced to the membrane structure to increase both permeability and selectivity.[221–223] FTMs rely on reversible reactions between CO_2 and functional groups like amines, and they exhibit higher performance in flue gas decarbonization due to their ability to operate at moderate feed pressures. PVAm membranes, with high amine content, are a leading candidate for FTMs, particularly when coupled with mobile amine carriers.

PEO and related materials, along with nanofillers, have been intensively researched as MMMs to enhance membrane performance. The addition of nanomaterials like MOFs, COFs, and carbon-based materials has improved both permeability and selectivity, with promising results in pushing beyond the Robeson upper bound. These developments, coupled with solvent and casting techniques, have improved the overall performance of gas separation membranes.

Recent advances in fabricating membranes for CCUS application along with the full technical details and performance results, including the effects of molecular weight, casting solvents, and different modifications, are discussed in the following subsection.

6. Advances in membranes for CCUS applications

Advancements in membrane fabrication for CCUS have been achieved through various functional modifications, including new monomer synthesis, altering the membrane backbone's chemistry,[224] or impregnating the base membrane with functionalized MOFs,[216] zeolitic imidazolate framework (ZIF),[212,225] COFs,[226] 2D and 3D carbon-based structures (graphene oxide (GO),[227–229] carbon nanotubes (CNT))[230,231]. For example, increasing the oxygen-to-carbon (O/C) ratio from 0 to 0.5 by using polyethylene oxide instead of polyethylene has been shown to enhance solubility-selectivity from 13 to 50.[214,232] These membranes are developed with diverse design approaches to meet the specific challenges of CCUS applications. This section will cover the latest research works performed on different CCUS membranes.

6.1. Polyethylene glycol and similar materials

The ethylene oxide (EO) family, which includes both low-molecular-weight polyethylene glycol (PEG) and high-molecular-weight polyethylene oxide (PEO), represents a common class of membrane materials with acceptable CO_2 separation performance. The high content of polar oxygen functional groups in PEO grants it a higher affinity for CO_2 permeation. However, these polar structures also increase the crystallinity of the PEO matrix, which reduces overall permeability. For example, amorphous PEO exhibits a permeability of 140 Barrers, while semicrystalline PEO has a permeability of only 13 Barrers. The crystalline structures obstruct free pathways within the membrane, reducing the FFV and, consequently, the permeability.[233]

To address the crystallinity-related permeability loss, enhancing the molecular weight of the ethylene oxide segment has been employed as a strategy to improve membrane-forming capability, reduce crystallinity, and enhance mechanical stability in low-molecular-weight PEO. The micro-domains of the polymeric backbone can also be fine-tuned to further mitigate the permeability loss.

The selectivity of modified-PEO membranes is determined by the EO soft segments. For CO_2/N_2 binary mixtures, the selectivity performance remains comparable to that of neat PEO. However, the permeability of these membranes is heavily influenced by factors such as the length of both hard and soft segments, their spatial arrangement, and the copolymerization approach. By incorporating hard segments *via* co- or block-polymerization with materials such as polyamides, polyimides, polyether block amides (Pebax), and aryl sulfones, PEO-based membranes can achieve better control over crystallinity, maintaining both permeability and selectivity.[135,218,219]

Adding a hard segment to the EO membrane family is an effective method to maintain CO_2 solubility while enhancing the mechanical stability of the membranes. This modification is commonly achieved through transesterification or polycondensation reactions involving aliphatic diols, diamines, and aromatic diacids. The resulting copolymer structure may undergo interactions at the interface between the hard and soft segments, necessitating an optimal design that minimizes disruptions. An ideal PEO-based membrane for CCUS should exhibit weak interpolymer interactions.[234]

One prominent example of an EO-containing copolymer is polyether block amide (PEBA), commonly known as Pebax. In this copolymer, the ether-containing soft segment enhances

solubility through strong dipole-quadrupole interactions with polar components in the feed gas, while the crystalline polyamide (PA) segment provides mechanical strength and higher solubility selectivity due to its polar content. The PA segment also directly controls gas diffusivity by regulating the FFV and intersegmental polymer spaces. Pebax's affordability and favorable characteristics have made it a popular material for CO_2 separation and other polar/non-polar gas mixtures such as CO_2/CH_4, CO_2/N_2, CO_2/H_2, H_2S/CH_4, CH_4/N_2, O_2/N_2, NH_3/N_2, NH_3/H_2, ethylbenzene/N_2, and hydrofluorocarbons (HFCs)/hydroflurolefin (HFO).[235]

Given its popularity, Pebax is now considered a distinct class of gas separation membrane material with various production and modification methods. Among the different grades of Pebax, Pebax 1657 is commonly used due to its superior CO_2 selectivity, while Pebax 2533 has the highest soft segment content, resulting in higher permeability.[220] Table 7 provides further details on various Pebax membrane materials and their separation performance.

While Pebax is one of the most widely studied materials for post-combustion CCUS applications, its low permeability limits its performance, prompting various modification strategies to enhance its efficiency. Although there is significant interest in Pebax-based CO_2 separation membranes, only a few studies have focused on how fabrication parameters affect their structure and performance. For instance, Isanejad *et al.* examined the influence of organic solvents on the microstructure and performance of Pebax 1657.[237] Their study demonstrated that even though the chemical structure of the membranes remained identical, the boiling points of the solvents used during fabrication played a crucial role in altering the crystallinity and free volume (*d*-spacing) of the membranes, as shown by X-ray diffraction (XRD) measurements. Dimethylacetamide (DMAC), for example, produced a membrane with the highest crystallinity. Initially, the *d*-spacing increased with crystallinity, but excessive crystallinity led to reduced free volume due to slower solvent evaporation, resulting in a more interconnected membrane matrix.

Solvent characteristics, such as specific volume, also impact membrane structure. Solvents with higher specific volumes create larger *d*-spacing by reducing van der Waals interactions, leading to membranes with higher FFV and, consequently, increased permeability.[238] Karamouz *et al.* studied the effect of drying temperature on the structure and performance of Pebax 1074 membranes and found that drying temperatures of 60–80 °C resulted in denser membranes with better permeability and selectivity. However, temperatures above 80 °C caused the formation of non-selective micro-voids, which reduced selectivity due to rapid solvent evaporation.[239]

Modifying Pebax membranes can be done by blending Pebax with a base polymer such as polyethersulfone (PES) or by coating a thin Pebax film onto a nanoporous sublayer. Solvent compatibility is essential for successful casting solutions, with a 70/30 wt% ethanol/water mixture proving to be an effective solvent for minimizing structural impacts. Since the highly polar structure of Pebax requires a solvent with a high dielectric constant, several solvents have been proposed.[240,241] Formic acid has also been shown to be a highly effective solvent for dissolving Pebax and preventing gelation at low temperatures, although its large-scale viability remains a concern.[242] After dissolving Pebax and its modifiers, the mixture is typically refluxed at 70–80 °C for 2 hours, followed by post-treatment drying to remove residual solvents.

Crosslinking has emerged as another effective strategy for modifying Pebax membranes. Reported examples include Pebax/PVDF crosslinked with 2,4-toluylene diisocyanate (TDI),[243] Pebax/PAN crosslinked with polydimethysiloxane (PDMS),[244] PES/Pebax composite membrane crosslinked with poly ethylene glycol diacrylate (PEGDA),[245] and Pebax/chitosan crosslinked with glutaraldehyde.[246] The characteristics of the crosslinker and its impact on the membrane's final structure are crucial factors to consider when designing such modifications. Silane coupling agents containing amine groups can be incorporated for polymer crosslinking while enhancing polar interactions of CO_2. Sanaeepour *et al.* conducted such amino-silane modification by enhancing the selectivity of Pebax 2533 using (3-aminopropyl(diethoxy)methyl silane (APDEMS)).[222] They highlighted the benefits of R-(CH2)*n*-Si-X3 crosslinkers (where R and X represent amino and hydrolyzable groups), which reduce the gas diffusion energy barrier due to Si–O local mobility. These crosslinking modifications are designed to increase selectivity without significantly sacrificing permeability.[246]

The incorporation of nanofillers into Pebax membranes has been intensively studied, and various classes of nanofillers for CCUS applications have been comprehensively reviewed. The performance changes of the membranes were reported in Fig. 14.[247] Among all the fillers, ranging from the novel MXene structures to more established fillers like graphene and carbon nanotubes, the bimetal oxide nanosheet $ZnCo_2O_4$ demonstrated the most significant improvements, enhancing permeability and selectivity by 166% and 76%, respectively. The better enhancement ratios were linked to the generation of oxygen vacancies ($O^{-\delta}$), which ultimately create more CO_2 adsorption sites ($C^{-\delta}$).[248] Another significant additive with a 628% selectivity enhancement ratio was NaY zeolite due to creating a diffusional path by micro-sized voids.[249] Permeability-oriented enhancement strategies are particularly prominent among Pebax modification approaches, aiming to surpass the binary gas Robeson's trade-off.[235]

Copolymerization of polyesters and EO derivatives represents another family of CCUS membranes with improved inner microregions. A commercialized copolymer in this family is poly(butylene terephthalate) (PBT), known as polyactive. The

Table 7 Different grades of Pebax polymers and the composition of their hard/soft segment (Open access policy from) (reproduced through MDPI open access policy from ref. 236, copyright 2025)

Pebax	Soft segment (polyether, wt%)	Hard segment (polyamide, wt%)
1657	40	60
1074	55	45
5513	60	40
2533	80	20

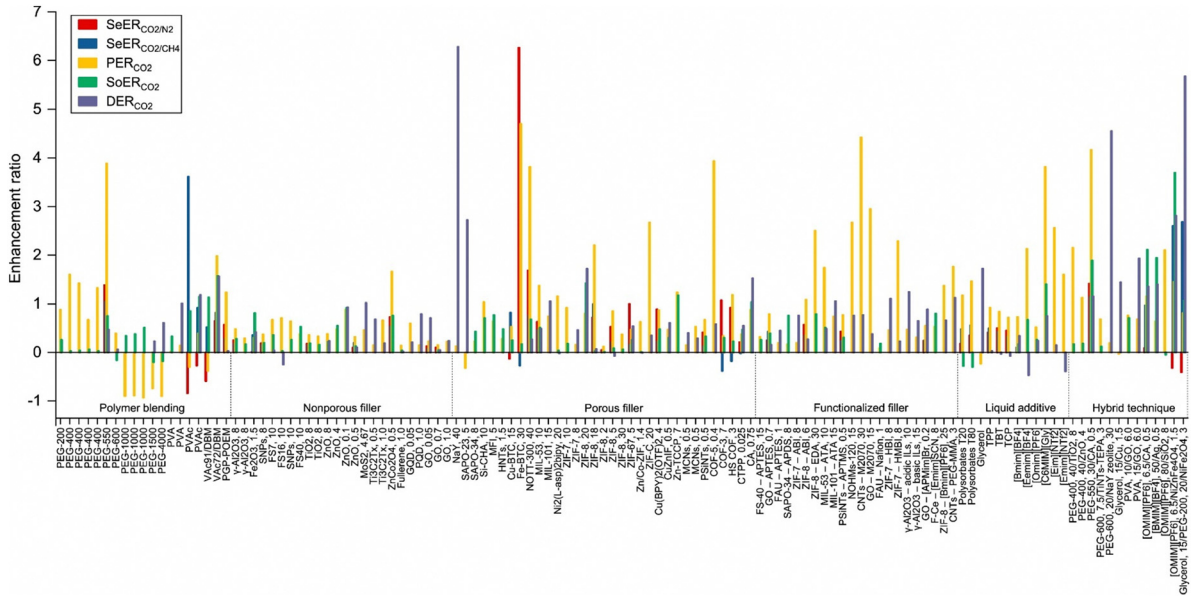

Fig. 14 Selectivity, permeability, diffusivity, and solubility enhancement ratios for mixed matrix Pebax membranes (reproduced from ref. 247 with permission from Elsevier, copyright 2025).

ease of copolymerization for this combination enables systematic studies on the effects of segment length, molecular weight, and weight percentage of each block on transport and mechanical properties.[250] Experiments suggest that the chain length, molecular weight, and thermal characteristics of polyactive segments have similar influences on membrane performance as those in Pebax. In combination with ester segments, PEO with a molecular weight within the range of 2000 to 2500 g mol^{-1} has been found to achieve the highest permeability.[251] Imide copolymers are reported to outperform amides and esters when the PEO segment is sufficiently long to form a continuous phase. The enhanced performance of polyethylene imide is attributed to the limited hydrogen bonding interactions between the segments, resulting in complete phase separation.[252]

6.2. Facilitated transport membranes (FTMs)

The addition of the functionalized selective layer to the gas separation membranes bearing amine carriers can lead to the fabrication of FTMs. FTMs are well-suited candidates for post-combustion CCUS scenarios where the main flue gas elements are nitrogen and CO_2.[253] Current FTMs exhibit moderate selectivity (50–100) with high CO_2 permeability (exceeding 1000 GPU).[221–223] Compared to traditional solution-diffusion membranes, FTMs offer superior performance at moderate feed pressures, making them more cost-effective for flue gas decarbonization by reducing the need for high compression costs.[254]

FTMs take advantage of CO_2-philic structures and functional groups to create more CO_2 adsorption sites on and within the selective top layer of the membrane, resulting in higher permeability and selectivity of the membrane. CO_2 reacts reversibly with the target functional group on the surface of the selective layer and turns into an alternative species. It then diffuses through the membrane body due to the chemical potential difference driving force, originating from the partial pressure or concentration difference of CO_2, and dissociates on the opposite side of the membrane in the form of CO_2 (Fig. 15(a)). While the transport of the polar gases happens by reaction and diffusion, the inert gases like methane and nitrogen pass through only by diffusion. Thus, FTMs can selectively separate CO_2. Several structures have been investigated for their CO_2-philicity, with polymers containing a high content of amines reported as the most effective carriers for FTMs. The functional group can either be integrated into membrane's polymeric backbone (fixed-site amine carriers) or incorporated into the membrane matrix through modification strategies (mobile carriers).

Fig. 15(b) illustrates two main pathways for amine-facilitated transport in FTMs.[255] Primary and secondary amines possess an unshared electron pair on the nitrogen atom, allowing them to act as nucleophiles and engage with the electrophilic carbonyl group of CO_2, forming a zwitterion. The zwitterion undergoes a quick deprotonation process facilitated by another amine, yielding a more stable carbamate ion. In this pathway, converting one mole of CO_2 requires two moles of amines. When a tertiary amine is used in FTM, acting as a Brønsted base only, bicarbonates are formed instead of carbamates. Carbonic acid is neutralized after the reaction of CO_2 and water. This pathway requires one mole of amine for each mole of CO_2. Although the second pathway is more efficient, the slow formation of carbonic acid hinders the reaction rate.[257]

An ideal example of FTM is the polyvinyl amine (PVAm) membrane, which is highly valued for its high content of primary amine groups.[209,258] Compared to other polymers, including amine fixed-site carrier-containing polymers such as polyallylamine (PAAm),[259] chitosan,[246] and polyethyleneimine (PEI), PVAm has the highest amine content,[260] making it a leading candidate for CO_2 separation applications. Its compatibility with porous PES

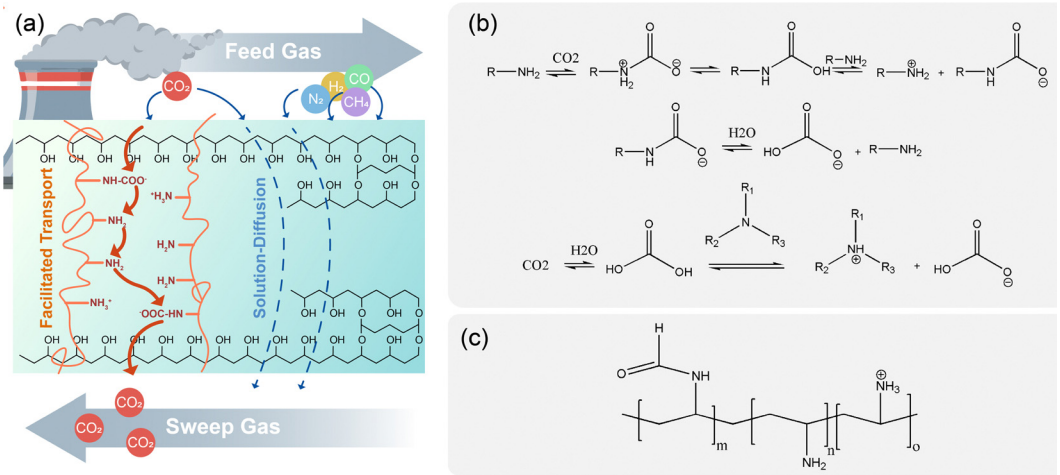

Fig. 15 (a) CO_2 transport through amine-containing facilitated transport membrane,[255] (b) reaction pathways for CO_2 passage through facilitated transport membranes, and (c) chemical structure of PVAm or polyvinyl formamide-*co*-vinylamine (PVNF-*co*-Vam); $m:n:o$ = 85 : 12 : 3 at pH of 11.7[256] (reproduced from ref. 255 and 256 with permission from Elsevier, copyright 2025).

UF sublayers has increased its commercial potential as a composite membrane material.[261,262]

PVAm membranes are typically synthesized using *N*-vinyl formamide (NVF), a water-soluble isomer of acrylamide, in a solution polymerization process that involves free radical polymerization under nitrogen ambient in an aqueous solvent containing reactive initiators like α,α′-azodiisobutyramidine dihydrochloride (AIBA).[209] The resulting poly(*N*-vinylformamide) (PVNF) undergoes a partial acid hydrolysis step using aqueous HCl, followed by a strong base anion-exchange process to adjust the pH to 10. This approach produces PVAm with a molecular weight between 0.8 to 1 kDa. An alternative synthesis method, inverse emulsion polymerization (IEP), offers higher viscosity[263] and better control over the polymerization process. The aqueous monomer solution is distributed in an organic phase throughout the IEP, and the polymerization takes place in multiple dispersed polymer phases encircled by an emulsifier. Instead of the hydrophobic continuous phase, polymerization occurs inside the separated micelles. The reaction system can benefit from facilitated heat and mass movement, and the likelihood of developing gels greatly decreases. A recently less practiced approach for PVAm production is polyacrylamide conversion through the Hoffman reaction.[260] Polyacrylamide is readily available and reasonably priced, making this strategy promising. However, the Hofmann process requires sodium hypochlorite treatment at a high pH, which might cause adverse effects, including chain scission.

Much research has focused on enhancing the molecular weight (MW) of PVAm. Increasing the MW of the casting solution improves the density of the selective layer, reducing the diffusion of non-polar gases while increasing chain mobility for better gas separation performance.[264] An effort toward enhancing the MW of PVAm (from 20 000 to 80 000) was reported to significantly reduce the permeance of CH_4 and increase the CO_2/CH_4 selectivity (10-fold growth).[264] However, maintaining consistent reaction conditions during MW growth is challenging,[264] and alternative methods, such as synthesizing sterically hindered PVAm to favor the bicarbonate pathway, are being explored.[265] Attaching a bulky structure, such as a methyl group, to the amine hinders the carbamate pathway, promoting the chemisorption of CO_2 as bicarbonate. As this requires fewer amine sites, more CO_2 can pass through the membrane with the constant amine functional group content.

Crosslinking substances bearing CO_2-philic carriers to a fixed carrier membrane may improve CO_2 transport, CO_2/N_2 selectivity, and mechanical integrity of the PVAm membranes.[266] Crosslinking introduces hydrogen bonding into the polymer matrix, further enhancing amine carrier effectiveness.[266,267] Several studies have investigated improving the performance of PVAm membranes through the incorporation of mobile amine carriers such as piperazine.[261,268] Piperazine-modified PVAm membranes have outperformed those modified with ethylenediamine (EDA),[266] showing a more than twofold improvement in selectivity. A team from Ohio State University, led by Winston Ho, has further advanced this field by optimizing PSF membranes with PVAm, piperazine, and glycinate carriers.[261] Adding 0.1 wt% polyvinylpyrrolidone (PVP) improved hydrophilicity and pore size, achieving a CO_2 permeance of 843 GPU and a CO_2/N_2 selectivity of 160. However, excessive crosslinking may lead to carrier depletion or polymer matrix densification, negatively affecting membrane performance.[269,270]

A significant portion of PVAm membranes is sourced from commercial aqueous Lupamin solutions or similar products, such as Polymin® VX[271,272] (Fig. 15(c)). In such cases, PVAm is precipitated from the concentrated, viscous solution using ethanol. After separation and drying, the white precipitate is either exposed to another round of dissolution and precipitation or Soxhlet extraction for further purification. A final ion exchange-assisted pH adjustment is performed to transform the functional groups.[273,274] pH adjustment is identified as a crucial step due to the improvement of free amine groups without protonation (elimination of ammonium salts), which eventually improves the CO_2 reactivity of PVAm membranes (discussed and

approved at different pHs by Kim *et al.*[275]). Casting solutions for wet or Petri dish casting, with an approximate concentration of 2 wt% PVAm, are commonly used with mobile amine carriers or inorganic modifiers. Undiluted PVAm membranes derived from commercial solutions often result in fragile, uneven films.[271]

In a recent pilot-scale study conducted in Wilsonville, Alabama, PVAm-based spiral-wound modules were tested on real coal-based flue gas (Fig. 16(a)).[197] The membranes demonstrated a CO_2 permeance of 1450 GPU and a CO_2/N_2 selectivity of 185. The study also examined the effects of feed flow rate, pressure, and temperature, as well as long-term stability under varying CO_2 concentrations and exposure to heavy metal deposition. These findings demonstrate the potential of PVAm membranes for large-scale carbon capture and separation applications.

FTMs face several challenges, particularly in their mechanical characteristics and performance under varying operating conditions. Most FTMs operate at near-zero differential pressure, making it difficult to assess their mechanical integrity under such conditions. Additionally, different processes lead to varying CO_2 concentrations and partial pressures in the exhaust, which can impact the efficiency of the separation process. Lower partial pressures are generally unfavorable because they reduce the driving force for separation. On the other hand, excessively high partial pressures of CO_2 can cause amine carrier saturation, leading to decreased efficiency in CO_2 transport and reduced overall performance.[276]

Flue gas decarbonization using FTMs typically occurs at moderate temperatures. However, if the gas stream is compressed, an inevitable rise in temperature can influence membrane performance. While FTMs can still perform well under such conditions, temperature optimization becomes essential to maintain efficiency. Humidity is another key factor in the performance of FTMs.[256] Competitive sorption between water and nitrogen can hinder N_2 passage and enhance CO_2/N_2 selectivity. Therefore, proper humidity control is crucial to ensure that FTMs operate effectively in gas separation processes, as water vapor content can significantly affect the selectivity and permeance of CO_2.[47]

6.3. Polymers of intrinsic microporosity

PIMs represent a significant class of materials for CO_2 separation, due to their unique combination of high permeability and selectivity derived from their intrinsic microporous structures. PIMs share certain similarities with COFs, as both possess highly porous structures that promote CO_2 removal from gas streams. However, unlike COFs, PIMs do not require a covalent bond network to achieve their microporous architecture.[277] Instead, their high permeability arises from their exceptionally high FFV, resulting from the incorporation of large, rigid, contorted polymer chains that disrupt efficient chain packing. This disruption creates a "ladder-like" structure that contributes to their microporous nature and enhances gas permeability.

The primary polymerization reaction responsible for the formation of PIMs involves double-aromatic nucleophilic substitution, which allows for the simultaneous creation of two covalent bonds, establishing the polymer backbone.[278] This process results in a highly tortuous structure made up of interconnected ring systems that restrict rotational motion along the polymer chain. The restricted rotational mobility prevents macromolecular sections from realigning, thereby maintaining the open, porous nature of the polymer. The bimodal narrow pore distribution within PIMs, typically ranging from 7 to 20 Å, provides selective molecular sieving, which is crucial for CO_2 separation.[279–281] These factors make PIMs highly effective for CO_2 separation, pushing the performance of gas separation membranes beyond the traditional Robeson upper bound, which limits the trade-off between permeability and selectivity (Fig. 17). The enhanced internal molecular free volume (IMFV), as shown in Fig. 18, combined with the ability to finely tune their structure, contributes to the superior gas transport properties of PIMs, making them as a prominent material for CO_2 separation.

In FTMs, high pressures lead to 'carrier saturation,' where the ability of CO_2 carriers to facilitate gas transport diminishes due to the overwhelming influx of CO_2. As a result, the transport mechanism shifts from facilitated transport to solution diffusion, reducing efficiency. Furthermore, high pressures

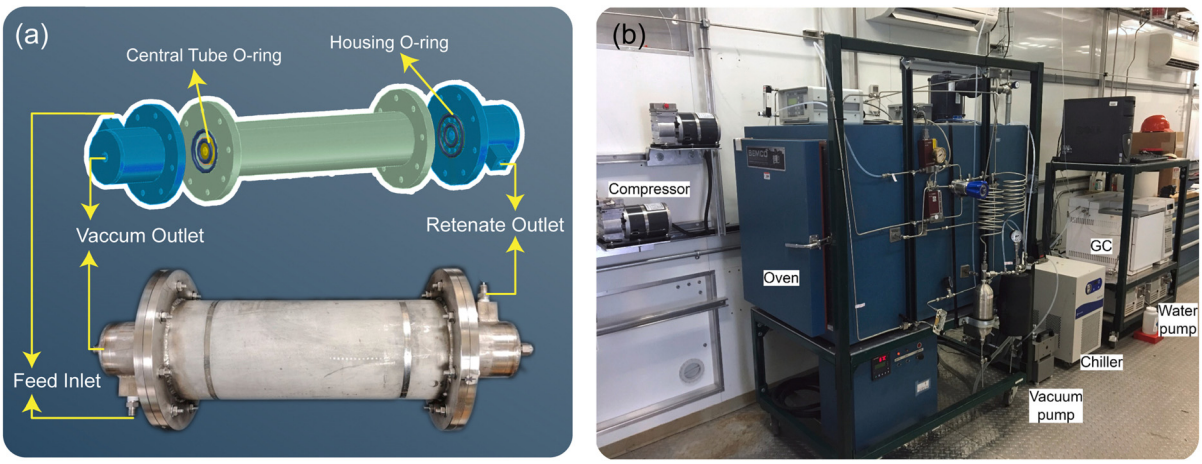

Fig. 16 Spiral wound module test rig for facilitated transport membrane assisted decarbonization; (a) schematic of the module's housing, (b) test setup (reproduced from ref. 197 with permission from Elsevier, copyright 2025).

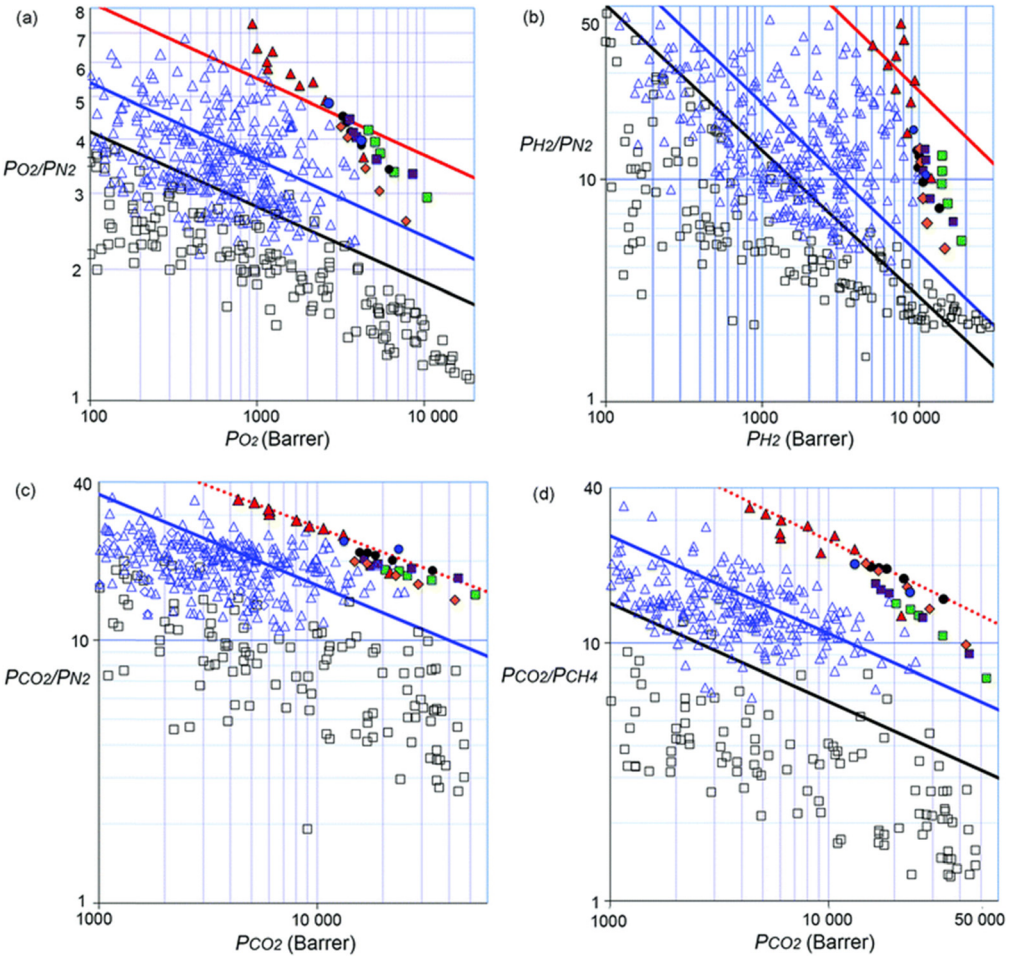

Fig. 17 Selectivity-permeability log–log plots for (b) H_2/N_2, (a) O_2/N_2, (c) CO_2/N_2, and (d) CO_2/CH_4 and their evolution through time by different membrane materials introduction to the market; solid black lines (1991), solid blue lines (2008), and red dot lines (2015) upper bounds (reproduced through RCS open access policy from ref. 282).

compress swollen membranes, leading to water loss, reduced polymer flexibility, and decreased free volume for gas diffusion. This issue is further exacerbated by the fact that, at high pressures, water vapor permeates more readily than CO_2, reducing the water vapor content essential for FTM function and leading to lower permeance and selectivity. Despite these advancements, PIMs face several limitations. One major drawback is their susceptibility to physical aging, where the polymer structure collapses over time, reducing its gas transport efficiency.[284] Additionally, PIMs exhibit moderate selectivity compared to other advanced gas separation materials. Their chemical stability, while superior to some other high-FFV polymers such as poly(trimethylsilyl propyne), still presents a challenge, particularly under harsh industrial conditions. Efforts are ongoing to enhance the chemical robustness of PIMs through copolymerization and blending with more stable materials to mitigate aging and improve their long-term performance.

6.4. Biomaterial-modified membranes for decarbonization

The polymeric membranes used for CO_2 separation are primarily made of synthetic materials. The growing interest in synthesizing biodegradable and sustainable membranes has spurred researchers to investigate the potential of renewable and biodegradable polymers as alternatives in membrane production. Due to their biocompatibility, biodegradability, and environmental sustainability, biopolymers are considered viable alternatives to conventional fossil-based/synthetic polymers for developing CO_2 membranes. Below, we explore key biopolymers utilized in membrane fabrication for CO_2 separation and capture.

6.4.1. Cellulose and its derivatives. Cellulose, the most abundant biopolymer on Earth, has long been suggested for gas separation due to its renewable nature.[285] Cellulose is a homopolysaccharide composed of β (1 → 4) linked D-glucose units. The equatorial orientation of the D-glucose substituents gives the cellulose polymer a flat, planar structure, allowing for rotation around the glycosidic bond, which keeps the polymer linear. Interactions between these polymers occur through inter-chain hydrogen bonds within the plane and van der Waals interactions out of the plane.[286,287] Cellulose has a high surface area, ample storage sites, and sustainability as a carbon capture material, with its hydroxyl groups serving as adsorption sites

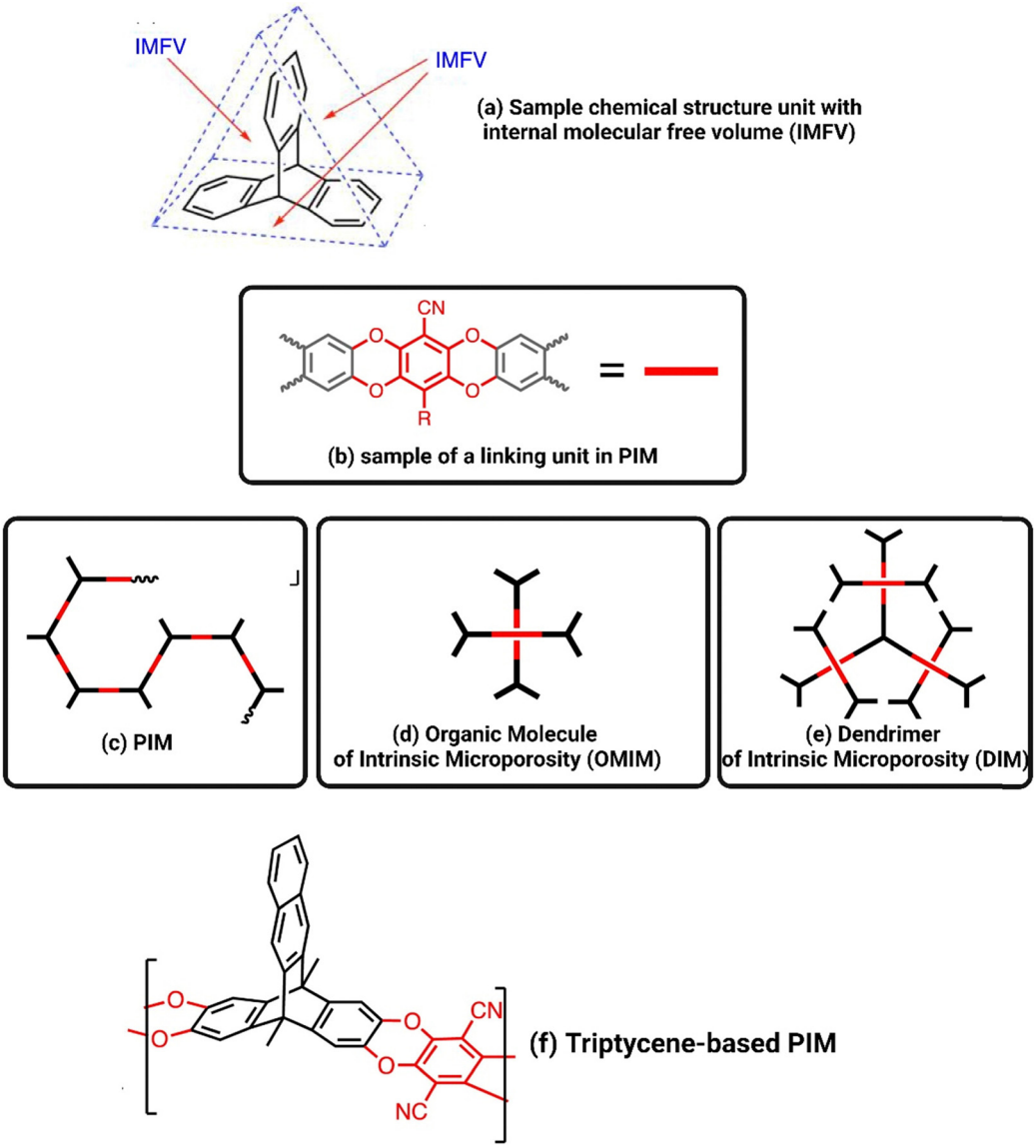

Fig. 18 Polymer of intrinsic microporosity (PIM); (a) sample structure with internal molecular free volume (IMFV), (b) chemical structure of a linker in a PIM, (c) PIM, (d) organic molecule of intrinsic microporosity (OMIM), (e) dendrimer of intrinsic microporosity (DIM), and (f) chemical structure of Triptycene PIM (reproduced from ref. 283 with permission from Elsevier, copyright 2025).

for CO_2, enhancing capture efficiency. To further optimize its performance, cellulose can be chemically modified or derivatized to improve adsorption, separation, and conversion properties.[288] Derivatives like ethyl cellulose, methylcellulose, and cellulose acetate have been used as membrane additives to enhance properties such as permeability, porosity, hydrophilicity, and fouling resistance. For instance, incorporating methylcellulose into NaA zeolite membranes has reduced crystal size and improved substrate membrane defect repairs.[289]

Cellulose acetate (CA), the most well-known derivative of cellulose, is produced by the acetylation of cellulose hydroxyl groups.[290] It is widely used in membrane production due to its good solubility in a range of organic solvents and its ability to form membranes with controlled pore structures. The hydroxyl groups within CA are readily available for various modifications, including oxidation, etherification, hydrolysis, esterification, grafting, crosslinking, and copolymerization.[291] CA membranes exhibit properties such as uniform pore structure, natural hydrophilicity, thermal stability, and suitability for gas separation, such as CO_2 and CH_4.[292] The degree of acetylation is a key factor affecting the gas separation efficiency of CA membranes. CA is partially crystalline and exhibits different substitution levels (DS = 1–3), indicating the extent to which hydroxyl (–OH) groups per repeating cellulose unit are acetylated. Based on the DS values, CAs display CO_2 permeability ranging from 1.8 to 6.6 Barrer at 35 °C.[293] The CO_2 gas permeability of membranes can be improved by employing cellulose acetate with higher DS without severe change in the gas selectivity because of the less internal hydrogen bonding among cellulose chains, providing a more porous structure.[294] Studies evaluating the influence of

the degree of acetylation (1.75–2.84) on the gas separation properties of cellulose acetate indicate that the gas permeability coefficient increases with a higher degree of acetylation.[295] However, limited CO_2 permeability poses a challenge when using CA as a membrane material in applications involving CO_2-containing streams. Nikolaeva *et al.* improved CA separation efficiency by integrating ionic liquid-like functionalities, namely 1-methylimidazole, 1-methyl pyrrolidine, and 2-hydroxyethyl dimethylamine (HEDMA), onto the CA structure.[296] Experimental evaluation of CO_2/N_2 mixed-gas permeation demonstrated a reduction in both CO_2 and N_2 permeability, with an initial decline in CO_2/N_2 selectivity followed by a gradual increase as the HEDMA content increased. CA membranes face drawbacks such as structural compression under high pressure, narrow pH tolerance (4.5–7.5), and temperature limits (up to 30 °C).[297,298] To optimize CA membranes, various solvents and additives are used during preparation, including *N*-methyl pyrrolidone, *N*,*N*-dimethylacetamide, and mixed solvents like *N*,*N*-dimethylformamide with acetone or 2-propanol.[299,300]

Among cellulose products, nanocellulose stands out for its exceptional surface area and mechanical properties, which make it highly effective in carbon capture.[301,302] Nanocellulose is classified into cellulose nanocrystals (CNC), cellulose nanofibers (CNF), and bacterial cellulose (BC). CNF is typically produced through a two-step process involving chemical or enzymatic pre-treatment followed by mechanical processing. This pre-treatment step not only enhances processability and uniform size distribution but also allows for tailoring the properties of the nanocelluloses for different gas separation applications, such as introducing CO_2 reactive groups. CNC and CNF exhibit differences in length and crystallinity, with CNC being predominantly crystalline and CNF often described as having amorphous regions with crystalline segments. CNC offers advantages such as uniform size with nanometric dimensions in both length and width. TEMPO-mediated oxidation is a key reaction for nanocellulose synthesis, where cellulose is converted into polyglucuronic acid due to the oxidation of C6 alcohol groups in the anhydroglucose unit.[303] CNFs with higher aspect ratios (5–50 nm diameter and several micrometers in length) and entangled networks are utilized as reinforcement agents or viscosity controllers in papermaking and polymer composites.[304] In contrast, CNCs, due to their higher crystallinity and shorter length (< 100 nm), represent better dispersibility, improving the *strain* at *failure* of *composites*.[305,306] A PVAm/nanocellulose hybrid membrane was developed for carbon capture applications.[271] The developed films with nanocellulose (30–70%) were analyzed through water vapor sorption experiments and humid gas permeation tests. Improvements in gas permeability and selectivity were achieved by increasing water vapor and the PVAm content in the films. The highest selectivity (135 for CO_2/CH_4 and 218 for CO_2/N_2 separation) was observed in blends containing nanofibrillated cellulose (CNF) with 70 wt% PVAm at 60% RH, while the maximum permeability of approximately 187 Barrer was achieved at 80% RH. Modifying CNFs with amine and aminosilane is a practical strategy to increase their CO_2 sorption capabilities. Chemical bonding of the aminosilanols from an aminosilane with cellulose hydroxyl groups occurs during the aminosilane functionalization of cellulose. In addition, the simultaneous self-attachment of amino silanols, due to an undesired side reaction, leads to the formation of siloxane bridges (Si–O–Si).[307] Regarding amino silane modification of CNFs, ethanol-water suspension, and toluene are two of the most common media used for cellulose modifications. *N*-(2-aminoethyl)-3 aminopropyl methyl dimethoxysilane (APMDS) is mainly attached to hydroxyl groups of C6 position in nanocellulose structure because of space structure of atoms in cellulose molecule during chemical modification of cellulose nanofibers for CO_2 adsorption. Amine loading of the modified CNF aerogels by APMDS is affected by the process parameters, such as the reaction time, the reaction temperature, silane proportion, and the kind of solvents. Tertiary butanol has been recommended as a highly efficient solvent, resulting in an amine loading of 9.02 mmol g^{-1} with 6% APMDS.[307]

6.4.2. Polyvinyl alcohol. PVA, a water-soluble synthetic polymer with a backbone composed only of carbon atoms, is biodegradable under both aerobic and anaerobic conditions. Due to its oxygen barrier, thermal stability, and CO_2 sorption properties, PVA is used as a host polymer, while additives such as nanocellulose materials are used to further improve their CO_2 permeance, selectivity, and mechanical strength. For example, the effectiveness of different nanocelluloses—including cellulose nanocrystals (CNCs), TEMPO-oxidized cellulose nanofibrils, and phosphorylated cellulose nanofibrils—as additives in PVA composite membranes was explored.[308] The findings indicate that PVA/CNC nanocomposites exhibit a higher CO_2/N_2 separation factor (39) and CO_2 permeance (127.8 GPU) than pristine PVA membranes, which have a separation factor of 36 and a permeance of 105.5 GPU. The membranes resulted from the PVA/CNC nanocomposite demonstrate performance comparable to that of membranes composed of PVA and carbon nanotube (CNT) while offering the added benefits of CNCs' non-toxicity and biodegradability. Although phosphorylated and TEMPO-oxidized nanofibrils enhance membrane performance, their effect is less pronounced than that of CNCs. Charging is used to enhance carbon nanofiber (CNF) dispersion in membranes, improving both permeance and selectivity. Phosphorylated-charged CNFs demonstrate superior permeance and selectivity compared to highly and low-charged CNFs. However, CNCs exhibit better dispersibility than all charged CNFs.[309]

Increasing the gas feed pressure reduces both the permeance and selectivity of the membranes. This is attributed to the stacking of polymer chains, which leads to membrane densification at higher pressures and restricts gas permeation. This effect becomes more pronounced at extremely high pressures, leading to membrane ''plasticization,'' where the polymer structure is permanently altered due to CO_2 swelling in the spaces between polymer chains. Plasticization can cause a loss of membrane performance as gas transport pathways become obstructed. Several strategies have been explored to mitigate high-pressure plasticization and membrane compaction, including crosslinking membranes and reinforcing polymers with inorganic or organic nanofillers to enhance mechanical strength.[309] To address these issues, maintaining high water

vapor content in the feed gas is essential for preventing membrane drying in high-pressure applications. Combining NC with hydrophilic polymers has been suggested to enhance permeance significantly. For instance, in membranes combining CNF and PVAm, permeability increased over 200-fold, with relative humidity (RH) levels up to 85%. Selectivity also improved by up to 65% RH but declined at higher RH levels due to excessive water activity, which caused membrane swelling. Optimization studies recommend a membrane composition of 70% PVAm and 30% CNF, achieving maximum permeance and selectivity at 85% RH in NC-based FTMs.[271,309]

6.4.3. Chitosan. Chitosan (CS) is a biopolymer derived from the deacetylation of chitin, a plentiful natural polysaccharide found in the outer shells of crustaceans. CS exhibits excellent stability, antibacterial properties, chelating abilities, and hydrophilicity. Additionally, it dissolves in water under acidic conditions and is biocompatible, biodegradable, and non-toxic. CS is a linear polysaccharide obtained by removing the acetyl functional group and liberating the amino groups from the backbone chain. It consists of *N*-acetyl-D-glucosamine and D-glucosamine units bonded by β-(1–4)-glycosidic bonds.[310] Nitrogen-rich chitosan is an excellent precursor for heteroatom-doped porous carbon, which finds application as a CO_2 adsorbent. This suitability stems from the presence of naturally occurring free amine groups within the D-glucosamine structure, enabling binding with weakly acidic CO_2. Although pristine chitosan demonstrates minimal CO_2 adsorption capacity (0.47 mmol g^{-1}), various chitosan-based composites—such as chitosan/SiO_2 nanoparticles (4.39 mmol g^{-1}), chitosan/zeolite (1.7 mmol g^{-1}), and chitosan/GO aerogel (4.15 mmol g^{-1})—exhibit enhanced adsorption capabilities. Ideally, a commercial membrane should have a CO_2/N_2 selectivity exceeding 100. However, pristine chitosan membranes typically display a CO_2 permeance of around 12.5 GPU and a CO_2/N_2 selectivity of approximately 54, falling short of making the technology competitive.[310] A promising approach for substantial improvement is introducing carriers into the membrane matrix, either by blending them with polymers to form the active layer or by impregnating them into the gutter layer. Generally, water-swollen CS exhibits significantly higher CO_2 separation performance compared to dry CS. Blending amine carriers enhances both CO_2 permeance and CO_2/N_2 selectivity. Composite membranes have been created by combining chitosan with amines, such as TEPA and PAA, forming a skin, selective layer over a porous support. TEPA, a small molecule amine, acts as a mobile carrier, while PAA serves as a fixed carrier. The TEPA-blended membrane shows a two-fold increase in CO_2 permeance (approximately 24 GPU) and a 1.5-fold enhancement in CO_2/N_2 selectivity (around 80) compared to the pristine CS membrane. Similarly, the chitosan/PAA membrane exhibits a three-fold increase in CO_2 permeance compared to the CS membrane.

6.4.4. Polylactic acid. Polylactic acid (PLA), the most extensively utilized biodegradable plastic, stands out as an intriguing biopolymer for membrane fabrication due to its flexibility in fabrication by phase inversion, electrospinning, and other common methods. Derived from renewable sources, PLA is highly sustainable and boasts attributes such as clarity, ease of manufacture, high tensile strength, biocompatibility, and non-toxicity. PLA has excellent processability, water resistance, solubility in various organic solvents, a melting point between 170 and 180 °C, and a glass transition temperature (T_g) ranging from 50 to 65 °C, depending on its crystallinity and structure.[311] However, a significant drawback is PLA's susceptibility to degradation *via* hydrolysis in the presence of water, bacteria, or UV sources. The incorporation of green plasticizers like oligomer of the lactic acid (OLA) and phenylphosphonic bis(2-aminobenzothiazole) (PBO) enhanced the ductility of PLA membranes, producing homogenous membranes suitable for gas separation applications. In recent years, PLA membranes have been investigated for gas separation applications, with promising results. For instance, PLA was used to develop biopolymer membranes through phase inversion techniques for purifying gaseous streams abundant in CO_2 and CH_4.[312] The resulting PLA membranes demonstrated high CO_2/CH_4 selectivity (220–230) and CO_2 permeability of approximately 11 Barrer at room temperature. The solubility, diffusivity, and permeability of gases decrease, along with increasing the crystallinity of a PLA membrane.[292] Therefore, PLA membranes with low crystallinity exhibit greater permeability compared to their more crystalline counterparts.

6.5. Mixed matrix membranes

The performance of polymeric membranes are inherently constrained by their permeability-selectivity trade-off, commonly represented by the Robeson upper bound. Strategies have been proposed to improve gas solubility—by creating chemical interactions between gas molecules and polymer chains—and increase gas diffusivity—primarily by enhancing the polymer's void fraction while minimizing the formation of non-selective voids.[313] These studies have resulted in the fabrication of MMMs that incorporate inorganic fillers into the polymeric matrices, simultaneously enhancing permeance and selectivity and thus lowering operating pressure, energy consumption, and the overall footprint of separation processes.

Embedding inorganic fillers facilitates the preferential transport of target gas molecules while obstructing the pathways of other molecules, thereby improving separation performance. An inorganic filler that is well-dispersed within a polymeric phase can substantially modify the FFV due to changes in the conformation, dynamics, or packing of polymer chains. This modification can effectively discriminate between smaller gas molecules and larger ones, leading to enhanced gas selectivity, such as H_2/CO_2.[314] Moreover, the interfacial interactions between inorganic fillers and polymer chains play a crucial role in directing the transport pathways of gas molecules, thereby enhancing selective transport and improving gas permeabilities.[315,316] Additionally, nanofillers in MMMs help prevent membrane plasticization by acting as crosslinking agents. Examples of these modifiers include CNT, GO, cellulose nanofibers (CNF), cellulose nanocrystals (CNC), MOFs, COFs, layered double hydroxides (LDHs), transition metal dichalcogenides (TMDs), and MXenes. Although these fillers have the potential to enhance both permeability and selectivity, the

extent of these improvements depends on several key factors. Simply blending non-homogeneous phases does not always guarantee optimal membrane performance.

While MMMs are promising, they have several challenges that must be addressed. These challenges include inconsistencies at the phase interfaces, uneven distribution of fillers, and reduced stability compared to homogeneous systems.[236] Larger fillers are prone to agglomeration, forming clusters that disrupt the membrane's homogeneity. As a result, the mechanical strength of the membrane deteriorates, leading to undesirable performance under high pressure. Thus, a modifier/filler should remain in the nanometric size range at its highest loading and should allow for controlling size distribution and preventing aggregation. Moreover, the interaction between the surface of nanomaterials and polymers plays a critical role in maintaining the membrane's mechanical integrity, requiring careful optimization. Fig. 19 depicts perfect and imperfect interactions (*e.g.*, polymer rigidification, pore blockage, and interfacial defect) along with their possible impact on the selectivity-permeability trade-off, where losses in permeability and selectivity may occur depending on the nature of the filler and the polymer matrix.[317]

One major strategy to enhance nanomaterial-polymer interfacial compatibility is surface functionalization of the nanofiller using CO_2-philic moieties (NH_2, OH, COOH, and SO_3), attaching polymeric chains, or connecting it with other nanomaterials. Modifications on the polymer backbone also promote electrostatic and hydrogen bonding interactions, improving compatibility.[318] Drying and redispersion of nanomaterials induce agglomeration to reduce surface energy. To resolve the challenges of aggregation, multistep nanomaterial synthesis and size control, as well as one-

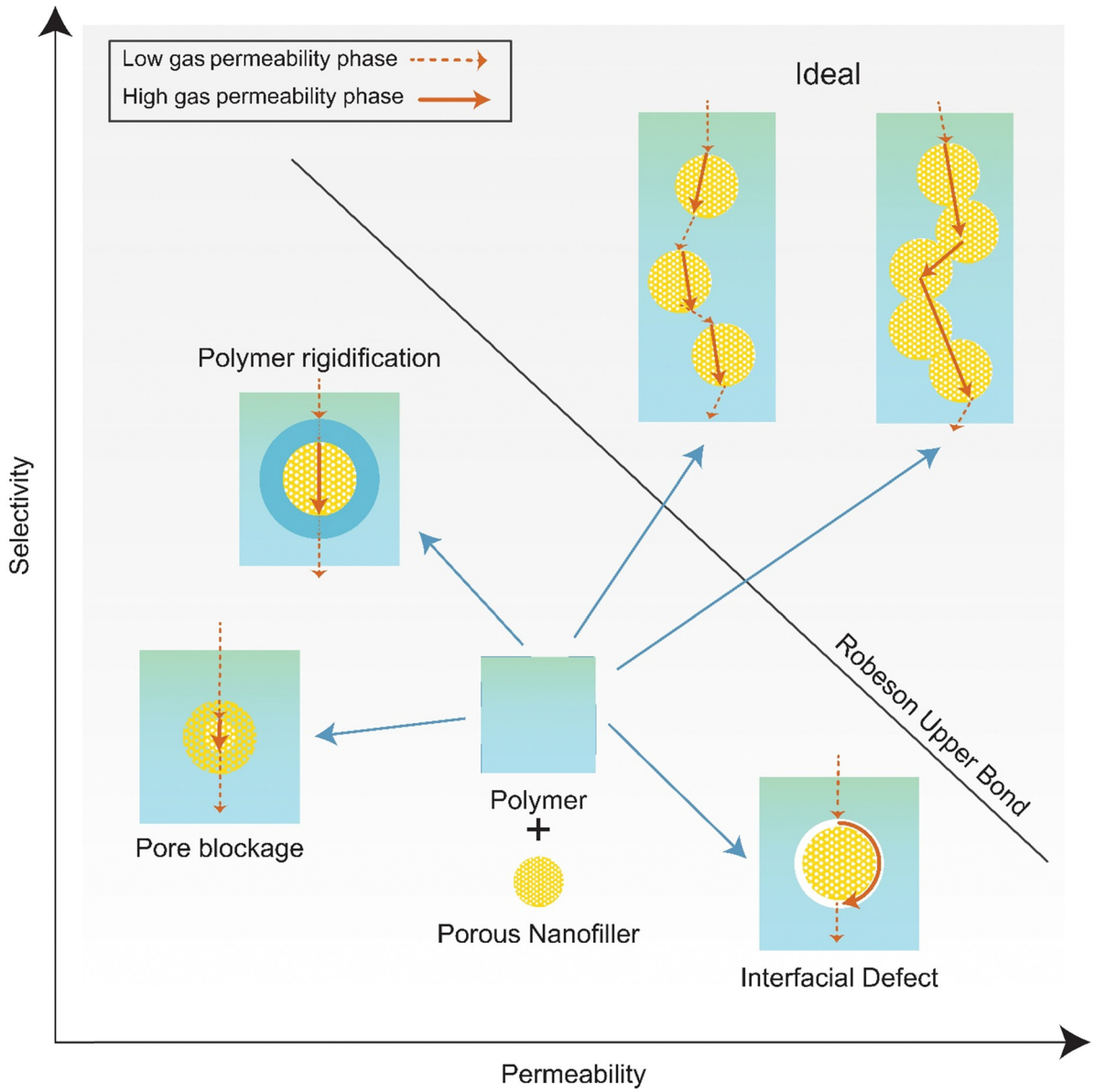

Fig. 19 Various nanomaterial-polymer interactions and their related consequences (reproduced through RSC open access policy from ref. 317).

pot *in situ* growth, have been suggested. Synthesizing nanomaterials using polymer chains as a scaffold limits size growth, promoting a high load of evenly distributed nanosized fillers throughout the membrane.[319] However, selecting the right solvents for *in situ* growth is crucial, as they must be compatible with both the nanomaterial synthesis procedure and membrane fabrication. Another approach to reducing agglomeration is using wet nanomaterials, which excludes the drying step by exchanging the solvent in which the polymers will be dissolved.[320]

Nanostructured fillers, when properly applied, can significantly improve various membrane properties. Key factors include particle size, porosity, even distribution, and their affinity for CO_2 molecules—often called "CO_2-philicity." Correct particle sizing is crucial to avoid clustering, which could result in a non-selective, heterogeneous top layer. Moreover, the interaction between the surface of nanomaterials and polymers plays a critical role in maintaining the membrane's mechanical integrity, requiring careful optimization.

A major challenge in MMM fabrication is the compatibility of nanofillers with the polymer matrix and solvents. Poor dispersion of nanofillers can lead to phase separation, uneven film formation, and defects that degrade membrane performance. Inhomogeneities in thermal behavior and elastic modulus between the phases may also cause mechanical delamination.[321] Proper solvent selection during synthesis and fabrication is essential to maintain the chemical stability of nanomaterials and prevent phase inversion. Controlling the nanomaterial load and adjusting the viscosity of the polymer solution can mitigate phase separation and improve nanofiller distribution.

The porosity and functional groups of the fillers can further enhance both the performance and mechanical stability of the membrane. Non-porous fillers increase diffusion-path tortuosity, which typically reduces permeability. However, the presence of functional sites can enable selective diffusion, potentially enhancing effective permeability for targeted species. In contrast, porous fillers act as molecular sieves, facilitating gas transport based on kinetic size and shape. The connectivity of the filler network also plays a crucial role in optimizing gas diffusion pathways, significantly improving membrane performance. A schematic illustration of filler impact on gas transport in MMMs is shown in Fig. 20.

Several inorganic modifiers have so far been introduced to polymeric membranes with impermeable, surface-functionalized nanomaterials, porous, and non-3D (one, 2D) enhancers. Examples of these modifiers include CNT, GO, cellulose nanofibers (CNF), cellulose nanocrystals (CNC), MOFs, COFs, layered double hydroxides (LDHs), transition metal dichalcogenides (TMDs), and MXenes. Among these, MOFs and MXenes have gained particular attention due to their high surface area, tunable pore structures, and unique chemical functionalities, which enhance molecular selectivity and improve separation performance in polymeric membranes. MOFs represent a unique class of porous nanostructured compounds that have gained prominence as alternatives to conventional inorganic microporous materials like zeolites. MOFs consist of a metal core and an organic linker (ligand), and their hybrid organic/inorganic composition provides high surface area and tunable pore sizes, making them suitable for diverse

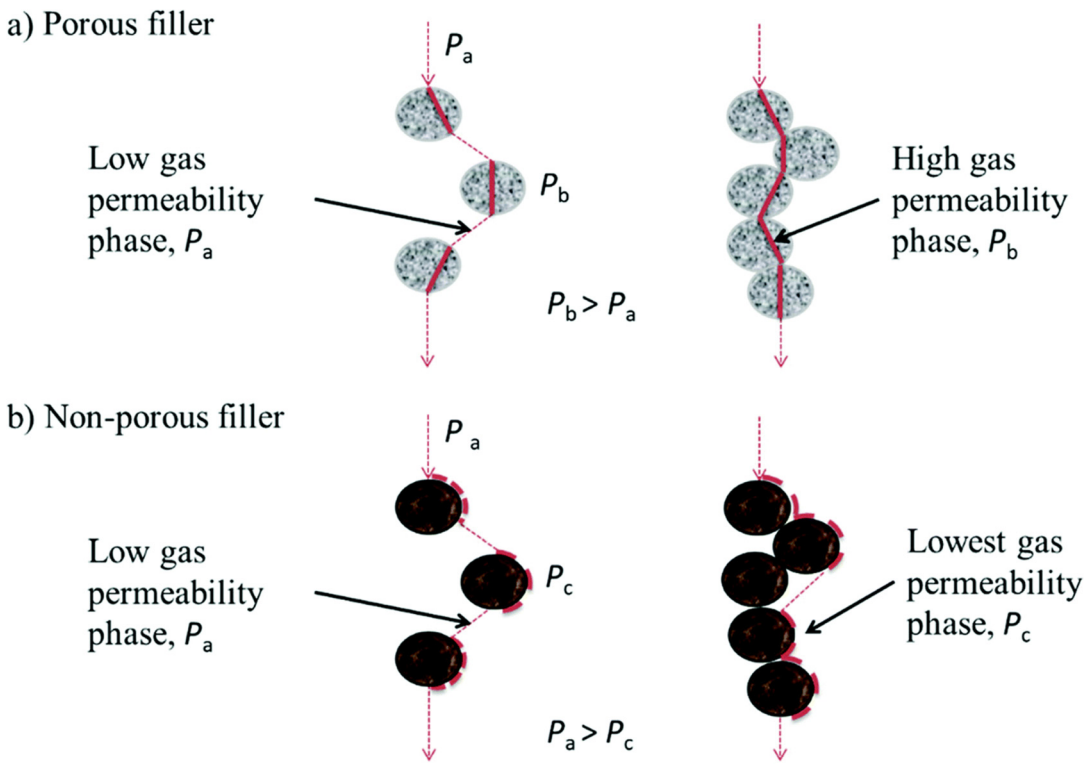

Fig. 20 Gas diffusion in mixed-matrix membranes with (a) porous and (b) non-porous fillers (reproduced from ref. 280 with permission from RCS, copyright 2025).

separation applications.[322–326] A key advantage of MOFs is their highly customizable molecular structure, allowing for precise control by selecting specific metal cores and organic ligands. Stabilized by chemical bonds, these metal centers resemble those found in metal oxide nanoparticles (NPs). The bonds within the MOF structure are strong enough to ensure material robustness while maintaining the activity of the metal centers.[327] The active metal sites in MOFs are uniformly distributed throughout the entire structure, enhancing their affinity for CO_2 molecules if properly selected. Additionally, the organic ligands used in MOFs often carry polar functional groups like $-NH_2$ or $-SO_3$, which synergistically improve CO_2 adsorption and increase the dispersion of the MOF within polymer matrices compared to inorganic NPs.

In recent years, continuous advancements in MOF-based MMMs have been driven by the development of new organic linkers paired with different metals to improve decarbonization performance.[328] These newly designed ligands not only protect the metal core from nucleophilic attacks but also support the stability and functionality of the framework. The chemistry behind MOF synthesis is crucial, as factors such as pore volume, aperture size, particle size, and filler distribution all influence the membrane's CO_2 separation performance. Specifically, the aperture size determines molecular sieving capabilities, while other properties, such as pore shape and size, impact the overall separation efficiency.

Despite significant progress, several challenges remain in the commercialization of MOFs. Only MOFs with effective heat and mass transfer properties, such as Universitetet i Oslo (UiO)-66, are suitable for continuous flow reaction production.[329] One key consideration for researchers is the development of environmentally friendly synthesis methods that use green solvents and moderate processing conditions.[330] However, achieving repeatability in MOF synthesis remains difficult, particularly under intense operational conditions. These challenges can lead to poor dispersity, low reactivity, and hindered mass transfer, resulting in issues like undesired size distribution, material collapse, aggregation, and pulverization of MOFs.[329]

Although MOFs can potentially achieve satisfactory separation performance, their tendency to agglomerate and form non-selective voids restricts their full potential for gas separation. One practical method to overcome agglomeration is immobilizing or decorating MOFs on larger support structures, creating MOF-based templates. This hybridization significantly reduces surface energy and the tendency to agglomerate, forming a more stable structure for MOF deposition and growth. Such templates enhance the composite's multifunctional features, including increased adsorption capacity, enhanced porosity, improved permeability, and greater mechanical strength than standalone MOFs. Promising materials for MOF nucleation and growth include CNTs,[331] GO,[332,333] reduced GO (rGO),[334] CNCs,[335] and halloysite nanotubes (HNT).[336] The synergy between the MOFs and these support materials offers significant performance improvements by combining adsorption and molecular sieving capabilities.

Furthermore, achieving homogeneous dispersion within the matrix remains a challenge. Synthesizing fillers with well-defined physical and chemical properties and leveraging their synergistic effects with 2D fillers holds promise. Carbon-based nanomaterials such as CNTs and GO have gained significant attention as promising membrane materials.[337] However, their separation performance is heavily influenced by the degree of dispersion and chemical modifications. Functionalizing the surface of these carbon-based nanomaterials enhances their overall performance, leading to improved separation and durability in membrane applications.

Generally, GO exhibits a higher tendency for dispersion and is easier to functionalize compared to CNTs, primarily due to the presence of multiple functional groups on its surface. GO, an allotrope of carbon, consists of sp^2-bonded carbon atoms arranged in a hexagonal honeycomb lattice.[338] It forms 2D nanosheets with a high specific surface area and an atomically thin laminar structure, presenting a new class of highly permeable and selective nanomaterials for membrane-based separations.[339,340] The physicochemical properties of GO nanosheets, such as morphology, size distribution, density of oxygen-containing functional groups, electronic mobility, and carbon radicals, significantly influence their potential for further modifications. Several oxygen-containing functional groups exist on GO, including hydroxyl and epoxide groups on the basal plane, and carboxylate groups primarily at the edges.[341,342] The presence of both ionic groups and aromatic sp2 species enables GO to serve as a nucleation site for metal cations and further growth when organic linkers interact. Metal cations deposit on GO nanosheets through π–π interactions, hydrogen bonding, and Ag–O coordination.[343,344] Due to these superior characteristics, GO is a promising template for developing MOFs-based hybrids. The use of GO-based hybrids in developing efficient MMMs for CO_2 separation has been regarded as one of the promising solutions. By decorating MOFs on GO, it is possible to control the interlayer structure, improving permeability and separation performance due to the molecular sieving properties of the hybrid material.[334]

For example, different types of MOF nanosheets (such as ZIF-7, ZIF-8, CuBTC, and MIL-100) have been systematically integrated into the interlayers of reduced GO (rGO), benefiting from its polar oxygen groups, increased interlayer spacing, and high electronegativity.[334] These properties facilitated strong anchoring of rGO and created a porous structure with uniform nanochannels, enhancing separation performance. In one study, ZIF-8@GO hybrids incorporated into a Pebax matrix improved CO_2 separation by increasing both CO_2 permeability (191%) and CO_2/N_2 selectivity (174%).[333] Two main functions enhanced membrane performance: (i) the high-aspect ratio of GO nanosheets augmented the tortuous path length for gas diffusion within the polymer matrix, thereby limiting the diffusion of larger molecules while facilitating the passage of smaller ones, which improved diffusivity selectivity; and (ii) the intrinsic high permeability and ultra-microporosity of similarly, ZIF-8/GO hybrid composites incorporated into a polysulfone (PSF) matrix achieved a 7-fold increase in CO_2/CH_4 selectivity and an 87% increase in CO_2 permeability compared to pristine membranes.[332] Additionally, bimetallic ZIFs with different Co/Zn ratios were incorporated into the Pebax matrix, leading to a significant 250.37% enhancement in selectivity, surpassing the

Robeson upper bound, due to finely tuned pores of the bimetallic Co60Zn40ZIF hybrid.[345]

CNTs have also attracted considerable research attention across various fields due to their unique structural, electronic, thermal, chemical, and mechanical properties, all of which can improve permeability, selectivity, and long-term stability.[346,347] However, challenges remain in dispersing CNTs uniformly within the polymer matrix and eliminating interfacial defects, which can hinder the development of CNT-based MMMs with high gas selectivity.

To address these challenges, hybridizing CNTs with MOFs by growing MOFs on the surface of CNTs has been explored. For instance, NH2-MIL-101(Al) was deposited on CNT surfaces to introduce polar amino groups, improving interfacial adhesion. Polyimide-based MMMs incorporating MOF/CNT hybrids showed improved CO_2 permeability and CO_2/CH_4 selectivity, surpassing the Robeson upper bound.[331] Fig. 21 shows SEM images of MOF particle growth on the outer surfaces of CNTs, with particle sizes around 50 nm. It also illustrates the separation performance of MOF/CNT MMMs compared to previously reported MMMs for the CO_2/CH_4 gas pair relative to the Robeson trade-off line and a schematic of MOF/CNT composite dispersion within 6FDA-durene polyimide. This strategy of growing MOFs on CNTs was also applied to decorate UiO-66 on halloysite nanotubes (UiO-66@HNT), which enhanced the CO_2/N_2 separation performance of Pebax-1657 MMMs due to the fast transport pathways for CO_2 diffusion provided by the HNT lumen and the CO_2 affinity of UiO-66. This also conferred good long-term stability and excellent interfacial compatibility with the MMMs.[336]

Another class of 2D nanomaterials for membrane-assisted decarbonization is crystalline COF, a porous structure formed by covalent bonds between light elements (carbon, hydrogen, nitrogen, oxygen, *etc.*). COFs possess a high surface area, tunable pore sizes, and excellent structural stability due to their covalent bonds, offering an advantage over MOFs, which rely on coordination bonds between metal clusters and ligands. Recent reviews on COF-based membrane gas separation highlight their potential for flue gas decarbonization.[348] Notable examples include a PVAm-functionalized COF-based MMM

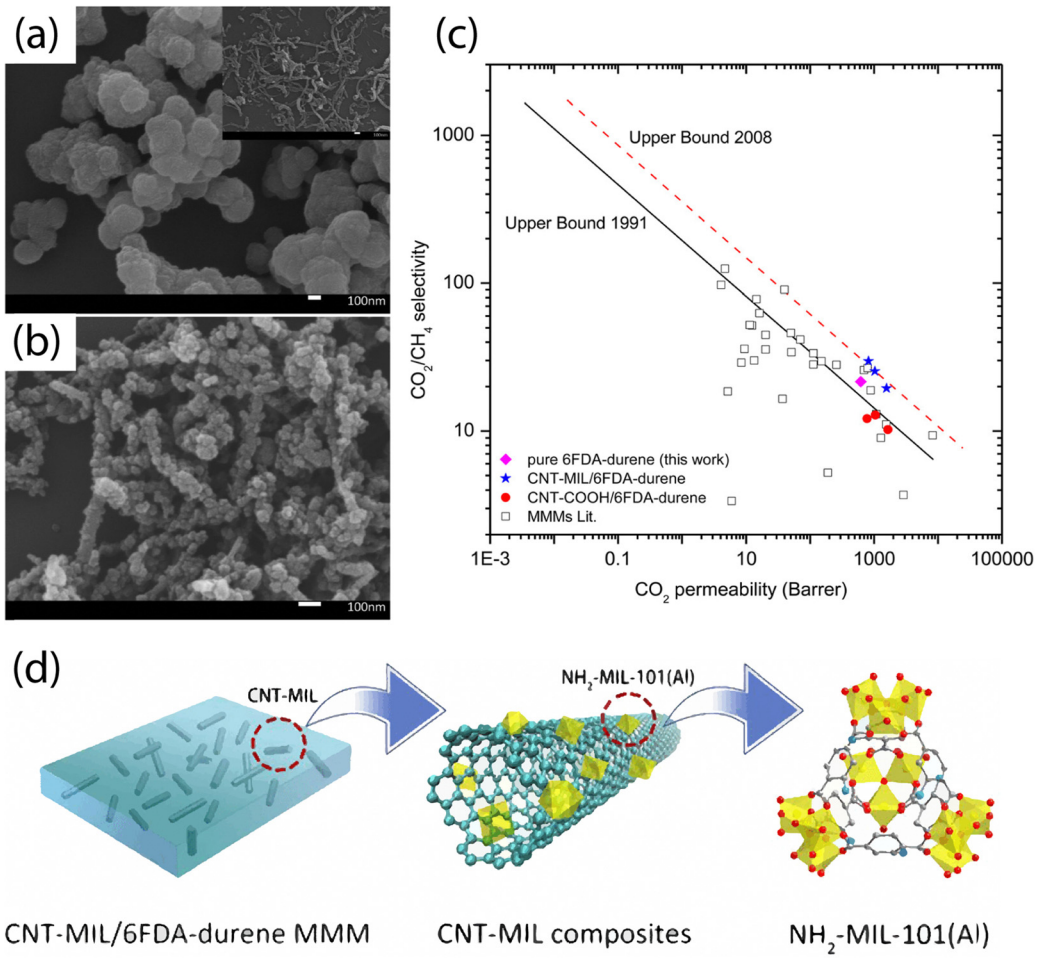

Fig. 21 SEM images of (a) NH_2-MIL-101(Al), with CNT-COOH (inset), and (b) CNT-MIL composite. (c) Gas separation performance of the CNT-MIL MMMs for the CO_2/CH_4 pair with respect to Robeson trade-off line in comparison with single MOF- or CNT-based MMMs reported in the literature. (d) Schematic of 6FDA-durene MMM containing NH_2-MIL-101(Al)-decorated CNTs (Al, yellow; C, gray; O, red; and N, blue) (reproduced from ref. 331 with permission from Elsevier, copyright 2025).

with a permeability of 1738 Barrer and a CO_2/N_2 selectivity of 89[349] and a COF-5-based Pebax 1657 membrane synthesized from 4-benzene boronic acid and 2,3,6,7,10,11-hexahydroxytriphenylene, achieving permeability of 493 Barrer and CO_2/N_2 selectivity of 49.3.[350] Bilayer membranes having imine- and azine-based COF have recently been reported to have superior performance due to the interlaced pore network.[351] Merging the capabilities of the two engineered materials has led to a hybrid membrane with MOF grown on the COF layer.[352] For example, MMMs were fabricated through attaching UiO-66-NH_2 to TpPa-1 COF[353] (Fig. 22(a)). However, permeability values of these MMMs were not as high compared to other studies, as this hybrid was incorporated into a polysulfone (PSF) membrane rather than a more selective layer. A recent innovation introduced the concept of MOF-in-COF, where MOFs are grown as strings through the 1D channels of COFs, addressing the trade-off concerns typical in conventional membranes[354,355] (Fig. 22(b)). The molecular sieving effect of these MOF-in-COF membranes has been particularly effective for hydrogen (H_2) purification from gas mixtures. For instance, a membrane designed for biogas green hydrogen purification (H_2/CO_2) achieved a separation efficiency of 34.9. Although this selectivity may seem modest compared to flue gas decarbonization membranes, it is important to recognize that this process involves extracting hydrogen from a CO_2-rich stream. A selectivity value of 34 is quite significant in this context compared to other membranes used for H_2 purification and CO_2 capture. The MOF-in-COF concept shows great promise, offering the potential to tailor pore sizes for specific gas separation applications.

Graphene analogs, including exfoliated hexagonal boron nitrides (h-BNs), graphitic carbon nitride (g-C3N4), transition metal dichalcogenides (TMDs), and MXenes (metal carbides, nitrides, or carbonitrides), are emerging as promising 2D materials for membrane-assisted decarbonization.[356] MXenes, in particular, stand out due to their distinct physicochemical properties, rich surface chemistry, and versatility for post-synthesis functionalization, making them a highly flexible superfamily of nanostructures that offer unprecedented design potential for gas separation membranes.[357]

MXenes are derived from MAX phases, represented by the formula $M_{n+1}AX_n$, where M is an early transition metal such as Ti, Cr, Mo, and V, A is an element from groups 13–16 (*e.g.*, Al, Ga, or Si), and X represents carbon and/or nitrogen. The resulting MXene structure, $M_{n+1}X_nT_x$, where T_x refers to surface terminations such as –OH, =O, and –F, is usually produced through selective etching of the A element using acids such as hydrofluoric and hydrochloric acid.[358] MXene nanosheets can be incorporated into MMMs, where they act as molecular sieves, enhancing both the permeability and selectivity of polymeric membranes.[359] MXenes alter the tortuosity and solubility of gases in these composite membranes, enhancing the solution-diffusion mechanism for gas transport by leveraging their interlayer nanogalleries and surface terminations.[360] MXene, as a filler within the polymer matrix, alters the tortuosity and solubility of gases in composite membranes compared to pristine polymeric membranes.[361,362] Additionally, surface terminations on MXenes enhance interfacial interactions with the polymer, increasing the affinity of composite membranes for condensable gases (*e.g.*, CO_2).[363]

For example, Shamsabadi *et al.* reported remarkable advancements in CO_2 separation technology by incorporating $Ti_3C_2T_x$ MXene nanosheets within Pebax-1657.[363] With just 0.1 wt% $Ti_3C_2T_x$ loading, CO_2 permeability increased by 43%, while CO_2/N_2 selectivity doubled compared to pure Pebax membranes. This

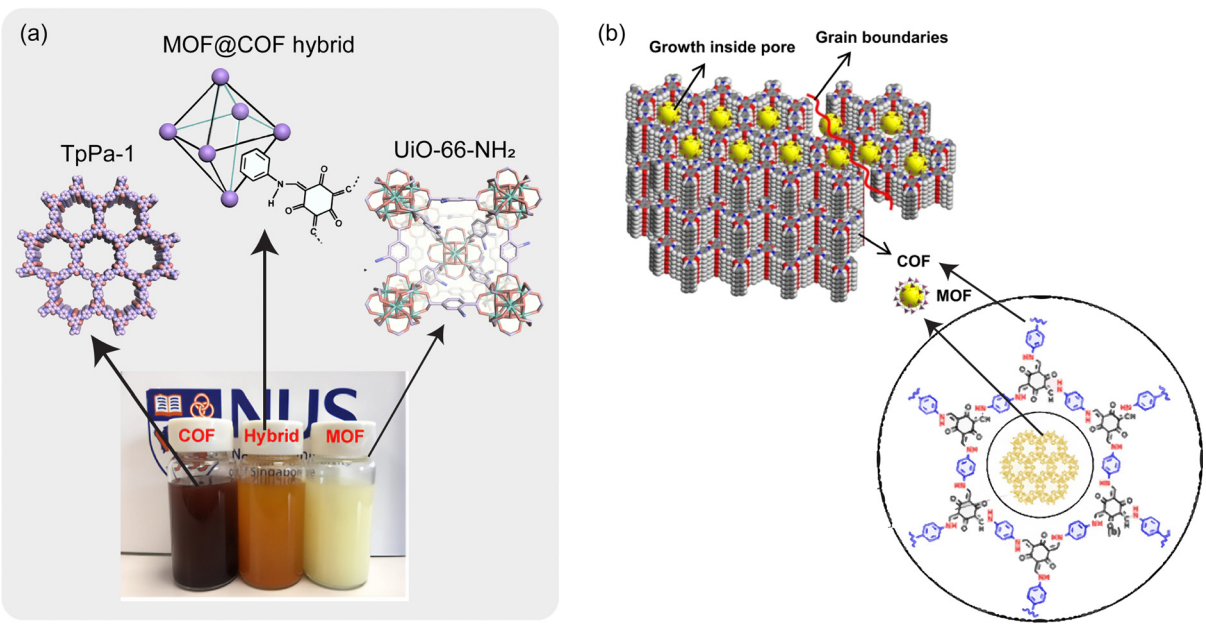

Fig. 22 (a) Attaching UiO-66-NH_2 to COF as a modifier of PSF membrane for gas separation membranes[353] (with permission from Elsevier), and (b) Growing ZIF MOFs in COF porous structure as the selective membrane material for gas separation purposes.[354]

enhanced performance was attributed to strong interactions between the $Ti_3C_2T_x$ nanosheets and the polymer matrix (Fig. 23(a)), as confirmed by characterizations and molecular dynamics simulations, facilitating higher CO_2 solubility and selectivity. The nanochannels between the MXene layers also contributed to improved CO_2 diffusivity, while the molecular sieving effect efficiently blocked N_2 molecules. The high CO_2 adsorption capacity of the hydroxyl groups on $Ti_3C_2T_x$ and the altered morphology and phase separation within the Pebax matrix contributed to the improved performance (Fig. 23(b)). However, at loadings above 0.1 wt%, permeability decreased due to nanosheet agglomeration, which created nonselective voids at the MXene–polymer interface. Liu *et al.* showed similar improvements in CO_2 permeance and CO_2/N_2 selectivity for Pebax MMMs containing 0.15 wt% $Ti_3C_2T_x$ (Fig. 23(c)).[364] Hu *et al.* took this approach further by synthesizing a $Ti_3C_2T_x$-carboxylated nanocellulose composite to improve interfacial compatibility and prevent nonselective void formation. Their composite membrane, containing 15.4 wt% $Ti_3C_2T_x$, achieved a CO_2 permeability of 156.7 Barrer and a CO_2/N_2 selectivity of 47.8 (Fig. 23d).[365] With the incorporation of 23.1 wt% $Ti_3C_2T_x$ MXenes, the CO_2 permeability increased, while the selectivity

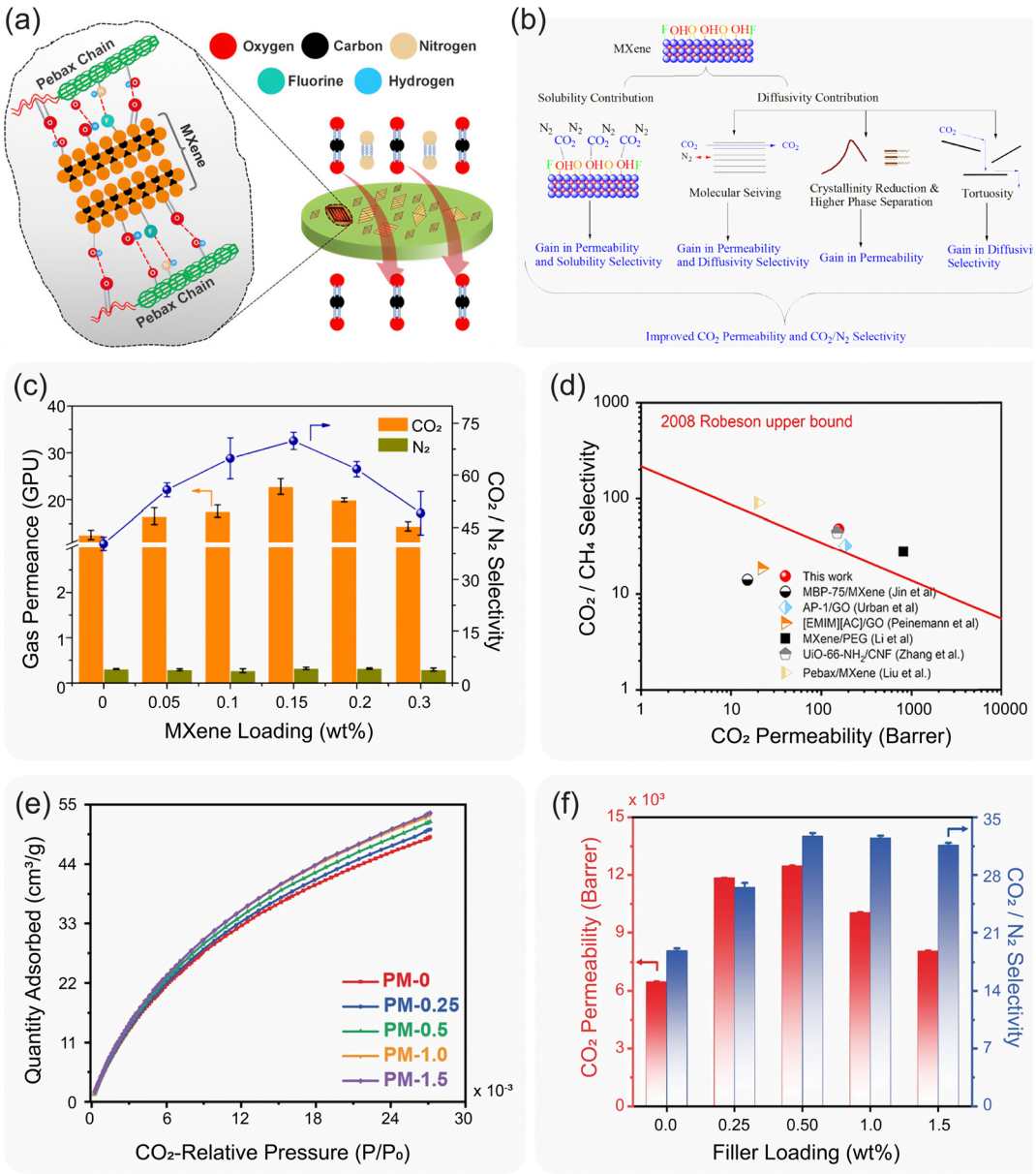

Fig. 23 (a) Schematic illustration of the formation of hydrogen bonds between $Ti_3C_2T_x$ surface terminations and Pebex chains. (b) Proposed CO_2/N_2 separation mechanisms in $Ti_3C_2T_x$-Pebax membranes.[363] (c) Single gas separation properties of $Ti_3C_2T_x$-Pebax membranes as a function of the MXene loadings.[364] (d) CO_2 separation performance of carboxylated nanocellulose membranes containing 15.4 wt% $Ti_3C_2T_x$ MXene compared to Robeson upper bound.[365] (e) CO_2 adsorption isotherms of the pristine PIMs and $Ti_3C_2T_x$-PIM MMMs. (f) CO_2/N_2 separation performance of $Ti_3C_2T_x$-PIM MMMs with a constant feed flow rate of 300 Nml min^{-1} at 3 bar and 25 °C.[368]

decreased due to MXene agglomeration. In another study, the structure and CO_2 separation performance of Pebax-GO and Pebax-MXene membranes were systematically compared.[366] Pebax-MXene membranes were able to accommodate up to 20 wt% MXene due to improved dispersion and interfacial interactions, whereas Pebax-GO membranes reached a maximum loading of only 5 wt%. However, for both membranes, optimal performance was achieved at a 1 wt% filler content under dry conditions. Under humidified conditions, Pebax-MXene membranes with higher loadings exhibited significantly enhanced separation performance. This improvement is attributed to water molecules trapped within the MXene nanogalleries, which facilitate the transport of CO_2 molecules through the membranes.[367]

Despite the numerous advantages of PIMs, including low density, high specific surface area, and favorable physicochemical properties, unloaded PIM membranes often exhibit low CO_2 selectivity compared to CH_4 and N_2.[369,370] To address this limitation, Wang *et al.* fabricated MMMs by integrating $Ti_3C_2T_x$ MXenes into the continuous phase of PIM-1.[368] This innovative approach yielded significant enhancements in CO_2 separation performance. The resulting MMM achieved a CO_2 permeability of 12 475.3 Barrer (Fig. 23(e)), marking an impressive 92.7% increase, and a CO_2/N_2 selectivity of 32.7, a notable improvement of 73.9%. These enhancements were attributed to a 46.1% increase in diffusion selectivity, facilitated by the ~0.35 nm interlayer spacing between MXene layers within the PIM-1 matrix. Furthermore, sorption selectivity improved by 37.9% due to the incorporation of MXene sheets with polar functional groups (–OH, –O, –F), which enhanced the affinity for CO_2 molecules and modified the pore size distribution and volume within the membrane (Fig. 23(f)). These advancements, driven by the synergistic effects of solution-diffusion and molecular sieving mechanisms, have led to a remarkable enhancement in both CO_2/N_2 selectivity and CO_2 permeability.

Research on MXene-based membranes for gas separation is in its early stages and requires further study. Thus far, most published papers have focused on using $Ti_3C_2T_x$ for the fabrication of mixed matrix membranes. However, with over 30 types of MXenes reported, their potential separation performance remains largely unexplored. Additionally, several critical aspects require clarification: the orientation of MXenes within the continuous phase, the effects of high MXene loading, the physical aging of MXene-based membranes, and the impact of MXenes on membrane plasticization. Addressing these areas is crucial for advancing the application of MXene-based membranes in gas separation technologies. Table 8 reports some of the selected performance results for the polymeric membranes used for decarbonization purposes, along with their operational test condition. Table 9 offers more details on the membrane units that have been used on pilot scale for the same purpose.

Despite their superior separation performance in the lab scale, MMMs may not show the same performance real-world operating conditions in the industrial scale. Before commercialization, they must meet certain minimum requirements.[377] Table 10 provides a summary of membrane-based gas separation performance requirements for various commercial applications, including pre-combustion, post-combustion, air separation, and air dehumidification. Additionally, the long-term stability of MMMs in practical applications is a very important.[378] The stability depends on the type of materials used, operating conditions, and the specific application. Harsh environmental conditions, including exposure to aggressive chemicals, high pressure, and high temperatures, can impair the separation performance of MMMs. Both the filler and polymer components govern their thermal and chemical stability. Considering the typical longevity of current polymeric membranes (3–5 years) and the challenges in MMM commercialization, MMMs demonstrate enhanced long-term stability compared to conventional polymeric membranes.[379] This can be attributed to inorganic fillers, which not only improve resistance to plasticization by condensable gases at high pressure but also prevent the reduction in FFV because of physical aging.[380] Therefore, strong interfacial interactions between the polymer and fillers can enhance the longevity of MMMs in practical applications.

7. Challenges of gas separation membranes

Physical aging in glassy polymers occurs due to lattice contraction and chain rearrangement after solvent removal, particularly at temperatures below the glass transition temperature (T_g).[392] This aging process leads to a reduction in the FFV within the polymer matrix, decreasing membrane permeability and overall separation performance over time.[393] Both thin film selective layers and intermediate gutter layers are susceptible to aging, which poses a significant challenge to long-term membrane stability. For instance, gutter layers with a glassy nature, such as poly(trimethylsilyl propyne) (PTMSP), can lose up to 90% of their permeability due to physical aging.[191] The rate of physical aging, r, can be quantified using the following equation[394]:

$$r = -\frac{1}{V}\left[\frac{\partial V}{\partial \ln t}\right]_{P,T} \quad (20)$$

where V is the specific volume of the polymer and t is the performance test duration. Studies show that controlling the FFV can effectively limit the rate of physical aging.

Plasticization is another issue that negatively impacts polymer membranes. The polymer matrix loses its size-sieving capability, leading to diminished selectivity. Plasticization typically occurs when membranes are exposed to polarizable gases (like CO_2) and heavy hydrocarbons under intense operating conditions. The phenomenon involves solvation effects that interfere with polymer interchain interactions, allowing non-plasticizing gases such as N_2 and CH_4 to permeate more easily.[224] On a microscopic level, plasticization increases polymer chain mobility, disrupts the free volume within the polymer, and enlarges membrane pores. Macroscopically, the membrane becomes softer, exhibits increased ductility, and shifts toward a rubbery state with a lower T_g.[395] The presence of widened hysteresis patterns during pressurization-depressurization cycles with CO_2-rich streams further indicates plasticization.[396]

Plasticization is typically measured by observing the increase in CO_2 permeability as feed pressure rises. The plasticization

Table 8 Comparison of selected polymeric membranes performance and operation details for CO_2 separation (all at lab scale)

Selective layer	Support layer	Selective layer thickness (μm)	Operating condition	CO_2 transport factor	CO_2/N_2 Selectivity (or CO_2/CH_4) selectivity	Ref.
Pebax@1657	PES	1.25	25 °C, 4 bar	CO_2 permeability of 22	20	331
Pebax@1657	PMP	25	25 °C, 7 bar	CO_2 permeability of 240	(15)	332
PEO	N/A	N/A	25 °C	CO_2 permeability of 204.3 and N_2 permeability of 3.8	53.7	209
PEO-PBT	PAN	0.05	25 °C, 10 bar, mixed gas CO_2/N_2 feed composition of 28/72 vol%	CO_2 permeability of 150	51	173
PEO-PBT (64–36 v%)	N/A	N/A	25 °C	CO_2 permeability of 100 and N_2 permeability of 2	50	209
PEO-PBT (77–23 wt%)	N/A	60 to 80	25 °C, 0.3 bar	CO_2 permeability of 115	45.6	210
PVAm (from commercial source) with piperazine glycinate as mobile amine carrier	PSF with PVP as an additive (pore size 38 nm, porosity 13.4%)	30	57 °C, 17% relative humidity, 1.5 psig	843 GPU	160	221
PVAm (made from NVF monomer) with piperazine as a mobile amine carrier	PSF with a molecular weight cut-off of 6000	0.78	50 °C, 0.11 MPa	2.17 (μmol m^{-2} s^{-1} Pa^{-1})	277	236
PVAm (from a commercial source) with 2-(1-piperazinyl)ethylamine sarcosine modified with a multiwalled carbon nanotube as a mobile amine carrier	PSF with PVP as an additive (pore size 30.6 nm, porosity 12.9%)	0.17	Mixed feed pressure of 1 atm, CO_2 partial pressure of 0.166 atm	975 GPU	165	235
PIM-1@NUS-8-NH_2 (10 wt%)	N/A	N/A	Room temperature, 2 bar	14 000 Barrer	30	333
PIM-1 with g-C_3N_4 (1 wt%)	N/A	60–90	25 °C with a transmembrane pressure of 1 bar	5785 Barrer	16.3	334
PIM-1 with MOF-801 (5 wt%)	N/A	45	0.4 Mpa, 35 °C	9686 Barrer	27	335
PIM-1 with Ag^+/UiO-66-NH_2 (30 wt%)	N/A	120–140	25 °C, 1 bar	15 000 Barrer	30	336
Pebax@2533 with ZIF-8 decorated graphene oxide	Non	55–65	25 °C, Mixed feed of CO_2/N_2 (15/85 vol%) at pressure of 0.1 MPa	CO_2 permeability of 249 Barrer	47.6	289
PSF with ZIF-8 decorated graphene oxide	Non	90	25 °C, CO_2, CH_4, and N_2 at pressure of 250 kPa	CO_2 permeability of 1.76 Barrer	CO_2/CH_4 selectivity of 6.3	288
Pebax@1657 with bimetallic (Zr and Co) ZIF-decorated graphene oxide	Non	50–70	30 °C, CO_2 and N_2 at pressure of 12 bar	CO_2 permeability of 95.06 Barrer	57.53	301
6FDA-durene polyimide with MIL-101 (Al) decorated carbon nanotube	Non	20–40	25 °C, CO_2/CH_4 (50/50%) mixture at 2 atm	CO_2 permeability of 818 Barrer	CO_2/CH_4 selectivity of 29.7	287
MMM	Pebax	75–90	25 °C, CO_2/CH_4 (50/50%) mixture at 5 bars	CO_2 permeability of 119.08 Barrer	76.26	292
PEO@Zn-TCPP MMM (2.5 wt%)	N/A	100–150	35 °C and 12 atm	198 Barrer	81	337
Cu-TCPP-Pebax MMM (0.1 wt%)	N/A	160	Room temperature, 1 bar	1183 Barrer	57.6	338
$Ti_3C_2T_x$-Pebax MMM (0.1 wt%)	N/A	60–70	25 °C, 4 bar	126 Barrer	96	319
$Ti_3C_2T_x$-Pebax thin-film composite containing 0.05 wt% of $Ti_3C_2T_x$	poly[1-(trimethylsilyl)-1-propyne as the gutter layer on a polyvinylidene fluoride support	0.07	25 °C, 4 bar	1986.5 GPU	41.8	319

Table 9 Comparison of facilitated transport membrane-based decarbonization pilot scale tests

Membrane	Team	Membrane geometry/ module type	Active area	Size	Gas source	Ref.
PVAm-2-(1-piperazinyl)ethylamine-Sarcosine modified with multiwalled carbon nanotube; no brand has been mentioned yet	Ohio State University, US	Spiral wound module with 4 envelopes of flat sheet	1.4 m^2	880 MW_e[a]	Coal-based flue gas	197
Polaris	Membrane technology and research (MTR) Inc., US	Spiral wound		1 TPD[b]	Coal-fired power plant	371
Polaris	Membrane technology and research (MTR) Inc., US	Spiral wound		20 TPD[b]	Natural gas power plant	372
PVAm	Norwegian University of Science and Technology (NTNU), Norway	Hollow fiber	4 m^2 to 20 m^2		Propane burner, cement factory	254, 373 and 374
Polyactive	Helmholtz-Zentrum Geesthacht (HZG), Germany		10 m^2		Coal-fired power plant	375
Chilled PI	Air Liquide, US	Hollow fiber		0.3 MW_e	Coal-fired power plant	376

[a] Megawatt electrical. [b] Ton of CO_2 per day.

Table 10 Membrane-separation performance ranges for industrial viability in different applications

Application	Market size (USD/year)	Gas pair	Operation condition	Required permeance/ permeability	Required selectivity	Ref.
Pre-combustion	1.8 B	H_2/CO_2	Feed pressure of 20 bar 250–400 °C	200–1000 GPU	>10	381 and 382
Post-combustion	700 M	CO_2/N_2	5% CO_2 Low CO_2 partial pressure	1000–5000 GPU	30–50	381–383
Air separation	800 M	O_2/N_2	79% N_2, 21% O_2 Feed pressure of ~10 bar	>0.8 Barrer	>8	384 and 385
Air-dehumidification	900 M	H_2O/N_2	~ 60–80% RH 22–30 °C	>11 900 GPU	>1500	386
Natural gas upgrading	300 M	CO_2/CH_4	Feed pressure of 70 bar 50 °C 10% CO_2	>100 GPU	20–35	387
Hydrogen recovery from ammonia purge gas	200 M	H_2/N_2	40 bar 20% N_2, 60% H_2	>1000 GPU	>290	388–390
Olefin production from steam cracking	37 B	C_2H_4/C_2H_6 C_3H_6/C_3H_8	Feed pressure of 6 bar	>30 GPU >1 Barrer	>30 >3	391
Hydrogen production by gas steam reforming	120 M	H_2/CH_4	4 bar 40 °C	>85 GPU	>37	378

pressure is defined as the minimum pressure at which this increase is observed. Yuan *et al.* studied the effect of wet thickness on PVAm membrane performance and noted that thinner membranes are more prone to accelerated plasticization.[266] Thinner selective layers, achievable through intermediate/gutter layer usage, wet coating thickness reduction, and coating parameter adjustments, are crucial for higher CO_2 permeability. However, reduced thickness leads to accelerated plasticization due to a decrease in glass transition temperature.[397] To mitigate this, crosslinking approaches using ethylenediamine have been proposed, as crosslinked membranes exhibit improved resistance to plasticization. Consequently, thinner crosslinked films can be produced without compromising CO_2 separation performance.[266]

Wessling and his team conducted an in-depth assessment of plasticization across various membrane materials (polysulfone, polyethersulfone, cellulose acetate, cellulose triacetate, polyetherimide, copolyimide, Matrimid 5218, poly(2,6-dimethyl-*p*-phenylene oxide), bisphenol A polycarbonate, bisphenol Z polycarbonate, and tetramethyl bisphenol A polycarbonate). Their study aimed to correlate the critical plasticization pressure, CO_2 concentration, FFV, and functional group density. Interestingly, they found that plasticization is not solely influenced by CO_2 polarity-segment interactions, as even non-polar gases like argon can induce plasticization at high pressures.[398] Their findings suggest that plasticization is more closely related to the absorbed CO_2 content than to gas polarity. Plasticization depends on both pressure and a relatively constant critical CO_2 concentration of approximately 38 ± 7 cm^3(STP) cm^{-3}. Therefore, the key factor is the sorption of CO_2 rather than its polar characteristics. Table 11 provides plasticization data, permeability, and testing conditions for various membrane materials.[399]

Crosslinking enhances the mechanical stability of the membrane by forming covalent bonds between polymer chains, reducing the polymer matrix's flexibility and thereby limiting swelling under high-pressure conditions. This makes it a viable approach not only for preventing plasticization but also for addressing physical aging issues, where polymer membranes tend to densify and lose performance over time.[222] However,

Table 11 Plasticization pressure for different membrane materials

Membrane	Plasticization pressure (bar)	Permeability at plasticization pressure (Barrer)	Permeability at zero pressure (Barrer)	CO_2 equilibrium plasticization concentration (cm^3(STP) cm^{-3})	Operating temperature
Polysulfone	34	3.6	5	47	23
Polyethersulfone	27	2.6	3.7	43	21
Polyetherimide	28	0.84	1.1	37	21
Bisphenol A polycarbonate	31	4.7	7.5	33	25
Bis13phenolZ polycarbonate	24	1.0	1.4	32	23
Tetramethyl bisphenol A polycarbonate	13	13	16	36	25
poly(2,6dimethyl-*p*-phenylene)oxide	14	8.2	99	34	25
Polyimide matrimid 5218	12	4.8	5.7	47	22
CopolyimideP84	22	0.92	1.1	48	23
Cellulose acetate	11	6.0	6.7	31	27
Cellulosetriacetate	10	7.3	9	31	24

crosslinking can negatively impact the FFV within the membrane. The reduction in FFV results in fewer free spaces for gas molecules to diffuse through, leading to a decrease in permeance. While the mechanical integrity and selectivity are improved through crosslinking, the trade-off often comes at the cost of gas permeability. To balance this, careful tuning of crosslinking density is required to ensure that the membrane maintains sufficient FFV to allow for gas transport while mitigating plasticization and aging effects. Advanced crosslinking strategies, such as the use of flexible crosslinkers or partial crosslinking, are being explored to minimize the adverse impact on permeability while maintaining stability and selectivity.

While the topic is generally tailored toward looking at the phenomena around CO_2 filtration, the effect of other components and impurities in the target stream must not be ignored. Flue gas might contain NO_x, SO_x, humidity, H_2S, CO, NH_3, or even heavy metals depending on the source of the fuel in combustion processes.[400] The presence of impurities could reduce the adsorption capacity of the membranes, reduce the driving forces of the permeation or negatively affect the structure of the membrane leading to reduced performance of the membrane separation unit.

SO_2, a more studied element from the SO_x family, has larger kinetic diameter compared to CO_2 and deterioration of the performance is not mainly due to the diffusion of the gas molecule.[401] The increased permeability of SO_2 can be attributed to its higher critical temperature, which results in a greater affinity constant and higher adsorption in Langmuir free volume sites. MMMs with higher share of rubbery polymers have higher affinity toward SO_2 and higher loading of Langmuir free volume sites. Due to its more condensable nature, SO_2 has a higher plasticization effect. While the SO_x components' concentration is much smaller than CO_2, it is important to note that each decarbonization process must be separately assessed with regards to the flue gas characteristics. On the other hand, the cogenerative effect of the impurities deteriorates the performance much more when humidity plays a major role. The presence of humidity triggers the conversion of SO_2 to sulfuric acid, within the free volume of the MMM and degradation of the MMM's structure. Similar effects are identified with the formation of nitric acid because of NO_2 and humidity reaction. From the NO_x family, NO is more frequently observed in flue gas streams with concentrations not exceeding 500 ppm. NO has lower kinetic diameter in comparison with CO_2 yet its lower adsorption affinity results in lower permeability. H2S, present in natural gas, and fermentation-generated biogas could reduce the performance of polymeric membranes. As an instance, in the case of PDMS membrane, CO_2 permeability was reduced by 8% due to the diffusion competition of impurities.[402] More importantly, N_2's mass transport resistance was reduced due to the swelling of the polymeric matrix, explained by the Flory–Huggins theory.[402] Nanoparticle's structure could also be sensitive to interaction with H_2S. Metals such as copper could react with sour gas. This could jeopardize the performance of MMMs with Cu-based MOFs such as ZIF-8.[400] On the other hand, porous organic polymers and carbon based nanomaterials could resist acid gases with due to their less exposed nature.[400] This could highlight the opportunity for PIM-like structures and graphitic carbon nitrates (GCN) as acid-gas resistant decarbonization membranes. Nevertheless, the concern of sour gas is more attributed to the natural gas decarbonization or biogas purification, rather than the flue gas decarbonization.

8. Computational studies, artificial intelligence and machine learning contribution to membrane-based CCUS

8.1. Computational effort in membrane-based CCS technologies

As discussed earlier, the transport of gas molecules through the membrane matrix is controlled by the adsorption and diffusion characteristics of the penetrating molecules. If the desired molecules adsorb too strongly or too weakly, it can hinder membrane performance, causing slow diffusion or a low concentration of the targeted molecules.[403] Additionally, separation performance can be significantly influenced by multicomponent phenomena, particularly when highly sorbing gases, such as water vapor and CO_2, are present. Experimental data have revealed that multicomponent phenomena can decrease the solubility and increase

the diffusivity of less soluble species in gas mixtures.[189,404–406] This suggests that the intermolecular interactions between polymer chains and gas molecules, as well as the competition among gas molecules in a mixture, are not straightforward to interpret. Therefore, optimizing membrane properties is crucial to creating ideal interactions between the membrane and the desired molecule for effective adsorption and diffusion, ensuring optimal separation performance.

Membrane modeling involves various methods to estimate membrane properties and consider multicomponent effects, primarily focusing on two fundamental performance metrics: gas permeability and membrane selectivity.[403,407]

Extensive efforts have been made to explain experimental results by considering various assumptions at the molecular scale. One of the most widely used theories is the dual-mode sorption model, developed for glassy polymers, which assumes that each gas molecule can be adsorbed either directly on the polymer chains (Henry's sorption law) or in the non-equilibrium voids between the chains of a glassy polymer (Langmuir sorption).[408,409] Saberi *et al.* applied this theory to develop their model to explain gas permeation and CO_2-induced plasticization in glassy polymers.[410] Additionally, the dual-mode sorption model was extended using artificial intelligence methods to model mixed-gas sorption in PIM-1 and TZ-PIM.[411] However, the need for mixed-gas sorption data may limit the applicability of this model to specific polymers and operating conditions.

Alternatively, thermodynamic methodologies such as non-equilibrium thermodynamics for glassy polymers (NET-GP) have been effectively applied, leveraging the inherent non-equilibrium characteristics of glassy polymers. Within this framework, equation of state (EoS) models, expanded to account for non-equilibrium conditions, are used to compute gas sorption and describe the non-equilibrium states in glassy polymers. This is achieved by introducing polymer density as an internal state variable to explain the system's degree of non-equilibrium.[406,407] The advantage of this method is that it can be applied to multi-component gas mixtures using sorption data acquired from experiments with pure gas or binary mixtures. Subsequently, the diffusion coefficient can be represented as the product of a kinetic factor (mobility) and a thermodynamic factor, calculated using the NET-GP methodology to compute the permeability of the penetrating species.[412,413]

Classical molecular simulation is another approach used to study membrane properties and the transport phenomena of gas species. The accuracy of these interactions strongly depends on factors such as the gas models used and the methods for assigning partial charges. The accuracy of these interactions strongly depends on several factors, such as gas models and methods used for assigning partial charges. The importance of this type of simulation becomes more apparent when studying composite membranes.[414,415]

In computational studies involving MMMs, various molecular techniques are employed, including grand-canonical Monte Carlo (GCMC), equilibrium molecular dynamics (EMD), non-equilibrium molecular dynamics (NEMD), transition-state theory (TST), and even density functional theory (DFT), a quantum-based simulation. GCMC simulations are widely used to determine the gas adsorption properties of membranes (*e.g.*, gas uptake or affinity). In contrast, gas diffusion properties within membranes are explored using MD simulations or the TST approach.[416,417] After calculating gas adsorption and diffusion, permeability and membrane selectivity are determined based on the solution-diffusion model. This approach integrates adsorption and diffusion data to determine the membrane's effectiveness in a specific separation process.[418]

A distinct advantage of molecular simulation is its ability to approximate intermolecular interactions to ensure an intimate interface between the species that make up the composite membrane. This feature can pave the way for making compatible polymeric composites where emerging materials with unique properties can be embedded in the membrane matrices to promote separation performance. Thus, it provides guidance for selecting filler/polymer pairs by identifying noncovalent and covalent bonds between fillers and polymer chains. Typically, functional groups (*e.g.*, –NH2 or –CN) on the surface of fillers or structural defects intentionally created in the crystalline structure of fillers can lead to a favorable interface and reduce non-selective voids, maintaining the level of selectivity.[403] For instance, simulations showed that MXene nanosheets could form an intimate interface with the Pebax membrane matrix, supporting the cost-effective separation performance of the resulting membrane.[363] In another study, Sadeghi and Howe used DFT simulations to examine how polymer fragments (specifically, Kapton and 6FDA-Durene) interact with ZIF-8 and Co-BDC surfaces.[419] Their investigation uncovered that the presence of unsaturated sites can promote strong compatibility between the MOF and polymer. Conversely, when there was a deficiency of undercoordinated surface species, the adhesion between the MOF and polymer was weaker, particularly in cases where dispersion forces played a dominant role. It is noteworthy that molecular simulations can also calculate various structural properties of polymer membranes, including density, glass transition temperature (T_g), FFV, polymer solubility, and mechanical properties, which can reveal whether a polymer is suitable for a specific separation.[420–422]

8.2. A data-driven approach for membrane-based CCS studies

As previously mentioned, MMMs stand out as a highly advantageous membrane type due to their cost-effectiveness, ease of processing, and superior performance. The unique properties of fillers can also be imparted to the membrane when they are dispersed within the membrane matrix. However, choosing compatible polymers and fillers to prepare a defect-free composite remains a significant challenge. As a result, researchers have focused on applying cutting-edge computational approaches, such as data-driven methods, to make optimal choices.[403,417]

The highly detailed atomistic simulations offer precise outcomes but come with substantial computational expenses.[403] Hence, typically, the permeabilities of MMMs are calculated utilizing permeation models like Maxwell,[423] Bruggeman,[424] and Felske.[425] These models integrate the gas permeabilities of fillers obtained through atomic simulations with experimental data on gas permeability in polymers. Consequently,

once the gas adsorption and diffusion properties of fillers are known, the permeabilities of MMMs can be estimated without further simulations.[403,426]

In this regard, numerous studies on both real and hypothetical materials, including MOFs, COFs, and 2D materials, have examined their potential for diverse applications and objectives.[427–434] Budhathoki *et al.* performed high-throughput atomistic simulations on 112 888 real and hypothetical MOFs to obtain CO_2 permeability and CO_2/N_2 selectivity.[435] Afterward, using experimental data attributed to nine polymers and applying the Maxwell model, they estimated the separation performance of over one million possible hypothetical MMMs resulting from combining those MOFs and polymers. The results were then used for a techno-economic evaluation of membrane-based carbon capture, showing that many potential MMMs are predicted to have a carbon capture cost of less than $$50 per ton of CO_2 removed. Altintas and Keskin also performed high-throughput computational screening (HTCS) to evaluate a MOF database for membrane-based CO_2/CH_4 separation.[436] They applied GCMC and MD simulations to identify the separation performance of those MOFs. They then calculated the permeability and selectivities of possible MMMs, where the best MOF candidates were embedded as fillers. This revealed a significantly improved CO_2 separation performance compared to pristine membranes.

Meanwhile, Yuan and Sarkisov proposed an efficient approach using lattice models and dynamic mean field theory to estimate gas permeability in MMMs.[437] This model considers interfacial effects, suggesting potential gas transport hindrances due to unfavorable interface interactions. Although these models lack the resolution of molecular simulations due to the absence of long-range interactions, they serve as effective initial screening tools for probing diffusion in various MOF-based MMMs. The idea was that the identified candidates could then undergo detailed molecular simulations for a more comprehensive analysis.

The rapid advancement of high-performing MMMs can be achieved by integrating diverse modeling, simulation tools, and data science techniques, offering valuable insights to experimentalists. Transitioning MMMs from laboratory research to practical application requires significant effort and time. However, this transformation can be efficiently accomplished through the cohesive integration of experimental knowledge, theoretical knowledge, and big-data science methodologies. At this point, the conversation pivots toward exploring the application of artificial intelligence (AI) techniques for material classification or membrane performance regression.[437]

Apart from the studies that AI was implemented to find a correlation between parameters or build a model to predict the output *versus* inputs, AI-assisted methods have widely been used to optimize the operational parameters of carbon capture processes such as temperature, operating pressure, flow rates of species, and geometry of the reactors to increase the overall efficiency of the process.[438,439] However, AI-assisted methods are often applied for polymeric membranes to select or discover the optimal polymeric structure or the best combination of polymers and additives to achieve high-efficiency separation performance. Data-driven analysis (including AI-assisted methods) aids in identifying the pros and cons of different materials to overcome certain drawbacks, such as weak intermolecular interactions between continuous and dispersed phases in a polymer composite, non-selective voids at the interface, or chain rigidity.[279,440]

The emergence of machine learning (ML) techniques has led to precise predictions for diverse material properties. Simultaneously, the availability of vast repositories containing both experimental and simulation data has facilitated the use of machine learning to uncover new materials through data analysis.[441] Fig. 24 displays a typical ML model workflow that utilizes data sources to ultimately accelerate the identification of high-performance materials.

Resources, including crystallographic data and molecular simulations, can provide chemical, structural, or energetic properties of substances. However, the first step in utilizing these large data sets is converting the information into formats, such as scalars or vectors, that are readable by ML models and accurately describe the properties of materials. Once material representations are acquired from experimental or computational data, ML models can be implemented for two purposes: regression and classification. The regression task, often applied to predict separation performance metrics, may lack accuracy due to factors such as limited data or the absence of physically relevant features. In such cases, classification methods are useful, categorizing materials as stable or unstable, or high performance or low performance, instead of providing precise numerical values. This approach can expedite identifying potential materials for use in MMMs for CO_2 separation.[442,443]

Zhang *et al.* combined HTCS and ML models to evaluate the potential of ionic liquid-incorporated MOFs (IL@MOF) as fillers to overcome the trade-off limitation in membrane separation.[390] They prepared a dataset of 8167 IL@MOF composites by considering the [NH2-Pmim][Tf2N] molecule and using the CoRE MOF 2019 database.[444] All IL@MOF composites were assessed for CO_2/N_2 (15/85) separation under ambient conditions. To obtain a better understanding of the structure-performance relations, some chemical characteristics (*e.g.*, unsaturation degree, metallic percentage, and oxygen/metal ratio), as well as textural properties (*e.g.*, crystal density, pore-limited diameter, and surface area), were considered to train an ML model based on the random forest (RF) regression algorithm. The ML outputs demonstrated that the most effective descriptors for CO_2/N_2 selectivity and CO_2 permeability are accessible pore volume and mass-accessible surface area. [NH2-Pmim][Tf2N]@ZIF-67 was eventually selected as the best filler due to its promising CO_2/N_2 separation performance observed in molecular simulations. The selected filler was then integrated into PIM-1 to fabricate a high-performing MMM. The experimental results for the MMM exhibited superior CO_2/N_2 selectivity and CO_2 permeability compared to both the pristine PIM-1 membrane and the ZIF-67/PIM-1 MMM, surpassing the redefined Robeson upper bound for CO_2/N_2 separation in 2019.[282]

8.3. Future directions of ML/AI modeling: inclusion of degradation and ageing effects

Despite the recent advances, we still observe that membrane degradation and ageing are not explicitly addressed in AI/ML

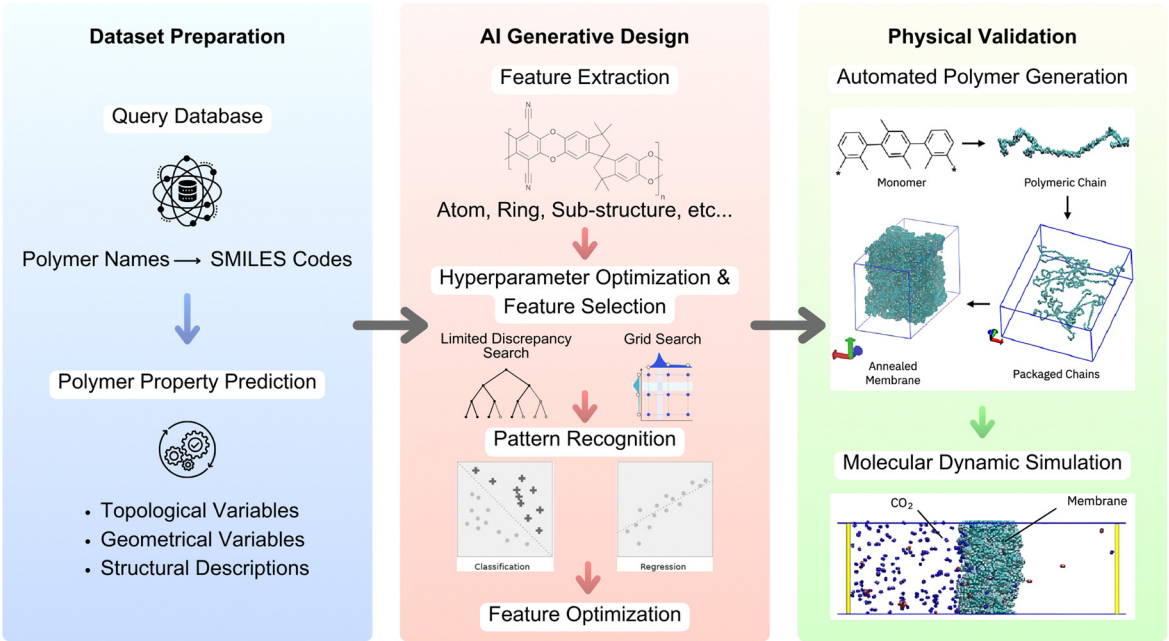

Fig. 24 A typical workflow of ML models developed for high-performing membrane identification.

models, specifically in the case of polymer membranes. One approach recently presented by Giro *et al.*[440] has implicitly accounted for degradation effects through inclusion of the half-decomposition temperature as a target figure-of-merit. The main reason for the methodological gap is the lack of high-quality training data. Experimental data on degradation are scarce and, if available, they are often qualitative. Moreover, there is a lack of standardization with regards to how these data are obtained in the lab. One potential route to address this gap could be the generation and use of synthetic data. Nevertheless, nowadays the problem complexity limits the AI/ML model efficiency, model accuracy and predictive power.

Going forward, an important challenge will be to include into the ML models the physical degradation effects observed in polymer membranes, such as plasticization, competitive sorption, and aging.[445] Plasticization in polymer membranes occurs at high pressure, due to CO_2 related swelling. The effect increases the segment mobility of polymer chains, the free volume and the interchain spacing. This leads to an increasing permeability[446] and a loss of selectivity.[447] Competitive sorption is an effect that tends to reduce the solubility of gases due to competition for the adsorption of the more soluble gas in the mixture.[448] Physical aging occurs in glassy polymers due to the relaxation of the nonequilibrium chain conformation towards an equilibrium state, below the glass transition temperature. Glassy polymer chains gradually relax into their favored higher packing density (densification), which decreases membrane permeability.[445] A potential pathway for mitigating these degradation effects is the addition of polymer crosslinking.[449]

In the case of nanoporous membranes, such as MOF membranes, some advancements towards inclusion of degradation effects have emerged. In recent works, a natural language processing (NLP)-based approach was used to extract information with regards to MOF solvent removal and thermal stability from the literature.[450,451] The data was then used to train ML models for predicting the stability of new MOFs with quantified uncertainties. In a similar approach, Terrones *et al.* enlarged a training data set for predicting MOF stability against water.[452] Inclusion of the additional data improved the ML model performance in the prediction of both stability against water and stability under acidic conditions. As an extension of previous work and an example of generative design including degradation effects, Nandy *et al.* employed ML models to identify MOFs that are stable against heating and solvent removal.[453] Nevertheless, ML models do not yet capture degradation caused by corrosive and acid substances. For example, substances such as H_2S, SO_X, and NO_X can disrupt weak ligand-metal linkages in MOF OMS.[454,455] In addition, MOF stability could be further improved by exploring structural changes and functional modifications.[454]

We conclude that future ML approaches to membranes should explicitly include degradation effects. In generative design, the inclusion of suitable figures-of-merits in the design workflow could lead to improved, higher-stability membranes.

9. Process simulation and design challenges

The process of upscaling membrane samples from the lab to larger scales facilitates the transition of the technology from its initial developmental stages to pilot- and industrial-scale applications. Process modeling and simulations allow the identification of several technological and economic aspects of a technology before implementation beyond the lab. Simulations can effectively analyze the performance of membrane filters and membrane contactors. It is generally believed that membrane systems are significantly simpler from an all-encompassing

standpoint, and more succinct, methodical comparisons are expected in the literature. In contrast, the carbon capture process is influenced by various factors such as industry type, geographic location, seasonal fluctuations in market demand, *etc.*, all of which impact the final costs and design criteria.

Industries emit streams with varying CO_2 concentrations, flow rates, pressure, temperature, and impurity levels. Scenarios from simulations help to understand the multitude of steps required and strike a balance between fixed/operating costs and the total quantity of CO_2 captured.[456] Small and medium-sized CCUS processes can benefit from the low cost of membrane separation. However, once a critical point is reached, as determined by process simulations, amine-based capture technologies become more technically and economically viable.[457] One major process challenge is optimizing both the number of steps and the purity and quantity of CO_2 removed from the flue gas. The primary goal for a single-stage membrane-assisted decarbonization system is to achieve an energy requirement of less than 2 GJ per ton of CO_2 recovered. Simulations indicate that such targets are achievable only when a vacuum pump is used on the downstream side or when the CO_2 concentration in the feed stream is high.[458] Membrane selectivity plays a crucial role in the system's feasibility; moderate selectivity values ($\sim$50) may be sufficient under optimized conditions. More cost-effective approaches, such as increasing the CO_2 concentration through partial recovery of the exhaust or coupling the membrane separation system with a cryogenic unit, have been proposed.[253,458] Two-stage membrane separation is more common and toward cost-function minimization by including/excluding/optimizing the process options of vacuum pump, partial recycle, step-vise pressure difference, purity and recovery ratio adjustment, energy recovery, humidification adjustment, and impurity removal.

Initial simulations were conducted based on fixed permeability, constant pressure change, and non-reactive systems. The next generation of simulations is now available based on variable permeability, variable pressure difference, and reactive FTM systems.[459,460] A major challenge for membrane-based decarbonization processes is the unique working specifications of each membrane or module. As the new generations of membranes integrate both reactive and molecular sieving properties, their permeability/selectivity coefficients, along with their behavior in modulated form, including concentration polarization, need to be evaluated individually. Accordingly, generic simulations may not be able to cover the broad spectrum of membranes currently available in the market.[458]

Jomekian *et al.* offered a perfect instance of a tailor-made simulation of precise process modeling using a specific MMM membrane.[461] ZIF-8 modified Pebax 1657 membranes containing up to 60% of the nanofillers were modeled by connecting an Excel sheet performance database to Aspen software. While this simulation approach is not the most optimum one, promising results were reported in terms of using simulation tools. Using an experimental mixed gas setup, they reported the permeance and selectivity of their lab-made MMMs. The flux for the CO_2 and the other gas, in their case, CH_4, was calculated using the generic solution-diffusion formula (eqn (23) and (24)), and the flux for the membrane unit was solved by rearranging the formulas (eqn (25) and (26)):

$$J_{CO_2} = \frac{yP}{A} = P_{CO_2}\left(p_{feed}x - p_{permeate}y\right) \quad (21)$$

$$J_{CH_4} = \frac{(1-y)P}{A} = P_A\left(p_{feed}(1-x) - p_{permeate}(1-y)\right) \quad (22)$$

$$\frac{y}{1-y} = \alpha\frac{p_{feed}x - p_{permeate}y}{p_{feed}(1-x) - p_{permeate}(1-y)} \quad (23)$$

$$\left(\frac{p_{permeate}}{p_{feed}} - \alpha\left(p_{permeate} - p_{feed}\right)\right)y^2 + \left(1 - x + \alpha x - \frac{p_{permeate}}{p_{feed}} + \alpha\left(p_{permeate} - p_{feed}\right)\right)y - \alpha x = 0 \quad (24)$$

where J_{CO_2} and J_{CH_4} are the flux of the CO_2 and CH_4, P_{CO_2} is the permeance of CO_2, p_{feed} and $p_{permeate}$ are the pressure values in the upstream and downstream of the membrane in cmHg, A is the membrane area in cm^2, and x and y are the mole fractions of the CO_2 in the feed and permeate sides, respectively. The above equations allow for calculating y and J_{CO2}. The total flux was calculated using:

$$J_{CO_2 total} = nJ_{CO_2\text{-single stage}} \quad (25)$$

and the effect of temperature using:

$$P = P_0 \exp\left(-\frac{E_p}{RT}\right) \quad (26)$$

where n is the number of filtration stages, P_0 is the experimental permeability (Barrer) obtained from lab tests, E_p is the gas permeation activation energy (kJ mol^{-1}), R is 0.008314 kJ mol^{-1} K^{-1}, and T is temperature (K). By creating spreadsheets and using Aspen Plus software, a comparative study was conducted, including four scenarios: single-step, single-step with recycling of the permeate, double-step with recycling of the permeate (with the highest recovery of methane), and double-step with recycling of the retentate. The coupled experimental-simulation work represents a simple, low-cost approach to observe the modified membranes' performance under different operating conditions before moving to the plant scale. However, the study lacked an economic assessment and critical information, such as feed impurities.

Another valuable report presented the simulation of two-stage membrane-based decarbonization of a 400 MW natural gas combined cycle (NGCC) power plant, along with the optimization of the carbon-to-electricity relative price (Fig. 25).[462] The objective was to maximize the total net present value (NPV) of the power plant, considering no constraints on production and demand, through the simultaneous optimization of design and operational parameters. The NGCC was modeled with part loads varying from 0.66 to 1, fixed fuel, and air flow rates to avoid fluctuations in the flue gas composition, maintaining a fixed CO_2 concentration of 3.9 mol%.

The two-stage membrane filtration was modeled under the assumptions of no pressure drop and no temperature change

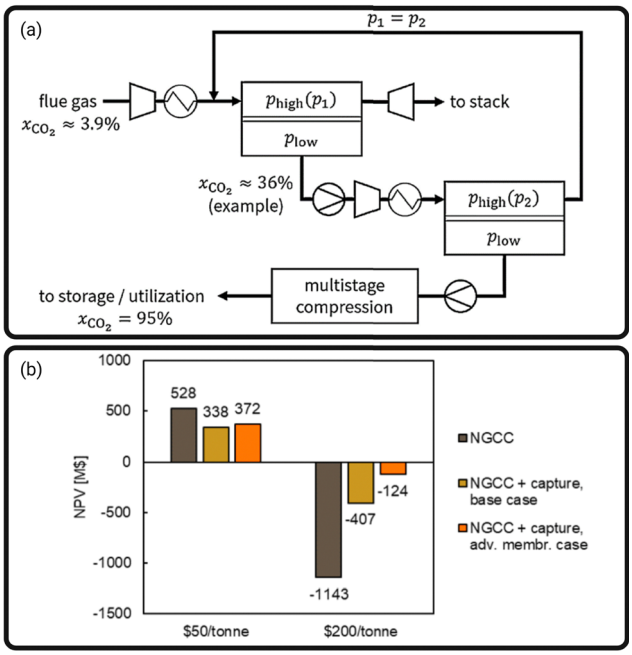

Fig. 25 (a) Schematic of two-stage membrane filtration model used for decarbonization of a 400 MW NGCC power plant, (b) Comparison of NPV for the power generation without carbon capture, with base membrane-decarbonization unit, and with advance membrane units (reproduced from ref. 462 with permission from Elsevier, copyright 2025).

within the membranes. The feed and operating temperatures were set at 45 °C, and 30 °C, respectively. The CO_2 concentration was 95 mol%, and the CO_2 outlet pressure at the end of the second filtration was 137.9 bar (6-stage compression). The compressor efficiency was 0.8, and the vacuum pump and expander efficiency were 0.7, with adiabatic expansion or compression considered in the calculations of the pumps and compressors. Time step of one hour was used for power cost estimation, based on twice the power price in California in 2015, with a natural gas price of \$3.13/GJ and a membrane cost of \$50/m^2.

A simplifying assumption was made that only CO_2 and N_2 permeated the membranes, and a crossflow model was applied for the simulation. A simplified crossflow symmetric membrane model was used, which is practical and easier to run compared to a more comprehensive asymmetric membrane model. Details of the membrane modeling for gas separation can be found elsewhere.[463]

The selectivity and permeance of the membrane were set to 50 and 1000 GPU, respectively, while four other design parameters, namely, the membrane surface area and the compressor size in each of the stages, were changed to create different simulation scenarios. Another scenario of improved membrane separation property was also developed (selectivity of 200 and permeance of 3500 GPU) for comparison purposes. Cycle load, each stage's feed pressure, each stage's permeate pressure, and the capture rate parameters were selected as the operation variables for the optimization. Interestingly, the comparison of the highly selective membrane and the base membrane in the lower carbon pricing range showed closer NPV values, while at a higher carbon price of \$200/ton, the difference was significant. While the study provides a good example of real scenarios, several aspects are not yet covered. For example, the NPV can be affected by the possible selling scenarios of the carbon captured for oil recovery purposes. A more comprehensive approach would consider avoided risks or regulatory compliance to prevent fines. A lower NPV with CCUS does not necessarily reflect less profit for the plant because of emitted carbon. Given the specific economic and regulatory context, the costs associated with capturing and storing carbon currently outweigh the financial benefits derived from such activities. According to Yuan *et al.*, decarbonizing power plants is inherently context-sensitive.[462] Power demand, energy prices, and carbon regulations within a region are examples of market circumstances that impact the model's sensitivity and optimal design and operation.

Simulation and modeling approaches can also target more detailed information on membrane properties with the possibility of altering the techno-economic aspect of the carbon capture process. As an instance, Budhathoki *et al.* considered a three-stage membrane separation design to investigate the TEA of the process for twelve hypothetical membranes with CO_2 permeance equal to 34, 1170 or 8000 GPU and CO_2/N_2 selectivity of 18, 35, 68 or 250.[435] This simulation setting, coupled with optimizing the operating parameters using the framework for optimization, quantifying uncertainty, and sensitivity (FOQUS) through Aspen Custom Modeler Software (ACM), highlighted the influence of membrane characteristics on the TEA. An interpolation of the cost of carbon capture was made as a function of permeability and selectivity, and it was further extended to a database on MMMs with different performance data. The TEA was assessed using the cost of CO_2 capture and cost of electricity production (COE), which is a function of total overnight cost (TOC), carbon capture operating variable cost (OC_{CC}), capital cost factor (CCF) and capacity factor (CF), and the parasitic load (MW $h_{parasitic\ load}$). The suffix "ref" indicates the same parameter for the plant without carbon capture, and the suffix "cc" refers to the parameters of the plant with carbon capture. Within the simulation framework described above, the cost of the CO_2 capture factor was calculated for each permeance/selectivity pair (Fig. 26(a)). Interpolation of the cost of CO_2 capture for several MMMs with different polymers and various nanofillers was then conducted to generate a cost sensitivity for MMMs-based carbon capture (Fig. 26(b)). Despite common assumptions, enhancing the permeability and selectivity of a membrane does not necessarily result in a reduced CO_2 capture cost. Interestingly, the lowest CO_2 capture cost does not result from the best MOF with the most suitable adjustments to pore and chemical characteristics. For a MMM to exhibit improved gas selectivity, the selectivity ratio between the MOF and the polymer should be at least ten times higher than their permeability ratio. This means that MOFs with the lowest cost of capture capacity (CCC) are not those with the highest permeability and selectivity. Instead, the optimal MOFs are those where the selectivity ratio surpasses the permeability

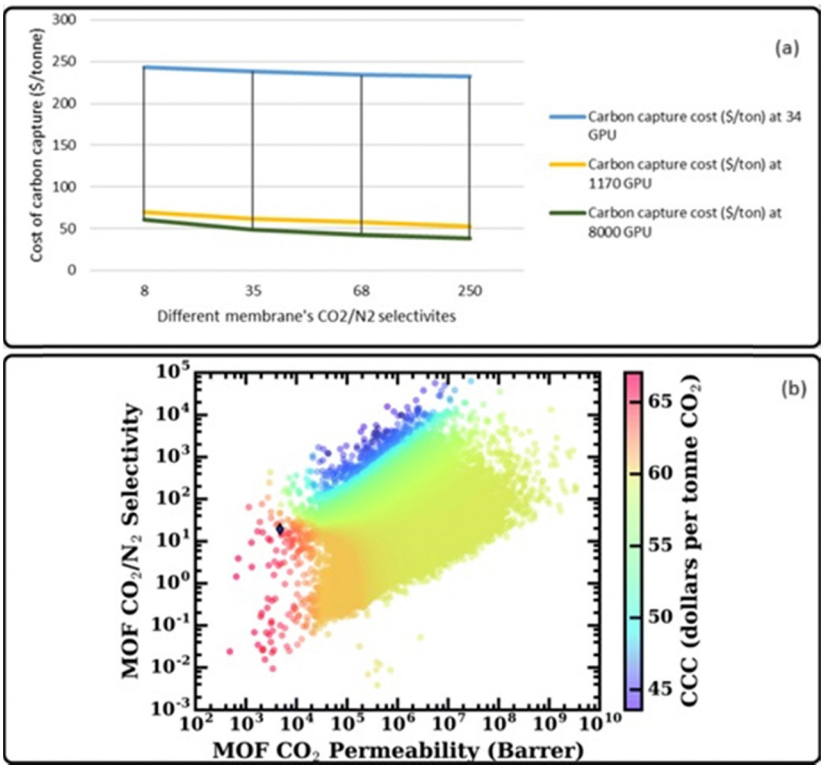

Fig. 26 (a) Carbon capture cost calculation using the simulated process for hypothetical membranes (3 different permeances and 4 different selectivities), and (b) carbon capture cost estimation using the interpolation driven from a 650 MWe power plant-carbon capture simulation and using it for hypothetical MMMs assessment (reproduced from ref. 253,435 with permission from RSC, copyright 2025).

ratio by at least an order of magnitude, provided that they also have higher permeability and selectivity than the polymer alone.

$$\mathrm{COE} = \frac{(\mathrm{CCF})(\mathrm{TOC_{ref}}+\mathrm{TOC_{cc}}) + (\mathrm{TOC_{FIX}}) + (\mathrm{CF})(\mathrm{TOC_{VAR_{ref}}}+\mathrm{TOC_{VAR_{CC}}})}{\mathrm{CF}(\mathrm{MWh_{ref}}\,\mathrm{MWh_{CC}})} \quad (27)$$

$$\mathrm{CCC} = \frac{\mathrm{COE_{cc}} - \mathrm{COE_{ref}}}{\text{captured } \mathrm{CO_2}} \quad (28)$$

9.1. Number of stages and its correlation with process efficiency and economics

Having CO_2 separated in a single-stage process could impose many limitations to the process.[464,465] Two-stage filtrations were studied and optimized by a few research teams. For instance, energy recovery from the CO_2-depleted stream and post-capture CO_2 liquefaction were taken into consideration when Shao *et al.* investigated a two-stage membrane technique for CO_2 capture from coal-fired power stations.[466] Vacuum pressure on the permeate side was found to be the preferred driving force after feed and permeate pressures were optimized. According to a cost analysis, the first-stage membrane accounted for the majority of overall expenses. For assumed parameters (1000 GPU permeance; CO_2/N_2 selectivity of 30, 50, and 200), the results showed that membrane technology is more economical than PSA and amine absorption for CO_2 capture in coal-fired flue gas.

Zhai *et al.* studied polymer membranes for capturing CO_2 after combustion in coal-fired power plants.[467] With a CO_2/N_2 selectivity of 50, a membrane permeance of 1000 GPU, and a flue gas flow rate of 500 $m^3\ s^{-1}$ (STP) with 13.0% CO_2, they discovered that the best way to minimize CO_2 avoidance costs is to combine compressors and vacuum pumps. A two-stage membrane system cost \$\$45.6/mt CO_2 to capture, but it recovered 90% of the CO_2 and was 95% pure. The cost was reduced to €31/t CO_2 by recycling CO_2 using a two-stage, two-step air sweep arrangement, which is in line with Kotowicz *et al.*[468] A parametric study on two-stage membrane designs for CO_2 collection in a 600 MW coal-fired power plant in North Rhine-Westphalia, Germany, was carried out by Zhao *et al.*[469] To find the best CO_2/N_2 selectivity and capture costs, they conducted a sensitivity analysis using PEBAX polymer membranes and PRO/II software. A two-stage cascade system that achieved 70% CO_2 recovery and 95% purity for a feed gas containing 14% CO_2 had a capture cost of €31/t CO_2 ($\sim$32.2 \$/t CO_2, assuming an exchange rate of 1 € = 1.04 USD), according to the data, making it a feasible retrofit option. Correlations between membrane characteristics and system performance were also discovered by the study. According to these investigations, two-stage membrane systems can achieve 90% CO_2 recovery and 90–95% purity, making them

competitive with traditional amine-based CO_2 capture methods. Further research is necessary to determine if membrane-based CO_2 capture can remain competitive if recovery and purity standards rise from 90% to 98%. Further process optimization also requires analyzing the effects of these higher targets on the ideal number of membrane stages, membrane area, operating conditions, and overall cost.

The primary methods for determining the best membrane-based CCUS system configurations -taking into account the number of filtration steps, membrane size, and operating conditions- are process optimization techniques. One important factor to keep in mind is that the permeability and selectivity of the membrane are inextricably tied to the final product purity, membrane size, and operating conditions. Therefore, if future developments result in the creation and commercialization of membranes with greater permselectivity, any process optimization based on projected membrane performance could become outdated. Arias *et al.* used a mixed integer nonlinear mathematical programming (MINLP) modeling approach to find the optimal number of membrane stages, membrane areas, and operating conditions that minimize the total annual cost of CO_2 capture from flue gas[470] (Fig. 27). The number of membrane stages is highly influenced by the targeted CO_2 purity (Table 12). A two-stage system with one recycle stream was shown to be ideal for purity levels between 90% and 93%, however three stages and two recycle streams were needed to achieve 94% to 96% purity. Four membrane phases were required to maintain efficiency for higher purity standards of 97% and 98%. This approach shows the trade-offs between increasing CO_2 purity and its associated expenses. Higher purity requires a greater membrane area and higher energy usage due to increased pressure and compression requirements. Furthermore, Arias *et al.* showed that these enhanced multi-stage designs are competitive in terms of affordability and power consumption not only with traditional absorption-based CO_2 collection techniques but also with other membrane-based separation procedures. In order to guarantee the economic viability of membrane-based CCUS technologies, these findings highlight the significance of carefully choosing the number of separation steps based on the intended CO_2 recovery and purity.

Accordingly, process optimization plays a crucial role in enhancing the efficiency and cost-effectiveness of membrane-based CCUS systems. The studies reviewed demonstrate that multi-stage membrane configurations can achieve competitive CO_2 recovery and purity levels compared to conventional amine-based methods, with the optimal number of stages being highly dependent on the target purity. As CO_2 recovery and purity demands increase, additional membrane stages and higher membrane areas are required, leading to higher energy consumption and costs. However, advancements in membrane materials and further optimization of system configurations can help mitigate these challenges. Future research should focus on refining membrane properties, exploring alternative driving force mechanisms, and integrating novel separation strategies to improve the economic and environmental viability of CCUS technologies.

10. Comparison of membranes and conventional processes for CCUS

The right CCUS approach is determined based on the different CO_2 streams that industries emit, which vary in concentration, flow rate, pressure, temperature, and impurity levels. Different strategies are needed for small, medium, and large industries to maximize technological efficiency and economic viability. While this paper insists on the benefits of membranes as one of the pioneer candidates for CCUS application, there are cons and pros when it is compared to the more conventional processes such as amine-based absorption. Because amine-based absorption has a high capture efficiency ($>90\%$), it is the preferable method for large-scale businesses (such as cement and power plants) that produce high-volume, low-CO_2-concentration emissions (~ 3–15%). Hybrid amine-membrane systems, in which membranes pre-concentrate CO_2 to lower the regeneration energy of amine solvents, can be advantageous for medium-sized companies (such as chemical plants and ammonia production). High-purity CO_2 streams are produced by small-scale enterprises (such as small hydrogen plants and biogas upgrading), which makes membrane separation more feasible because of lower startup and operating costs. Nevertheless, until large scale membrane-based plants with higher efficiency would not be in practice a real comparison would be irrelevant. To offer a current comparative vision between the absorption and membrane processes, Table 13 brings different aspects of the technologies together.

The scale of the industry and operating costs determine whether CO_2 capture is economically viable. 50% of yearly running costs are related to amines' high energy requirements for solvent regeneration. Membranes, on the other hand, are appropriate for small-to-medium applications due to their lower energy consumption and versatility. Large-scale companies where the high capture efficiency outweighs the high energy and maintenance costs favour absorption-based CCUS. Small and medium-sized businesses can save money by using membrane-based separation, especially in decentralized environments like hydrogen manufacturing and biogas upgrading. One approach that shows promise is process integration. By pre-concentrating CO_2 prior to solvent regeneration, hybrid membrane-amine systems can increase energy efficiency. Additionally, to increase CO_2 purity and lower operating costs, membrane-based separation in conjunction with cryogenic procedures is being investigated.

Developing membrane separation and improving hybrid strategies to get around present constraints are key to the future of CCUS technologies. High-performance polymeric and MMMs will be the focus of material advances to improve durability, permeability, and selectivity. It is also crucial to conduct research on FTMs that provide better CO_2 separation in industrial settings.

To decrease solvent regeneration energy and increase membrane longevity, process improvement will entail a hybrid integration of amine absorption and membrane separation. While the investigation of cryogenic-membrane hybrids can enhance separation efficiency in high-volume applications, the

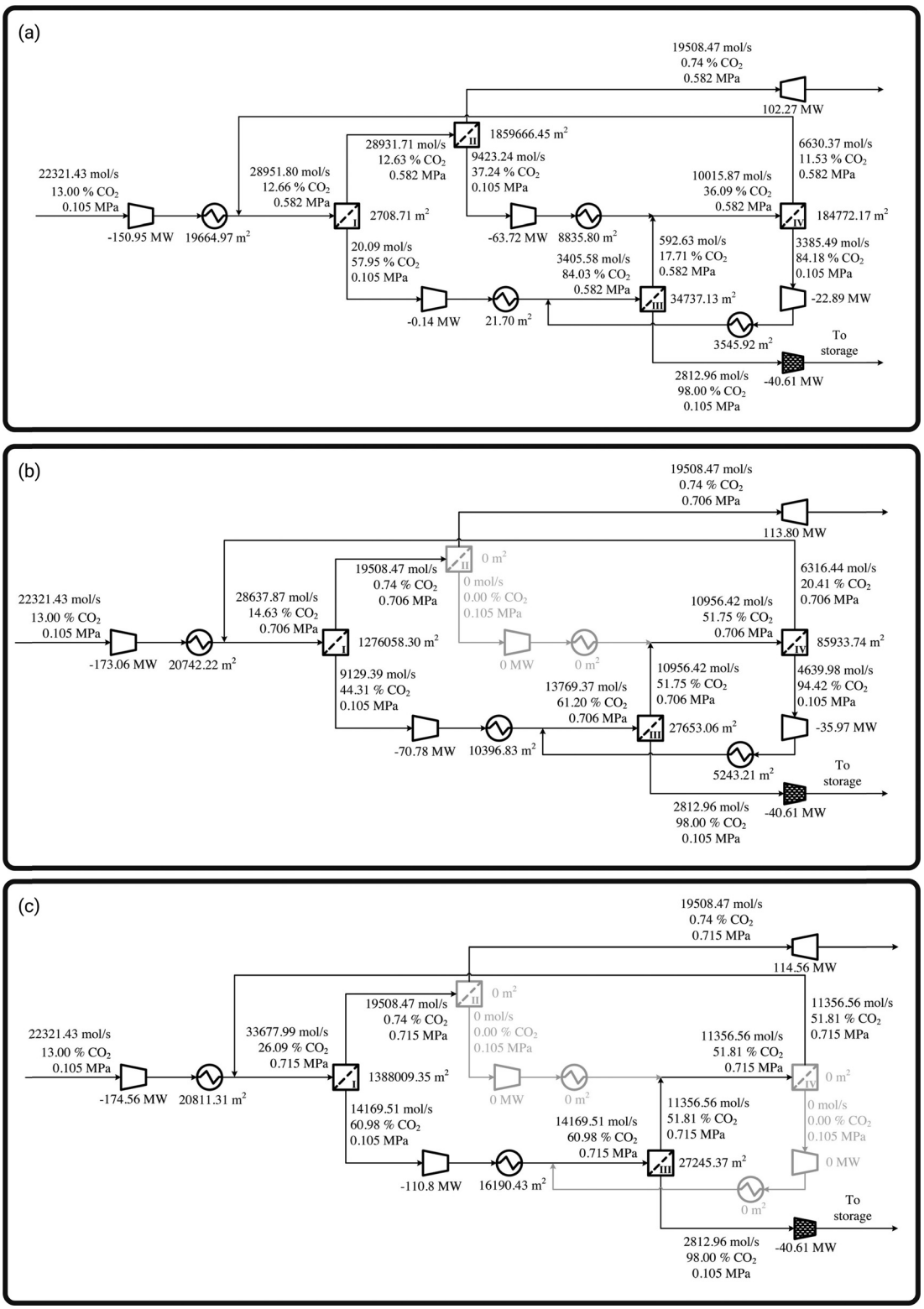

Fig. 27 Process simulation and optimization for membrane separation-based CCUS with different stages; (a) 4 stages, (b) 3 stages, and (c) 2 stages (reproduced from ref. 470 with permission from Elsevier, copyright 2025).

development of two-stage membrane systems will enable improved CO_2 purity and optimized energy consumption. When determining the cost break-even points at which membrane separation outperforms amine absorption, techno-economic analyses will be essential. It is necessary to assess long-term operating costs while taking membrane deterioration, replacement

Table 12 Parameter comparison for membrane-based CCUS processes with 4, 3, and 2 stages (reproduced from ref. 470 with permission from Elsevier, copyright 2025)

Variable	Optimal configuration (4 stages, Fig. 27(a))	Suboptimal configuration (3 stages, Fig. 27(b))	Suboptimal configuration (2 stages, Fig. 27(c))
TAC (M $ per year)	123.54	134.22	136.93
Total investment (M $ per year)	66.99	66.61	67.56
Total operating cost (M $ per year)	56.55	67.61	69.37
Total power (MW)	278.31	320.246	325.974
Power recovered in expander (MW)	102.272	113.8	114.55
Total net power (MW)	176.035	206.626	211.416
Total membrane area (m^2)	2082 164.65	1389 645.09	1415 254.71
Total heat transfer area (m^2)	32 523.82	36 382.26	37 001.73
Total compressed permeate flow rate (mol s^{-1})	12 828.82	13 769.37	14 169.51
High operating pressure (MPa)	0.586	0.706	0.715
Number of iterations	38	7	5

Table 13 Comparison of membrane separation and absorption for carbon capture

Feature	Amine absorption	Membrane separation
CO_2 capture efficiency	85–95%	50–90% (depends on membrane type & stages)
Energy consumption	3–6.5 GJ per ton CO_2	~1 GJ per ton CO_2
Selectivity	High for CO_2/N_2	Moderate, depends on membrane type
Operating pressure	Near ambient	Varies (vacuum-assisted options available)
Sensitivity to impurities	Highly sensitive (SO_2, NO_x cause degradation)	Plasticization and aging concerns but can be mitigated
Capital & operating costs	High due to solvent handling & regeneration	Lower due to modular design & no solvent regeneration
Scalability	Preferred for large-scale (>1 M ton CO_2 per year)	Best suited for small to medium industries
Commercial readiness	TRL 9 (Fully commercial)	TRL 6–7 (Pilot studies ongoing)

cycles, and scalability into account. It is also necessary to look at the viability of modular membrane modules designed for small-scale and decentralized industries.

Membrane separation and amine absorption each have unique benefits and drawbacks. Because of its high capture efficiency and commercial maturity, amine-based CCUS continues to be the industry standard for large-scale applications. Membrane-based systems, on the other hand, give small and medium-sized businesses a competitive edge by lowering energy and capital expenditure. The gap can be filled with additional hybridization and material developments.

11. Utilization of the captured carbon and the contribution of polymeric membranes

Utilization of captured carbon (CCU) is viewed as a promising pathway to address the limitations of conventional short-term solutions for carbon capture and storage (CCS). However, there is strong reasoning that CCS is the mature, well-understood, established, and only practical technique for meeting CO_2 emission reduction goals by 2050 and beyond, allowing ample time for a transition away from fossil fuels, thereby rendering CCU a highly unrealistic alternative to CCS.[471] The best approach to addressing conflicting reasoning among CO_2 emission reduction strategies is to view each process in its appropriate context. CCU should never be considered as the viable alternative to CCS for the mitigation of CO_2 emission challenge to meet net-zero to net-negative CO_2 emission milestones. It can rather be implemented in places where CO_2 is the only feedstock or process driver (*e.g.*, urea production or CO_2-enhanced oil recovery), CO_2 is the cheaper feedstock, or the CO_2-derived product can viably replace the alternative product, or the net CO_2 emission is not higher.[471] The fertilizer industry is the largest consumer, using approximately 130 Mt of CO_2 annually for urea manufacturing, while the oil sector follows closely, consuming 70 to 80 Mt of CO_2 for enhanced oil recovery (EOR).[472]

Polymeric membranes contribute to CCU in two major processes: (i) gas separation units, which are employed in membrane modules for the selective capture of CO_2 from flue gases, biogas, or natural gas streams, and (ii) membrane reactors, which enhance process efficiency and selectivity by integrating reaction and separation. The following discussion will focus on membrane reactors, as gas separation units were covered in previous sections.

11.1. Membrane reactors

Membrane reactors combine reaction and separation processes in a single unit, allowing for enhanced process efficiency, higher reaction rates, selectivity, and control.[473] The membrane component selectively separates one or more reaction mixture components, either by size, charge, or affinity, while allowing other components to pass through. This selective separation enables the continuous removal of reaction products or byproducts, shifting the reaction equilibrium towards the desired products and enhancing overall reaction rates. Membrane reactors find applications in CO_2 conversion processes, including hydrogenation of CO_2 to methanol, dry reforming of methane (DRM), reverse water gas shift (RWGS) reaction, CO_2 hydrogenation to formic acid, and

CO_2 methanation, among which the conversion to methanol and RWGS for fuel production is viewed as the most important CO_2 utilization pathway, presumably from a business perspective.

A membrane in a membrane reactor provides four basic functions: extractor to separate the desired products from the reaction mixture, distributor to introduce the required ratio of reactants into the reaction zone, contactor to enhance the surface contact of the reactants with the catalysts immobilized on the surface or embedded into the membrane layer, and extender of catalyst lifetime to enhance reaction rates by removing water (following Le Chatelier's principle), which acts as a reaction byproduct.[474] The two most common configurations for membrane reactors are the packed-bed membrane reactor (PBMR), where the membrane only separates products, and the catalytic membrane reactor (CMR), where the membrane acts as the catalyst support and separates products. There are four primary categories of membrane reactors: (i) electrochemical, (ii) thermocatalytic, (iii) photocatalytic, and (iv) biocatalytic. Among these, electrochemical membrane reactors typically do not utilize membranes for CO_2 or product separation.

Among these, electrochemical membrane reactors typically do not utilize membranes for CO_2 or product separation, nor do they serve as catalyst supports. Instead, the membrane acts as a barrier between the cathode and anode chambers, preventing the mixing of components while selectively conducting protons. This function is quite different from the concept of membrane reactors, where the membrane primarily serves as a means for selective reagent introduction, product separation (purification), and catalyst support. In membrane reactors, the membrane helps ensure the homogeneous distribution of catalysts and provides a large surface area for catalytic reactions. Consequently, the discussion will be confined to the remaining three categories, where membranes both support the catalyst and facilitate separation. Interested readers are encouraged to explore recent reviews on well-studied and industrially viable electrochemical CO_2 reduction technologies.[475–478]

11.1.1. Thermocatalytic membrane reactors. Thermocatalytic membrane reactors operate at higher temperatures (>100 °C). Therefore, thermocatalytic CO_2 conversion by a polymeric membrane reactor is limited by the thermal stability of the polymeric membrane, which has driven a vast interest in the development of low-temperature catalysts.[479,480] Inorganic membranes, such as zeolite membranes, perform better than cost-efficient polymeric membranes at high temperatures but suffer from deficiencies in selectivity in the separation process.[479] There are only a few studies on the use of polymeric membranes for thermocatalytic membrane reactors, where the membrane only serves the separation function,[481–485] and a few studies on using the membrane both as catalyst support and for separation.[486–488]

Zou *et al.* developed a WGS membrane reactor featuring a CO_2-selective polymeric membrane and a commercial Cu/ZnO/Al_2O_3 catalyst for hydrogen production suitable for use in proton-exchange membrane fuel cells (PEMFCs).[484] The membrane, made from cross-linked poly(vinyl alcohol) with fixed and mobile carriers that demonstrated good CO_2 selectivity and permeability at 110–170 °C, effectively removed CO_2 during the WGS, shifting the equilibrium towards more hydrogen production and reducing CO levels to below 10 ppm, meeting PEMFC hydrogen purity requirements. Lee *et al.* explored the use of polyimides (PI) membrane with 4,4′-(hexafluoroisopropylidene) diphthalic anhydride (6FDA) and hydroxyl aromatic diamines (2,2-bis(3-amino-4-hydroxyphenyl)hexafluoropropane (APAF) and 3,3′-dihydroxy-4,4′-diamino-biphenyl (HAB) copolymer) in a membrane reactor for CO_2 hydrogenation by the reverse WGS (Fig. 28(a)).[489] Integrating the polyimide membrane into the reactor enhances the yield of carbon monoxide (CO) by 2–3 times compared to reactors without the membrane by selectively removing the byproduct water. Additionally, the membrane exhibits high H_2O permselectivity at elevated temperatures due to bulky perfluoro moieties and local hydrophilicity provided by hydroxyl groups. The exceptionally high H_2O permselectivity at high temperatures is governed by the favorable solution-diffusion model, which is opposite to inorganic membranes, where adsorptive transport is the main mechanism for H_2O separation. These findings suggest that the use of polyimide hollow fiber membrane reactors can improve the efficiency of CO_2 hydrogenation reactions, particularly at low temperatures where equilibrium limitations typically hinder product yield.

The above studies involved membranes only for separation; the next studies will cover membranes acting mainly as catalysts or supports for catalysts in addition to separation. Considering the thermal stability concerns of polymeric membranes, exploring low-temperature CO_2 conversion pathways is deemed rational. Therefore, converting CO_2 to cyclic carbonate is a logical choice, as it is a 100% green reaction.[487] Liu *et al.* explored various compositions of ionic liquid monomers for preparing crosslinked block copolymer membranes for the conversion of CO_2 and propylene oxide (PO) to propyl carbonate (PC).[486] The variables considered for the monomer composition were the type of functional groups used for the quaternization of the tertiary amine groups of the 2-(dimethylamino)ethyl methacrylate (DMAEMA) block and the type of counterion for the positively charged quaternary ammonium ions. The best polymeric ionic liquid membrane (PILM) with a [DMAEMAE-tOH]Br-quaternized block resulted in the highest yield of PC (98%). The gas-phase PO conversion for PILMs was 28 times that of pure polymeric ionic liquids (PILs). The high catalytic activity of the PILM was attributed to the high density of catalyst active sites and the easy access of these sites to PO and CO_2 due to PO adsorption-induced swelling of the polymeric network, providing a microenvironment for the close contact of reagents. Despite a significant improvement in catalytic activity, this enhancement is brought about by membrane swelling, which can ultimately destroy the membrane under agitation; therefore, the stability of the membrane needs improvement. Process engineering, such as sandwiching the active membrane into a stable polymeric support, can play a crucial role in this case.

Xu *et al.* developed quaternized poly(4-vinylpyridine) (P4VP) membranes for selective CO_2 separation, followed by cycloaddition to epichlorohydrin to produce cyclic carbonates.[487] The (P4VP-C2-HCO3) membrane, made of quaternized poly(4-vinyl pyridine) (P4VP) followed by anion exchange of bromide (Br^- with bicarbonate (HCO_3^-), integrated both CO_2 capture from a

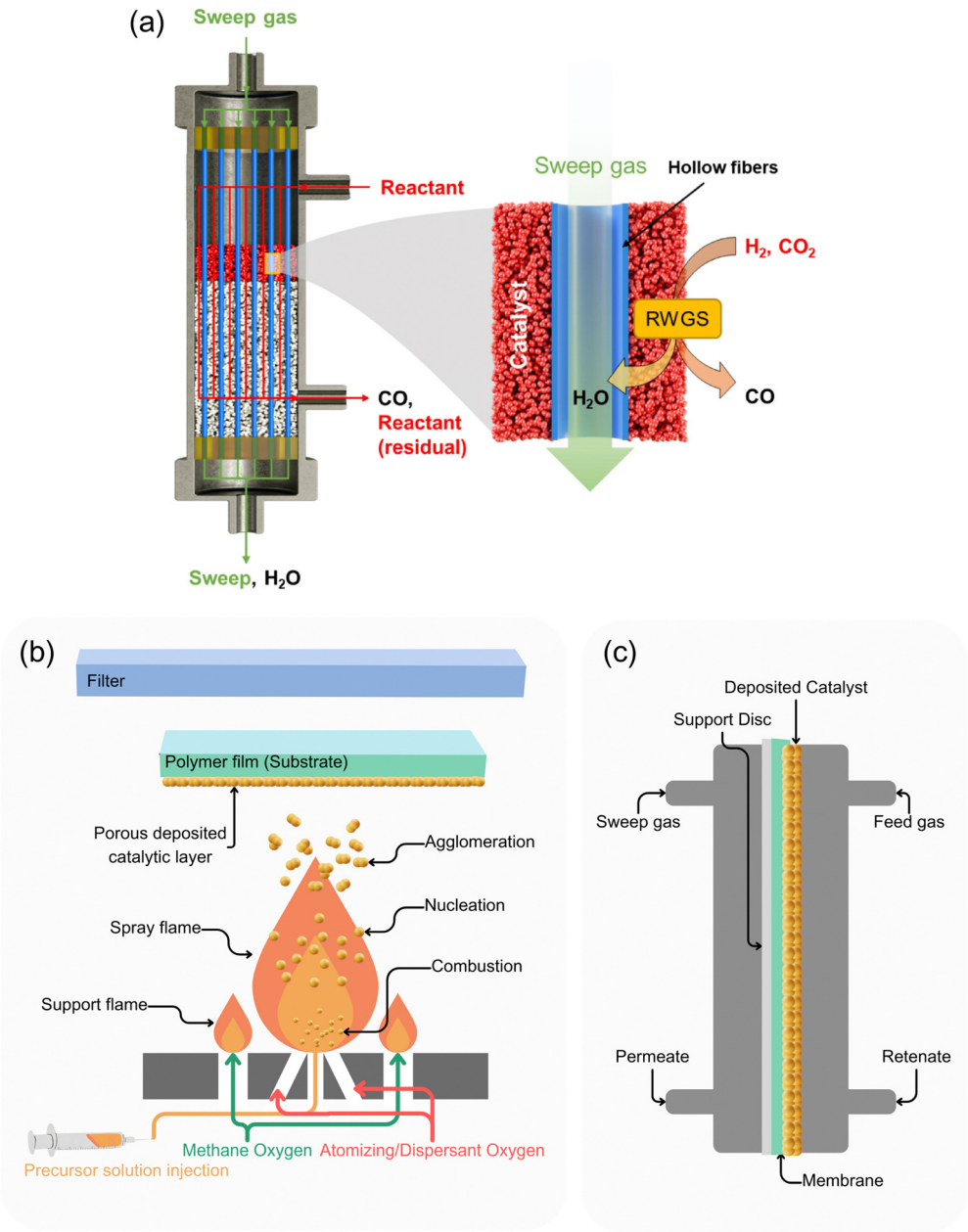

Fig. 28 Schematic illustration of: (a) the hollow fiber membrane reactor with membrane/catalyst and transport of gases (reproduced from ref. 489 with permission from Elsevier, copyright 2025), (b) flame spray pyrolysis-based deposition on the membrane, and (c) the resulting membrane reactor.[488]

dilute condition (similar to the concentration in air, 0.1 kPa of CO_2) and catalytic conversion to cyclic carbonate in a single platform under mild temperature (57 °C) and atmospheric pressure. The high catalytic activity of the (P4VP-C2-HCO3) membrane may be due to the favorable catalytic activity of HCO_3^- in the initiation step of ring-opening of epichlorohydrin and the final step of cyclic product release and HCO_3^- regeneration. Although the catalytic activity of the membrane was promising, the cyclic carbonate production rate decreased dramatically within 30 hours. The blockage of catalyst sites by strong adsorption of byproducts, such as glycidol or 3-chloro-1,2-propanediol, and the dissolution of the membrane in epichlorohydrin were associated with the decrease in production rate. Interestingly, the decline in rate over time was not considered. The reaction involves catalysis by HCO_3^-, which is generated by any quaternized polymeric membrane during the facilitated CO_2 transport process.[490,491] Therefore, any quaternized membrane will lead to a certain conversion rate, as in the quaternized membrane (P4VP-C2-Br) before the anion exchange used in this study. Therefore, it can be assumed that the initial reaction rate was higher due to the preexisting HCO_3^- in the P4VP-C2-HCO3 membrane, which depleted over time by reproducing CO_2, and the rate became similar to that of the quaternized membrane (P4VP-C2-Br) within 30 hours.[492] A remarkable advancement in catalytic membrane reactors for a commercially important product (methanol) was recently achieved by Pham *et al.* (Fig. 28(b and c)).[488] The authors

integrated strategies to enable high-temperature reactions (>200 °C) and enhance the reaction rate using high-temperature stable and highly water-permeable polyimide (PI) and polybenzimidazole (PBI) membranes, flame spray pyrolysis-based direct deposition of nanosized, highly porous, and active CuO/ZrO_2 thin layers on the membranes, and post-deposition reduction of CuO to Cu at a relatively low temperature (300 °C) under 5% H_2 in Ar. These strategies enabled the membrane to operate stably at 200 °C and 20 bar, with a 113% increase in CO_2 conversion and a 106% increase in methanol production compared to conventional reactors.

More interest and investment should be directed towards carefully selecting CO_2 utilization pathways that have no alternatives, are cost-effective, scalable, and incorporate efficient process design and integration. Efforts should also focus on improving polymeric membrane performance as both support and separator, and on ongoing research for low-temperature catalyst development. Polymeric membranes can play a vital role in enhancing the catalytic activity of encapsulated catalysts through coordination, in addition to their separation function. Birdja *et al.* used polymeric membranes to encapsulate the Indium(III) Protoporphyrin catalyst within a polymer matrix, improving the overall catalytic performance for CO_2 reduction.[493] The polymeric membranes examined were didodecyldimethylammonium bromide (DDAB), Nafion, poly(4-vinylpyridine) (P4VP), and poly(3,4-ethylenedioxythiophene) polystyrene sulfonate (PEDOT). They assessed the influence of different substrates and polymer encapsulation on catalytic efficiency. The study demonstrated that both the substrate and polymer encapsulation significantly impacted the efficiency and selectivity of CO_2 reduction to CO. The enhanced electrocatalytic CO_2 reduction performance by P4VP has been previously reported for catalysts like cobalt phthalocyanine (CoPc). This improvement is attributed to the pyridine residues in the polymer, which influence coordination with the catalyst,[433,434] P4VP can form strong interactions with the cobalt centers in the CoPc catalyst, improving the stability and distribution of the catalyst within the polymer matrix and enhancing overall catalytic activity and selectivity for CO_2 reduction[494]

Thermocatalytic membrane reactors offer key advantages over standard industrial thermocatalytic reactors by combining reaction and separation in one step, reducing the need for external purification. The membrane enables selective product removal, enhancing reaction efficiency and potentially increasing productivity by maintaining optimal thermodynamic conditions. These reactors can achieve high conversion rates, particularly for thermodynamically favorable reactions, though they require significant energy input to sustain necessary conditions.

11.1.2. Photocatalytic membrane reactors. Photocatalysis promotes sustainability and is considered green technology because it utilizes sunlight to drive chemical reactions under mild operating conditions, reducing energy consumption and environmental impact and offering a greener and less energy-intensive alternative to traditional thermo-catalysis methods.[495,496] Typically, polymeric photocatalytic membranes are produced using two fabrication methods, as illustrated in Fig. 29.

A large fraction of works on CO_2 conversion using membrane reactors are based on photocatalysis, which has been reviewed recently.[497,498] Only a few examples with high efficiency, feasibility, and process intensification will be discussed here. Pomilla *et al.* investigated the conversion of CO_2 to liquid fuels using photocatalytic methods within a continuous membrane reactor, where C_3N_4 nanosheets were embedded in a Nafion membrane.[499] Their setup achieved successful CO_2 conversion to liquid fuels at a rate of 32.8 μmol g^{-1} cat h^{-1}, with selectivity towards methanol (54.6%) and ethanol (45.4%). The continuous membrane reactor demonstrated a total carbon conversion rate more than 10 times higher compared to a batch reactor (Fig. 30). This enhanced performance is attributed to two key factors: (i) the dispersion of nanosheets within the Nafion polymer matrix provides greater exposure of active sites to light and reactants (ii) the continuous removal of products by the membrane promotes the forward reaction and frees active sites for further conversion. However, this method exhibited a low selectivity for methanol. Brunetti *et al.* improved both the alcohol production rate (48.8 μmol g^{-1} cat h^{-1}) and the selectivity for methanol

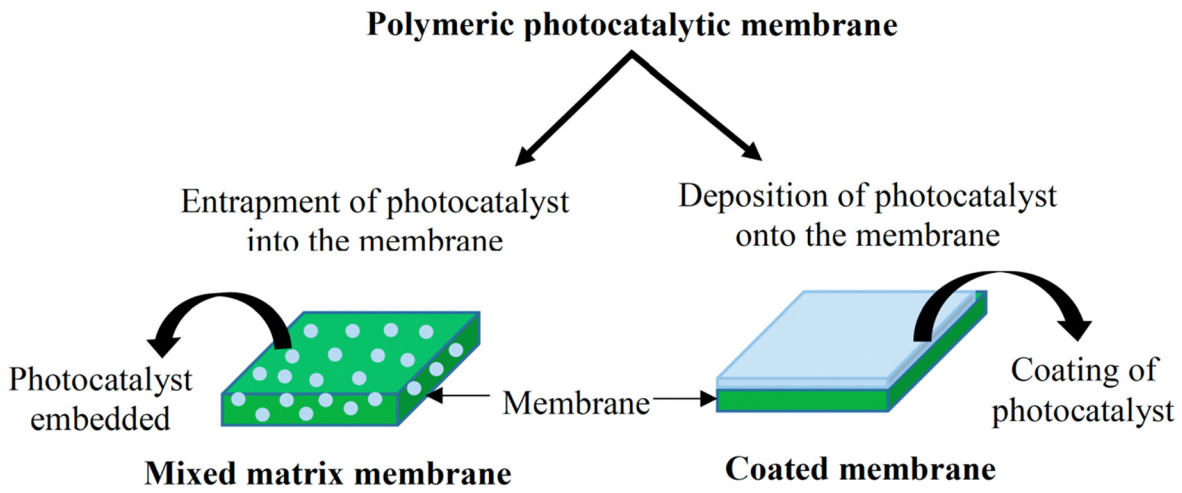

Fig. 29 Illustration of fabrication of polymeric photocatalytic membrane (reproduced from ref. 496 with permission from Elsevier, copyright 2025).

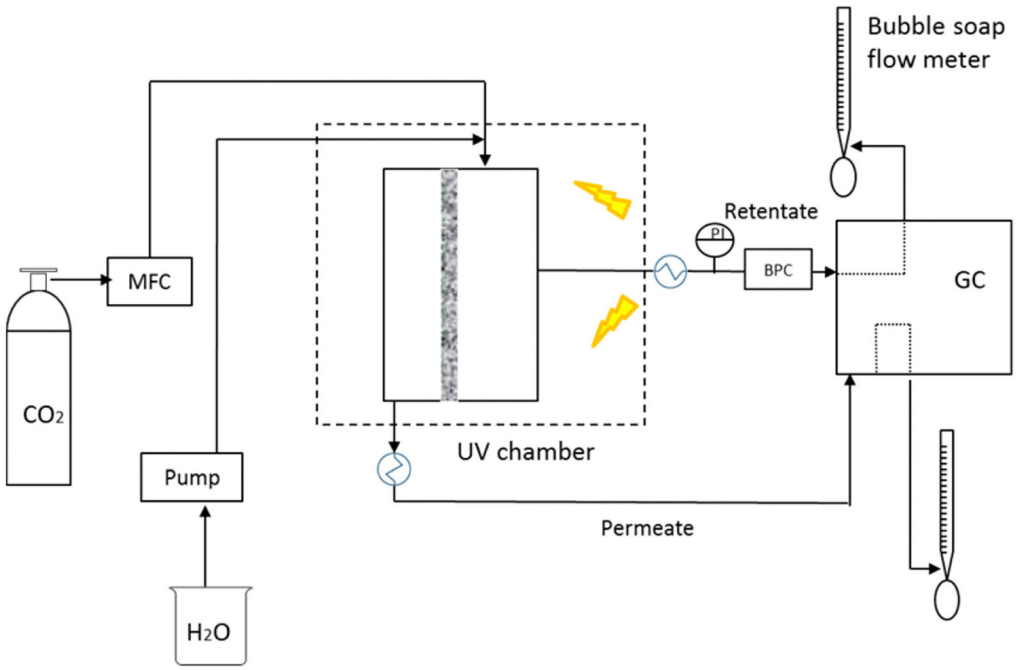

Fig. 30 Schematic for the continuous flow photocatalytic membrane reactor for the conversion of CO_2 to liquid fuels methanol and ethanol (reproduced from ref. 499 with permission from ACS, copyright 2025)

(83.2%) by incorporating a TiO_2–C_3N_4 composite into the Nafion membrane instead of using C_3N_4 alone.[500] The enhanced catalytic activity and selectivity for methanol were attributed to better charge separation at the heterojunction formed by the TiO_2–C_3N_4 interfaces.

In the quest to explore more efficient and selective photocatalysts, significant effort has been devoted to developing photocatalysts with tunable charge separation performance. This includes exploring MOF-based photocatalysts, as their photocatalytic activity and charge separation properties can be tuned by selecting photoactive organic ligands, doping with ions, or integrating photoactive materials.[497] Zhao *et al.* applied a comprehensive design strategy by incorporating CdS semiconductor nanorods and UiO-66-NH2 MOF into a chitosan-based membrane to enhance conversion efficiency and selectivity.[501] They selected CdS nanorods and UiO-66-NH2 MOF for efficient, broader light absorption and charge separation, thereby improving catalytic activity and selectivity. UiO-66-NH2 MOF served not only as a photoactive material but also as a highly selective CO_2 adsorption material, enhancing the reaction rate and selective reduction of CO_2 over other species in the reaction mixture. Chitosan was chosen as the membrane material for its highly selective adsorption of CO_2 and improved proton transport due to its abundant $-NH_2$ and –OH groups, which are critical for enhancing conversion rates and selectivity towards CO_2 reduction. These groups also interact favorably with the CdS nanorods and UiO-66-NH_2, providing uniform dispersion and suppressing agglomeration-induced photocatalytic deactivation. Consequently, the CdS/UiO-66-NH_2 membrane reactor demonstrated higher CO production (313.2 μmol g^{-1} cat) and selectivity (99%) than the mixed powder form (521.9 μmol g^{-1} cat, 95%) after 6 hours of irradiation.

Although incorporating photocatalysts into membrane matrices addresses many issues associated with bulk catalyst dispersion—such as aggregation, reduced active site availability, light-scattering, poor proton transfer, and catalyst recovery—the need for a pure CO_2 gas feed limits their applicability for selective product generation from crude gas mixtures.[497] Integrating a CO_2-selective gas separation membrane with a photocatalyst in a membrane reactor, where the membrane acts as a support for the catalyst and separates CO_2 from gas mixtures, can effectively resolve this issue.[497,502,503] Baniamer *et al.* designed a two-layer photocatalytic membrane reactor using Pebax 1657 as the CO_2-selective gas separation layer and BiFeO3@ZnS as the photocatalyst layer for simultaneous CO_2 separation and photoreduction to methanol.[445] Their reactor successfully demonstrated simultaneous CO_2 separation and photoreduction to methanol, with a methanol production yield of 5100 and 3360 μmol g^{-1} cat h^{-1} under UV and visible irradiation, respectively. This enhancement in methanol yield was attributed to the purified CO_2 feed provided by the Pebax membrane, the broader light absorption by the BiFeO3@ZnS photocatalyst, and efficient charge separation at the localized p–n junction between BiFeO3 and ZnS interfaces.

Most photocatalytic membrane reactors utilize high-concentration CO_2 feed gas, which requires costly separation and transportation steps. Direct air capture and conversion is the ideal scenario for addressing atmospheric CO_2 removal effectively and providing renewable resources for synthesizing value-added products. However, the low concentration of CO_2 in the air limits the rate of photocatalytic conversion, and other gases present in the air can adsorb onto the catalyst site, reducing efficiency and selectivity. To overcome this, Hu *et al.* developed a two-layered "Janus membrane" structure consisting of a polyimide (PI)

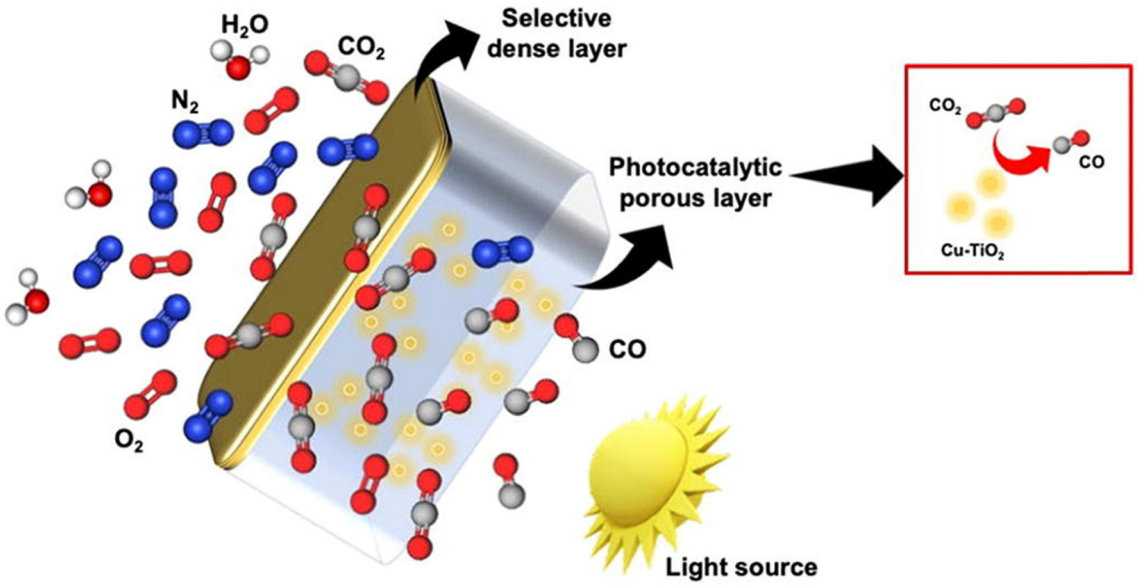

Fig. 31 Schematic for the direct capture and photocatalytic reduction of CO_2 from air using Janus Polyimide/Cu-doped TiO_2 membranes (reproduced from ref. 504 with permission from Elsevier, copyright 2025).

selective layer for CO_2 separation and enrichment from air, and a porous PI catalyst support layer embedded with Cu-doped TiO2 particles.[504] The dense PI layer separated and enriched CO_2 into the membrane, while the porous PI support layer allowed longer residence time for effective contact with the Cu-doped TiO_2 photocatalyst (Fig. 31). This approach was highly successful, achieving an optimum CO_2-to-CO conversion yield of 2.21 μmol g^{-1} cat h^{-1}.

Among various photocatalytic membrane reactors, direct air capture and conversion presents an economically viable renewable approach for producing CO_2-derived products and a reliable method for reducing atmospheric CO_2 levels. However, this process often has low efficiency, and the primary product is gaseous CO, which incurs additional isolation and storage costs. To address these challenges, a Janus membrane with broader solar light absorption, particularly visible light utilization (*e.g.*, BiFeO3@ZnS), should be developed. The selective layer of the membrane could be composed of CO_2-adsorbing and enriching materials like polyimide (PI), Pebax (PEBAX), or polybenzimidazole (PBI). The porous catalyst support layer could be fabricated from a blend of CO_2-philic and hygroscopic polymers or a block copolymer containing segments of both types to facilitate the enrichment and contact of CO_2 and H2O with the catalyst. This would enhance the production of liquid fuels such as methanol, which is easier to isolate, store, and serves as a valuable solvent and feedstock for various chemical processes.

Further process intensification strategies could be employed to improve CO_2 conversion efficiency and methanol storage. One such strategy involves placing the photocatalytic membrane on the surface of natural water bodies (*e.g.*, ponds, lakes, and rivers in urban areas) where sunlight is abundant. In these areas, CO_2 levels are generally higher due to human activities, infrastructure, and reduced vegetation. Additionally, elevated temperatures can facilitate humid air and CO_2-to-methanol conversion. The methanol collector could be submerged in the water, condensing the methanol, enhancing production rates, and maintaining a lower temperature for methanol storage.

Photocatalytic membrane reactors operate at lower temperatures and pressures than industrial thermocatalytic CO_2 conversion methods, making them more sustainable. However, their productivity is generally lower, which makes them more suited for small-scale or specialty applications focused on environmental sustainability. The membrane in these reactors offers the benefit of separating reactants and products, enhancing selectivity and efficiency by preventing undesired side reactions. Despite this, the slower reaction kinetics and limited light penetration hinder productivity compared to thermocatalytic or electrochemical systems, particularly at large scales. Solar-driven photocatalytic CO_2 reduction is appealing for its sustainability but faces challenges like low light utilization, scalability issues, and the need for new infrastructure. Large land coverage for solar light absorption and variability in sunlight intensity further impact its industrial feasibility. While not yet viable or profitable for large-scale industrial CO_2 conversion, solar-driven photocatalytic membrane reactors could serve as a long-term CO_2 removal strategy, potentially generating profit from conversion products in the future. In addition to advancing efficient photocatalysts, particularly in the visible light region, it is crucial to design reactors that optimize solar light use. This can be achieved by incorporating solar concentrators and strategically locating industries in regions with optimal solar light availability to enhance efficiency.

11.1.3. Biocatalytic membrane reactor. In a biochemical membrane reactor, microbial catalysts or enzymes can be integrated into the membrane to catalyze the reduction of CO_2 into value-added products, such as fuels. This approach presents a scalable, sustainable, and cost-effective method for the direct

production of bulk chemicals.[497] However, biochemical processes are currently limited by factors, including low CO_2 capture and conversion efficiency, complex processes, and the requirement for high temperatures for enzyme activation. Incorporating biocatalysts into a CO_2-philic membrane could address these challenges by improving CO_2 capture efficiency, enhancing the catalytic activity of enzymes *via* uniform distribution within the membrane matrix, optimizing contact with CO_2 in the membrane's porous microenvironment, and facilitating product separation from the reaction site for *in situ* catalyst regeneration. Additionally, photothermal materials can be incorporated into the membrane alongside enzymes to provide heat for enzyme activation. However, the development and application of biocatalytic membrane reactors remain largely unexplored.

Díaz *et al.* employed a hollow-fiber membrane for sparging H_2 into the bioreactor, which enhanced H_2 mass transfer into the liquid phase and improved the conversion of CO_2 and H_2 to CH_4. However, in this case, the membrane did not serve as a catalyst support or a medium for product separation.[505] On the other hand, Luo *et al.* pioneered the use of a membrane as support for biocatalyst immobilization by co-immobilizing or sequentially immobilizing three enzymes—formate dehydrogenase (FDH), formaldehyde dehydrogenase (FaldDH), and alcohol dehydrogenase (ADH)—within the porous structure of a membrane to promote sequential conversion of CO_2 to methanol.[506] Although this approach was innovative, the immobilization did not enhance the conversion of CO_2 to methanol. The complete conversion pathway from CO_2 to methanol involves three steps: (1) FDH-catalyzed conversion of CO_2 to formic acid, (2) FaldDH-catalyzed conversion of formic acid to formaldehyde, and (3) ADH-catalyzed conversion of formaldehyde to methanol. The primary bottleneck identified was the reversible step catalyzed by FaldDH, which converts formic acid to formaldehyde. Additionally, the slow conversion of CO_2 to formic acid by FDH produced insufficient substrate to activate FaldDH effectively in the second step. To overcome these limitations, future strategies could include engineering mutations in FaldDH, identifying alternative enzymes or cofactors for efficient formic acid to formaldehyde conversion, or designing layered membrane structures with supports optimized for each enzyme's catalytic activity. For example, embedding FDH into a membrane that maintains a slightly alkaline environment could facilitate formic acid to formate transformation, given that FaldDH and ADH efficiently convert formate to methanol.[507]

Interestingly, contrasting results were reported when the three enzymes were co-immobilized into siliceous mesostructured cellular foams, achieving a 4.5-fold increase in CO_2 conversion to methanol.[508] In this study, enzyme immobilization was performed through incubation, as opposed to the pressurized filtration method used for membrane pore immobilization, which may have led to enzyme agglomeration or over-compaction, hiding their catalytic active sites. Therefore, adopting ambient pressure conditions for enzyme immobilization and conducting conversion reactions under low pressure may help realize the full benefits of enzyme immobilization.

Biocatalytic membrane reactors operate under milder conditions, making them more sustainable than traditional reactors. The membrane helps with catalyst separation, reusability, and product separation, which facilitates purification. However, their scalability is limited by reaction rates and the stability of biocatalysts. While they excel in selectivity and sustainability, enzyme deactivation or microbial growth can reduce productivity. In contrast, traditional thermocatalytic reactors achieve higher productivity and are better suited for large-scale CO_2 conversion, although they require high temperatures and pressures. Biocatalytic systems offer moderate productivity in controlled environments but do not match the throughput of thermocatalytic or electrochemical systems. More focus should be placed on developing low-temperature, high-efficiency, and robust thermocatalytic membrane reactors for large-scale, profitable CO_2 conversion technologies.

11.2. Enhanced oil recovery

Enhanced oil recovery (EOR) is one of the most prominent and established methods of Carbon Capture and Utilization (CCU), playing a crucial role in both improving oil extraction efficiency and mitigating CO_2 emissions. The process involves injecting captured CO_2 into existing oil reservoirs to enhance crude oil recovery, typically following primary and secondary recovery stages.[509] Through EOR, CO_2 acts as a solvent that reduces the viscosity of the trapped oil and increases its mobility, enabling the extraction of otherwise inaccessible oil. In this process, a significant portion of the injected CO_2 remains sequestered underground, contributing to carbon storage while simultaneously increasing oil yield.[510,511]

The concept of EOR is grounded in the principle that the injection of CO_2 can improve oil displacement efficiency within the reservoir. CO_2-EOR is categorized into two main types:

(i) Miscible CO_2-EOR: this occurs when CO_2 fully dissolves in the crude oil, reducing its viscosity and increasing the oil's mobility. Miscibility typically occurs under high-pressure conditions. The injected CO_2 mixes with the oil, lowering its interfacial tension and causing the oil to swell, thus improving its flow toward the production wells.[512]

(ii) Immiscible CO_2-EOR: in cases where reservoir conditions do not allow full miscibility, CO_2 can still enhance oil recovery by displacing oil through its sheer pressure and causing the oil to move toward production wells. Although less efficient than miscible EOR, this method still improves recovery compared to conventional methods.[512,513]

EOR projects have been implemented in numerous regions worldwide, including North America, the Middle East, and Southeast Asia. In the United States, the Permian Basin is a leading example of CO_2-EOR deployment, where captured CO_2 from industrial sources is injected into mature oil fields. Approximately 400 000 barrels of oil per day were produced through CO_2-EOR in the U.S. as of 2019.[514] With the rising demand for carbon management solutions, the application of CO_2-EOR is expected to expand globally, particularly in regions with declining conventional oil reserves. It is worth noting that a major share of the injected CO_2 remains permanently sequestered underground,

contributing to carbon storage while simultaneously increasing oil yield. However, the focus on EOR as a justification for CO_2 sequestration requires a broader perspective, as many industrial carbon capture applications prioritize sequestration over oil recovery. For instance, facilities like the waste-to-energy plant at Klemetsrud in Norway and petrochemical plants in Europe focus primarily on capturing CO_2 for permanent sequestration rather than utilizing it for EOR. The facility at Oslo, is set to become the world's first waste-to-energy plant with full-scale CCS by 2026, targeting the capture of 400 000 tonnes of CO_2 annually. The project is part of Norway's 'Longship' initiative and demonstrates the potential for significant emission reductions in waste incineration through CCS.[515,516] On the other hand, projects such as the Port Arthur, Texas Carbon Capture Project demonstrate how CO_2 is captured, transported, and injected into geologic formations for long-term storage, with no connection to oil recovery. These cases demonstrate that the industrial demand for carbon capture extends beyond EOR and into permanent sequestration strategies to address climate change. In the Port Arthur Carbon Capture Project, Air Products and Chemicals retrofitted two steam methane reformers at their hydrogen production facility in Port Arthur to capture over 90% of CO_2 emissions. Since 2013, the project has captured approximately 1 million tonnes of CO_2 annually, which is transported *via* pipeline for use in EOR operations.[517,518]

11.2.1. Benefits and challenges of CO_2-EOR. The benefits of CO_2-EOR are as follows:[519–521]

Increased oil recovery: CO_2-EOR can increase the amount of recoverable oil from a reservoir by 10–20% beyond conventional methods. This represents a substantial economic benefit for oil producers.

Carbon storage: a major advantage of CO_2-EOR is its dual role in both enhancing oil recovery and sequestering CO_2 underground. Estimates suggest that for every ton of CO_2 injected, 0.5–0.7 tons can remain permanently stored.

CO_2 recycling: during the EOR process, a portion of the injected CO_2 is produced along with the oil, but it can be captured, separated, and re-injected back into the reservoir, further improving the CO_2 utilization efficiency.

Despite the high promise, the following challenges remain:[521,522]

Reservoir suitability: the success of CO_2-EOR depends heavily on the characteristics of the reservoir, including pressure, temperature, and rock properties. Not all oil fields are suitable for CO_2 injection, and achieving miscibility may require very high pressures, making the process energy-intensive.

CO_2 availability and infrastructure: a reliable supply of captured CO_2 is essential for large-scale CO_2-EOR operations. Establishing pipelines and storage facilities to transport CO_2 from industrial sources to oil fields requires substantial upfront investment.

Economic viability: the financial benefits of EOR depend on oil prices and the cost of CO_2 capture and transportation. While CO_2-EOR can be profitable under favorable economic conditions, fluctuating oil prices threaten its long-term viability.

11.2.2. Environmental considerations. CO_2-EOR represents a significant opportunity to reduce CO_2 emissions through permanent sequestration in geological formations. However, concerns have been raised regarding potential leakage from the storage sites over time. Proper site selection, monitoring, and regulatory oversight are necessary to ensure the long-term integrity of CO_2 storage in EOR operations.[523,524]

Furthermore, while CO_2-EOR offers a temporary solution for utilizing captured CO_2, it does not eliminate the need to transition away from fossil fuel dependence in the long term. The process, by increasing oil production, paradoxically contributes to higher overall carbon emissions from the combustion of the additional oil produced. As a result, EOR must be seen as part of a broader strategy for carbon management, in conjunction with other forms of storage and utilization technologies aimed at achieving net-zero emissions.[525,526]

11.2.3. Future prospects for CO_2-EOR. With advancements in membrane technology, polymeric membranes have the potential to further optimize the EOR process by enhancing gas separation and CO_2 purity prior to injection. Membrane-based gas separation units, covered earlier in this discussion, can help reduce energy costs and improve the overall efficiency of CO_2 capture and preparation for EOR applications. As the demand for CCU solutions grows, CO_2-EOR is likely to remain a significant application in the medium term. However, its contribution to carbon management goals will need to be balanced with considerations for renewable energy development and broader efforts to reduce fossil fuel reliance.[527,528]

12. Technology readiness level of membrane technologies for CCUS and impact measurement

CCUS (Carbon Capture, Utilization, and Storage) processes can be evaluated from multiple perspectives: environmental impact, feasibility and scalability, economic viability, and technology readiness. The Technology Readiness Level (TRL) serves as a classification tool to determine a technology's maturity. In general, the earlier TRL stages raise questions regarding a technology's likelihood of success, while higher TRL levels indicate commercial viability and practical scalability. However, it is crucial to note that a higher TRL does not necessarily equate to an optimal process or a flawless solution. For example, amine-based absorption, with a TRL of 9, is widely adopted in various industrial sectors but remains energy-intensive and economically unfeasible for smaller-scale applications.[99,529] Advances in the technical aspects of any field, process, or technology will influence both its TRL level and the overall costs associated with CCUS. Table 14 highlights the progress made in CCUS TRL levels since 2014 and their current status.

A closer examination of technologies within different sectors of the CCUS industry provides a clearer perspective on where each separation or utilization technology stands in terms of TRL. However, a region-specific experience can yield a more realistic evaluation of these technologies since cases are more practically assessed in local contexts. For instance, a report from the Government of Alberta presents the TRL status of existing technologies for CO_2 separation and utilization.

Table 14 Technology readiness of different CCUS technologies[99,529,530]

Technology		TRL 2014	TRL (current)	Examples of current practices	Comments
	Common amine solvents	9	9	Widely used in fertilizer, soda ash, natural gas processing plants, *e.g.* Sleipner, Snøhvit, and used in Boundary Dam since 2014	Commonly practiced in different industries, perfect for large-scale applications, energy extensive solvent regeneration, sensitivity of chemicals to impurities and oxygen,
	Physical solvent (Selexol, Rectisol)	9	9	Widely used in natural gas processing, coal gasification plants, *e.g.* Val Verde, Shute Creek, Century Plant, Coffeyville Gasification, Great Plains Synfuels Plant, Lost Cabin Gas plant	CAPEX and OPEX reductions are still a concern,
	Sterically hindered amine	6–8	6–9	Demonstration to commercial plants depending on technology providers, *e.g.* Petra Nova carbon capture	The environmental impact of the harmful chemicals is still a barrier
	Amino acid-based solvent*/ Precipitating solvents	4–5	4–5	Lab test to conceptual studies	
	Ionic liquids	1	2–3	Lab tests	
Solid adsorbents	Pressure swing Adsorption/vacuum Swing adsorption	3	9	Air Products Port Arthur SMR CCS	
	Temperature swing Adsorption (TSA)	1	5–7	Large pilot tests to FEED studies for commercial plants	
	Electrochemically Mediated Adsorption	1	1	Lab tests only	
Chemical looping	Calcium looping	6	6–7	Feasibility/cost studies for commercial scale	The technology uses a very cheap and abundant sorbent. The sorbent is susceptible to chemical deactivation due to competing reactions and deterioration in capture capacity
	Chemical looping combustion	2	5–6	Pilot tests	
Bioprocesses	Carbon biofixation	—	4–6	Microalgae cultivation and biomass co-firing for power generation	
Cryogenic	Cryogenic packed bed/ antisublimation system	—	3–4		Well-developed for natural gas decarbonization, uncertain to apply for post-combustion flue gas
Membranes	Gas separation membranes for natural gas processing	—	9	Petrobras santos basin pre-salt oil field CCS	Well-developed lab studies and a few pilot scale plants with variable CAPEX and OPEX depending on the scale
	Polymeric Membranes	6	7	FEED studies for large pilots	
	Electrochemical membrane integrated with MCFCs	—	7	Large pilots at plant barry	
	Polymeric membranes/ cryogenic separation hybrid	6	6	Pilot studies	
	Polymeric membranes/solvent hybrid	—	4	Conceptual studies	
	Room temperature Ionic liquid (RTIL) Membranes	2	2	Lab test	
	Inorganic membranes	—	3	Lab test	
	Facilitated transport membranes	—	6–7	The pre-pilot field testing was implemented at the cement industry	

Polymeric membranes are currently at the pilot study stage, but the operational scale may be smaller for high-performance FTM materials compared to other membrane types (Fig. 32). This underscores the significance of simultaneously exploring several promising polymeric membrane candidates to leverage a larger operational scale.

An essential insight from the Canadian Government's comprehensive study (carried out by Emission Reduction Alberta (ERA) and Alberta Innovates (AI)) is that the success of CO_2 utilization is strongly linked to the effectiveness of large-scale carbon capture technologies. Consequently, the scalability of membrane separation technologies for small- and medium-sized processes is a significant advantage. The utilization of captured carbon is projected to account for around 10% of the CCUS market, indicating that further technological and economic advancements in membrane-based utilization technologies are necessary to develop more practical applications.

The recent surge in interest in various carbon capture processes stems from climate change mitigation policies and the push towards sustainable development goals (SDGs) established both internationally and locally. Different approaches exist to measure various aspects of sustainability, with the most well-known being the triple bottom line (TBL) approach. TBL encompasses environmental, economic, and social dimensions of sustainability. Environmental sustainability focuses on measuring and reducing carbon and ecological footprints, preventing

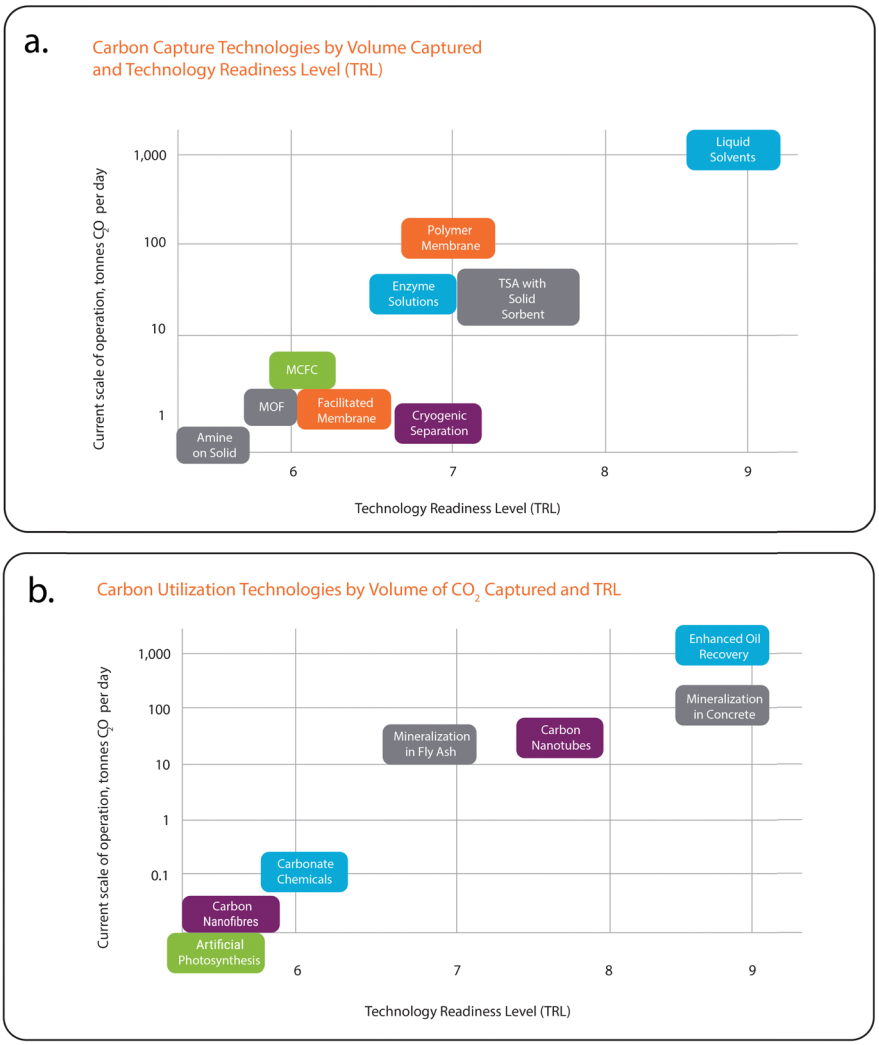

Fig. 32 Technology readiness level of (a) carbon capture technologies, (b) utilization technologies, reported by Alberta Innovates[531]

resource depletion, conserving biodiversity, and monitoring air, water, and soil pollution. Social sustainability addresses quality of life, equity, community well-being, and income distribution. Economic sustainability targets gross domestic product (GDP) and its adjustments to provide a holistic measure of economic progress, investment in renewable resources and efficiency, and the assessment of public and private debt relative to economic output.

Another important approach is the Environmental Life Cycle Impact (LCA), which evaluates the full process of a technology or product. A recent study has compared CCUS technologies for power plant decarbonization, including a membrane hybrid process.[532] Most LCA studies use the "cradle to grave" perspective, covering the entire lifecycle from raw material extraction to final disposal. Table 15 provides summarized data to offer comparative insights into the scale and environmental impacts of these projects. While this review emphasizes the importance of case sensitivity in CCUS processes and cautions against drawing broad conclusions, it is crucial to note that the use of membranes-either as standalone systems or in hybrid processes—can significantly reduce environmental impact. Membrane-based technologies demonstrate high capacity, suggesting their practicality for industries producing substantial emissions. However, focusing solely on power generation emissions is only part of the picture; a comprehensive assessment of other industries and processes is necessary, as suggested by the framework from Cuéllar-Franca *et al.*[532]

13. Outlook and concluding remarks

This review has provided an in-depth analysis of membrane technologies for CCUS applications, with a particular focus on polymeric, mixed-matrix, and emerging materials embedded with fillers such as MOFs and MXenes. Due to their compact design, high performance, and ease of scalability, membrance technologies are promising for carbon capture and separation in various industrial settings. Despite these advantages, several persistent challenges—such as plasticization, physical aging, and the inherent permeability-selectivity trade-off—must be addressed to fully realize the potential of membrane-based CCUS at scale.

Table 15 Environmental impact Life cycle assessment (LCA) of post-combustion carbon capture and separation (CCS) as well as carbon capture and utilization (CCU) (reproduced through Elsevier open access policy from ref. 532 with permission from, copyright 2025)

Case	Process	Storage or utilization	Functional unit[a]	Impact	Ref.
Cradle-to-grave LCA for coal-fired power plant	Chemical absorption, membrane and cryogenic separation, and pressure swing adsorption	Storage: geological and ocean	1 MW h	Global warming potential Acidification potential	533
Cradle-to-grave LCA for pulverized coal-fired power plant	Chemical absorption	Storage: geological	1 kW h	Abiotic depletion potential Acidification potential Eutrophication potential Fresh water aquatic ecotoxicity potential Global warming potential Human toxicity potential Marine aquatic ecotoxicity potential Ozone depletion potential Photochemical ozone creation potential Terrestrial ecotoxicity potential	534
Cradle-to-grave dynamic LCA of different power plants	Chemical absorption and oxy-fuel combustion	Storage: Ocean	1 kW h	Acidification potential Global warming potential Human toxicity potential Fresh water aquatic ecotoxicity potential Marine aquatic ecotoxicity potential Terrestrial ecotoxicity potential	535
Cradle-to-grave dynamic LCA of different power plants	Chemical absorption and oxy-fuel combustion	Storage: Ocean	1 MW h	Abiotic depletion potential Acidification potential Eutrophication potential Global warming potential Human toxicity potential Marine aquatic ecotoxicity potential Ozone depletion potential Photochemical ozone creation potential	536

[a] A unit of electricity generated, expressed either in kW h, MW h or TW h.

While conventional CCUS technologies like absorption–stripping, adsorption, and cryogenic methods continue to play a vital role, membrane-based approaches provide unique benefits that could make them the next frontier in CO_2 capture. The development of advanced materials and hybrid membrane systems, combined with ongoing innovations in separation mechanisms and membrane design, signals significant progress. However, achieving industrial adoption will require further research to enhance selectivity, durability, and economic feasibility.

Future efforts should focus on translating laboratory-scale breakthroughs into commercial applications, with a strong emphasis on collaboration across academia, industry, and policy. Such partnerships are crucial for addressing current limitations, optimizing hybrid solutions, and advancing technology readiness. With sustained innovation and strategic investment, membrane-based CCUS technologies have the potential to significantly contribute to global decarbonization efforts, helping to curb greenhouse gas emissions and support long-term climate sustainability goals.

13.1. Critical challenges in membrane technology for CCUS

Plasticization. Plasticization occurs when polymeric membranes are exposed to high CO_2 pressures, causing swelling, increased chain mobility, and reduced selectivity. This phenomenon compromises the membrane's effectiveness in separating CO_2 from other gases, such as nitrogen or methane. To mitigate plasticization, strategies include crosslinking polymer chains to restrict their flexibility, incorporating rigid nanofillers, and developing FTMs with CO_2-reactive carriers. Crosslinking, in particular, enhances membrane stability under high-pressure conditions, though it can reduce permeability if not carefully optimized.

Physical aging. In glassy polymers, physical aging gradually reduces free volume, leading to a decline in gas permeability and separation efficiency over time. This issue is especially problematic for thin-film membranes, which are more susceptible to aging due to their high surface area-to-volume ratio. Crosslinking has shown promise in addressing physical aging by restricting polymer chain mobility, thereby enhancing the membrane's mechanical stability and lifespan. However, the trade-off between enhanced stability and permeability must be carefully managed to maintain optimal performance.

Permeability-selectivity trade-off. The Robeson upper bound represents a significant barrier in membrane technology, where increases in permeability often result in decreased selectivity. MMMs, which embed nanofillers like MOFs, CNTs, or MXenes into polymer matrices, offer a potential solution by improving both properties. These nanofillers create selective pathways for CO_2 transport, enhancing diffusivity-selectivity while maintaining or even increasing permeability. Achieving uniform nanofiller dispersion and avoiding agglomeration, however, remains as the critical challenges as inconsistencies can lead to performance degradation.

Thermal, mechanical and chemical stability (resistance to degradation). Industrial CCUS processes frequently operate under harsh conditions, including high temperatures, elevated

pressures, and exposure to corrosive chemicals. While inorganic membranes, such as zeolites and MOFs, offer superior thermal and chemical stability, they often lack the selectivity and flexibility of polymeric membranes. Developing hybrid membranes that harness the thermal stability of inorganic components, and the flexibility of polymers will be essential for large-scale CCUS applications. Polyimide and polybenzimidazole (PBI) membranes, in particular, have shown considerable promise for high-temperature applications, providing a potential pathway forward in tackling this challenge.

A more in-depth discussion on how different impurities could affect the performance of the polymeric membranes was offered previously. Looking at the concept from the point of membrane structure itself, highlights the importance of "degradation-resistant" membrane material design. The ideal gas separation membrane should be resistant to other degradation risks depending on the process in which it is going to be applied. As an instance, FTMs are prone to degradation due to reaction with NH3 and H2S.[401] Acidic degradation of the polymeric membranes alters the free volume and changes the performance of the membrane. Chemical stability must be a major focus in the polymeric structure design for the membrane fabrication, as any undesired reaction between the functional sites of the polymer and the process stream could intensify the degradation.[158,537] Age-induced degradation is also a concept described earlier in "Physical aging" section. Temperature-induced degradation is also a concern in precombustion CCS processes suppressing the lifetime of the membranes.[537]

Degradation affects the lifetime, efficiency, and overall cost-effectiveness of membrane-based CCUS processes. The cost of polymeric membranes ranges from \$50 to \$400 per m^2, depending on material composition and fabrication complexity.[150–155] MMMs could cost similarly depending on the nanomaterial loading and synthesis expenses.[435] Compared to conventional amine-based absorption processes, membrane technology presents a lower operating cost due to its energy efficiency (2 to 5.5 GJ per ton CO_2 less energy consumption (Table 4)) and reduced solvent handling. To be able to push the CCUS membrane technologies toward commercialization, degradation—whether thermal, chemical, or mechanical— as a major challenge influencing maintenance and replacement frequency must be considered. To address assess this challenge, Table 16 summarizes the economic implications of degradation in different membrane types, including projected replacement cycles and cost per ton of CO_2 captured. It is worth mentioning that membrane-based technologies are highly process-dependent, *i.e.* the degradation profile and its effect on the scalability of the process highly depends on the operating conditions, harshness of the streams and the nature of the impurities. Optimizing materials and incorporating predictive AI/ML models for degradation forecasting can support material stability and boost economic feasibility. Nevertheless, more research should focus on developing stable, high-performance polymeric membranes with improved resistance to acidic gases (SO_2, NO_x) and thermal aging, which currently limit industrial scalability.

13.2. Potential solutions

Crosslinking and advanced functionalization. Crosslinking remains an effective strategy to combat plasticization and physical aging in membranes. Innovative approaches, such as flexible or partial crosslinking, are being developed to enhance membrane stability while preserving free volume and permeability. Crosslinkers like siloxanes, which add flexibility to the membrane matrix, are especially beneficial as they help maintain permeability while minimizing plasticization effects. Additionally, surface functionalization with CO_2-philic groups, such as amine groups, can significantly enhance CO_2 solubility and selectivity, thereby boosting membrane performance.

Incorporation of nanofillers and hybrid membranes. MMMs that incorporate nanofillers—such as MOFs, CNTs, and MXenes—show considerable promise in addressing the permeability-selectivity trade-off. These nanomaterials provide selective diffusion pathways and improve CO_2 adsorption, resulting in enhanced separation performance. Achieving uniform dispersion of nanofillers and ensuring strong polymer-nanofiller interactions are essential to fully realize the potential of MMMs. Among these, MXenes stand out due to their excellent CO_2 affinity and high permeability, making them a focal point for future research.

Facilitated transport membranes (FTMs). FTMs employ mobile or fixed carriers, like amines, to selectively bind and transport CO_2 across the membrane, yielding high selectivity and permeability—particularly valuable for post-combustion CO_2 capture. The primary challenge lies in refining carrier chemistry and optimizing membrane structure to maximize CO_2 transport efficiency while maintaining stability over extended periods. Recent advancements in FTMs have centered on enhancing carrier regeneration and preventing carrier saturation under high CO_2 pressures, which are essential for improving membrane lifespan and efficiency.

Table 16 Polymeric membrane degradation comparison, numbers are rough estimation could vary for different scenarios[21,538,539]

Membrane type	Cost (\$/m^2)	Degradation rate (% per year)	Lifespan (years)	CO_2 capture cost (\$ per ton)	Key Challenges
Polymeric (*e.g.*, Polyimide, PEBAX)	50	10	2	30	Prone to plasticization; lower thermal stability, short life time
Mixed matrix membrane (MMMs)	120	6	3	30	Dispersion issues; interface compatibility, reactivity of the nanomaterials with the impurities
Inorganic (*e.g.*, Zeolite, MOF)	300	3	4	40	High fabrication cost; scalability challenges
Hybrid (polymeric + inorganic)	200	4	4	30	Optimization of polymer–inorganic interactions

Hybrid membrane reactors. Membrane reactors, which integrate reaction and separation processes within a single unit, hold significant potential for process intensification in CCUS applications. Hybrid membrane reactors that combine catalytic reactions with CO_2 separation can greatly enhance overall process efficiency, especially in CO_2 conversion processes like methanation or hydrogenation. The development of stable, selective, and high-performance membranes for these reactors is a promising research direction, offering substantial benefits for CO_2 utilization and conversion in industrial applications.

13.3. Future prospects and research directions

Development of advanced materials. The future success of membrane technology in CCUS hinges on the development of advanced materials with application-specific properties. Research should prioritize synthesizing novel polymers and hybrid materials that combine high permeability, selectivity, and durability. Advanced nanomaterials, such as MOFs, MXenes, and COFs, present exciting possibilities for enhancing membrane performance. However, challenges around material stability, scalability, and cost must be addressed to make these materials viable for large-scale applications.

Computational and AI-driven design. AI and ML are revolutionizing the design and optimization of new membrane materials. By harnessing large datasets and predictive models, AI can accelerate the identification of promising polymer structures, optimize fabrication techniques, and predict long-term performance across diverse operating conditions. This data-driven approach could significantly reduce the time and costs associated with developing high-performance membranes for CCUS applications, enabling faster translation from research into industry.

Process intensification and integration. The integration of membrane-based separation processes with existing industrial systems is essential for maximizing efficiency and minimizing costs. Coupling membrane modules with other CCUS technologies—such as adsorption, absorption, or cryogenic separation—can yield hybrid systems that combine the strengths of multiple approaches. Additionally, research should focus on the design of membrane reactors that allow simultaneous reaction and separation, which could be transformative for CO_2 conversion and utilization applications.

Economic feasibility and scale-up. There are significant obstacles in scaling up membrane technologies for industrial usage, even with encouraging laboratory-scale developments. Future studies should focus on improving membrane durability in practical settings, streamlining fabrication processes, and lowering material prices. To assess the viability of large-scale deployment, techno-economic analysis is essential, particularly in energy-intensive industries like steel, cement, and power generation.

The process design criteria, such as the number of separation stages and membrane performance, impacts on how cost-effective CO_2 capture is. According to research, multi-stage membrane topologies offer a competitive recovery rate and purity levels while maximizing energy utilization, making them a strong substitute for conventional amine-based techniques. Process integration, operating pressure, and membrane selectivity are some of the variables that affect these systems' economic viability. It has been shown that two-stage membrane systems can recover up to 90% of CO_2 with purity levels of 90–95% at capture costs between \$32 and \$45 per ton CO_2. Further sophisticated multi-stage procedures can improve purity even further, but they come with higher energy and operational complexity costs. For example, surpassing 95% CO_2 purity frequently calls for more separation processes, bigger membrane surfaces, and higher compression energy, all of which raise expenses. According to optimization models, two-stage and three-stage systems can offer a more realistic balance between cost and performance, even though four-stage systems offer greater separation efficiency.

Advances in membrane materials, better process integration, and the use of energy recovery techniques are likely to keep the CO_2 capture prices on the decline going forward. Higher purity requirements (97–98%) are still difficult to meet, nevertheless, and necessitate careful balances between energy use and financial feasibility. To further lower costs and increase scalability, future research should concentrate on improving membrane materials, increasing system efficiency, and investigating hybrid capture systems.

Sustainability and green chemistry. As industries move towards sustainable practices, the development of eco-friendly and biodegradable membranes is gaining importance. Biopolymers, such as cellulose and chitosan, along with green solvents and sustainable manufacturing processes, are emerging as viable alternatives to conventional synthetic polymers. Research in this area should focus on optimizing the performance of biopolymer-based membranes while minimizing their environmental footprint, contributing to the broader goal of sustainable, green CCUS technologies.

Utilization. The economic viability of CCU is anticipated to increase dramatically in the upcoming years due to developments in catalysis, process integration, and renewable energy coupling. Despite being a niche option now in comparison to CCS, CCU's ability to convert CO_2 into chemicals, fuels, and construction materials is in line with the concepts of the circular economy and lessens dependency on products generated from fossil fuels. Future studies should concentrate on creating selective, scalable, and low-energy catalytic systems, especially for feedstocks made of polymers, synthetic hydrocarbons, and CO_2-to-methanol. By enabling continuous product separation and lowering energy usage, the coupling of membrane technologies with electrochemical and photocatalytic processes may further increase efficiency. Furthermore, the trend toward CO_2-derived synthetic fuels and DAC may make CCU a crucial component of industrial decarbonization, especially when fueled by excess renewable energy. Despite these developments, CCU still has problems with scalability, energy consumption, and the logistics of CO_2 delivery. To avoid transferring environmental costs rather than lowering net emissions, widespread adoption of CCU will necessitate a comprehensive assessment of life-cycle emissions, economic viability, and infrastructure adaption. The availability of low-carbon hydrogen and affordable CO_2 collection technologies, which are still

major obstacles, are also essential to CCU's success. Furthermore, there is currently little market demand for items created from CO_2, thus finding high-value uses that guarantee financial sustainability is essential. In order to develop a competitive and sustainable CCU sector, future research should tackle these issues through hybrid technology integration, process intensification, and policy-driven incentives. CCU can support CCS plans by generating income streams and lowering reliance on carbon-intensive raw materials, but it won't completely replace CCS in reaching deep decarbonization.

Data availability

No primary research results, software or code have been included and no new data were generated or analysed as part of this review.

Conflicts of interest

There are no conflicts to declare.

Acknowledgements

M. Sadrzadeh acknowledges the financial support for this work by the Natural Science and Engineering Research Council of Canada (NSERC) and Canada's Oil Sands Innovation Alliance (COSIA) under NSERC ALLRP 556293-20. J.-Y. Cho acknowledges the financial support by NRCan's Office of Energy Research and Development, National Research Council of Canada and Government of Canada. M. Soroush and M. Mozafari would like to acknowledge financial support from the U.S. National Science Foundation under Grant No. CMMI-2134607. Any opinions, findings, and conclusions or recommendations expressed in this material are those of the authors and do not necessarily reflect the views of the National Science Foundation.

References

1 C. Bataille, N. Melton, S. Stiebert and P. Eng, *The potential to decarbonize Canadian heavy industry*.
2 P. Warrian and A. Homeira, *Innovation and de-carbonization in the Canadian steel industry*, 2021.
3 T. Vass and M. Jaccard, *Energy and Materials Research Group*, Simon Fraser University, 2017.
4 K. Zaman and M. Abd-el Moemen, *Renewable Sustainable Energy Rev.*, 2017, **74**, 1119–1130.
5 T. Wilberforce, A. G. Olabi, E. T. Sayed, K. Elsaid and M. A. Abdelkareem, *Sci. Total Environ.*, 2021, **761**, 143203.
6 R. P. Bhatt, *Renewable hydropower technologies*, 2017, **1**, 75–98.
7 M. Aneke and M. Wang, *Appl. Energy*, 2016, **179**, 350–377.
8 S. Yu, L. Agbemabiese and J. Zhang, *Appl. Energy*, 2016, **165**, 107–118.
9 B. Metz, O. Davidson, H. De Coninck, M. Loos and L. Meyer, *IPCC special report on carbon dioxide capture and storage*, Cambridge University Press, Cambridge, 2005.
10 X. Xu, Y. Xu, J. Li, Y. Lu, A. Jenkins, R. C. Ferrier, H. Li, N. C. Stenseth, D. O. Hessen and L. Zhang, *iScience*, 2023, **26**(6), 106798.
11 N. R. Kabange, Y. Kwon, S.-M. Lee, J.-W. Kang, J.-K. Cha, H. Park, G. D. Dzorkpe, D. Shin, K.-W. Oh and J.-H. Lee, *Sustainability*, 2023, **15**, 15889.
12 L. Cameron and A. Carter, Why Carbon Capture and Storage Is Not a Net-Zero Solution for Canada's Oil and Gas Sector, International Institute for Sustainable Development, 2023.
13 T. Wilberforce, A. Baroutaji, B. Soudan, A. H. Al-Alami and A. G. Olabi, *Sci. Total Environ.*, 2019, **657**, 56–72.
14 R. Ben-Mansour, M. A. Habib, O. E. Bamidele, M. Basha, N. A. A. Qasem, A. Peedikakkal, T. Laoui and M. Ali, *Appl. Energy*, 2016, **161**, 225–255.
15 M. G. Plaza, A. S. González, C. Pevida, J. J. Pis and F. Rubiera, *Appl. Energy*, 2012, **99**, 272–279.
16 M.-B. Hägg and A. Lindbråthen, *Ind. Eng. Chem. Res.*, 2005, **44**, 7668–7675.
17 A. Mousavinejad, A. Rahimpour, M. R. Shirzad Kebria, S. Khoshhal Salestan, M. Sadrzadeh and N. Tavajohi Hassan Kiadeh, *Ind. Eng. Chem. Res.*, 2020, **59**, 12834–12844.
18 F. Pazani, M. S. Maleh, M. Shariatifar, M. Jalaly, M. Sadrzadeh and M. Rezakazemi, *Renewable Sustainable Energy Rev.*, 2022, **160**, 112294.
19 R. S. K. Valappil, N. Ghasem and M. Al-Marzouqi, *J. Ind. Eng. Chem.*, 2021, **98**, 103–129.
20 C. Z. Liang, T.-S. Chung and J.-Y. Lai, *Prog. Polym. Sci.*, 2019, **97**, 101141.
21 M. Rezakazemi, M. Sadrzadeh and T. Matsuura, *Prog. Energy Combust. Sci.*, 2018, **66**, 1–41.
22 A. R. Kamble, C. M. Patel and Z. Murthy, *Renewable Sustainable Energy Rev.*, 2021, **145**, 111062.
23 K. Xie, Q. Fu, G. G. Qiao and P. A. Webley, *J. Membr. Sci.*, 2019, **572**, 38–60.
24 Y. Alqaheem, A. Alomair, M. Vinoba and A. Pérez, *Int. J. Polym. Sci.*, 2017, **2017**, 4250927.
25 B. Sasikumar, G. Arthanareeswaran and A. Ismail, *J. Mol. Liq.*, 2018, **266**, 330–341.
26 W. F. Yong and H. Zhang, *Prog. Mater. Sci.*, 2021, **116**, 100713.
27 G. Li, W. Kujawski, R. Válek and S. Koter, *Int. J. Greenhouse Gas Control*, 2021, **104**, 103195.
28 G. Genduso, W. Ogieglo, Y. Wang and I. Pinnau, *J. Membr. Sci.*, 2024, 122533.
29 H. Li and J. Yan, *Appl. Energy*, 2009, **86**, 2760–2770.
30 Y. Zhang, T. Wang, W.-P. Pan and C. E. Romero, *Advances in ultra-low emission control technologies for coal-fired power plants*, Woodhead Publishing, 2019.
31 W. H. Organization, *WHO global air quality guidelines: particulate matter (PM2. 5 and PM10), ozone, nitrogen dioxide, sulfur dioxide and carbon monoxide*, World Health Organization, 2021.
32 P. Bains, P. Psarras and J. Wilcox, *Prog. Energy Combust. Sci.*, 2017, **63**, 146–172.
33 M. Ouikhalfan, O. Lakbita, A. Delhali, A. H. Assen and Y. Belmabkhout, *Energy Fuels*, 2022, **36**, 4198–4223.

34 R. Xu and B. Lin, *J. Cleaner Prod.*, 2017, **140**, 1330–1343.
35 M. Shen, L. Tong, S. Yin, C. Liu, L. Wang, W. Feng and Y. Ding, *Sep. Purif. Technol.*, 2022, 121734.
36 J. G. Speight, *Nat. Gas*, 2019, 59–98.
37 Q. Yang, Q. Lin, S. Sammarchi, J. Li, S. Li and D. Wang, *Greenhouse Gases: Sci. Technol.*, 2021, **11**, 52–68.
38 Á. A. Ramírez-Santos, C. Castel and E. Favre, *Sep. Purif. Technol.*, 2018, **194**, 425–442.
39 Á. A. Ramírez-Santos, C. Castel and E. Favre, *J. Membr. Sci.*, 2017, **526**, 191–204.
40 H. Li, Ø. Wilhelmsen and J. Yan, *Handbook of clean energy systems*, 2015, pp. 1–17.
41 C. Zhao, J. Lv, G. Li, Q. Zhang, Y. Zhang, S. Liu and Y. Chi, *Thermochim. Acta*, 2019, **676**, 20–26.
42 E. Luna-Ortiz, K. Szklarczyk-Marshall, M. Winter and E. McAllister-Fognini, Impact of hydrogen as impurity in the physical and transport properties of CO2 streams in CCS/CCUS transport systems: A technical discussion, in *Proceedings of the 15th Greenhouse Gas Control Technologies Conference*, 2021, pp. 15–18.
43 P. C. Chen and Y.-L. Lai, *Energies*, 2019, **12**, 2202.
44 Z. Liang, K. Fu, R. Idem and P. Tontiwachwuthikul, *Chin. J. Chem. Eng.*, 2016, **24**, 278–288.
45 M. Babar, M. A. Bustam, A. Ali, A. S. Maulud, U. Shafiq, A. Mukhtar, S. N. Shah, K. Maqsood, N. Mellon and A. M. Shariff, *Cryogenics*, 2019, **102**, 85–104.
46 R. Soltani, M. Rosen and I. Dincer, *Int. J. Hydrogen Energy*, 2014, **39**, 20266–20275.
47 X. Wu, C. Wu and S. Wu, *Chem. Eng. Res. Des.*, 2015, **96**, 150–157.
48 S. Cloete, M. N. Khan and S. Amini, *Int. J. Hydrogen Energy*, 2019, **44**, 3492–3510.
49 U. Zahid, S. S. Khalafalla, H. A. Alibrahim, U. Ahmed and A. G. A. Jameel, *Energy Convers. Manage.*, 2023, **296**, 117681.
50 A. A. Olajire, *Energy*, 2010, **35**, 2610–2628.
51 T. C. Drage, C. E. Snape, L. A. Stevens, J. Wood, J. Wang, A. I. Cooper, R. Dawson, X. Guo, C. Satterley and R. Irons, *J. Mater. Chem.*, 2012, **22**, 2815–2823.
52 D. Y. C. Leung, G. Caramanna and M. M. Maroto-Valer, *Renewable Sustainable Energy Rev.*, 2014, **39**, 426–443.
53 P. Fennell and B. Anthony, *Calcium and chemical looping technology for power generation and carbon dioxide (CO2) capture*, Elsevier, 2015.
54 Z. H. Liang, W. Rongwong, H. Liu, K. Fu, H. Gao, F. Cao, R. Zhang, T. Sema, A. Henni and K. Sumon, *Int. J. Greenhouse Gas Control*, 2015, **40**, 26–54.
55 R. Stanger, T. Wall, R. Spörl, M. Paneru, S. Grathwohl, M. Weidmann, G. Scheffknecht, D. McDonald, K. Myöhänen and J. Ritvanen, *Int. J. Greenhouse Gas Control*, 2015, **40**, 55–125.
56 H. I. Mathekga, B. O. Oboirien and B. C. North, *Int. J. Energy Res.*, 2016, **40**, 878–902.
57 M. Ditaranto and J. Hals, *Combust. Flame*, 2006, **146**, 493–512.
58 H. Liu, R. Zailani and B. M. Gibbs, *Fuel*, 2005, **84**, 833–840.
59 E. Koohestanian and F. Shahraki, *J. Environ. Chem. Eng.*, 2021, **9**, 105777.
60 A. Gopan, P. Verma, Z. Yang and R. L. Axelbaum, *Int. J. Greenhouse Gas Control*, 2020, **95**, 102936.
61 Y. Tan, K. V. Thambimuthu, M. A. Douglas and R. Mortazavi.
62 M. Simmonds, I. Miracca and K. Gerdes, *in Greenhouse Gas Control Technologies 7*, Elsevier, 2005, pp. 1125–1130.
63 F. Châtel-Pélage, R. Varagani, P. Pranda, N. Perrin, H. Farzan, S. J. Vecci, L. U. Yongqi, S. Chen, M. Rostam-Abadi and A. C. Bose, *Therm. Sci.*, 2006, **10**, 119–142.
64 M. B. Toftegaard, J. Brix, P. A. Jensen, P. Glarborg and A. D. Jensen, *Prog. Energy Combust. Sci.*, 2010, **36**, 581–625.
65 S. Seddighi, P. T. Clough, E. J. Anthony, R. W. Hughes and P. Lu, *Appl. Energy*, 2018, **232**, 527–542.
66 M. M. Hossain and H. I. de Lasa, *Chem. Eng. Sci.*, 2008, **63**, 4433–4451.
67 C.-C. Cormos, *Int. J. Hydrogen Energy*, 2012, **37**, 13371–13386.
68 L. Zhu, Y. He, L. Li and P. Wu, *Energy*, 2018, **144**, 915–927.
69 H. J. Richter and K. F. Knoche, *Reversibility of combustion processes*, ACS Publications, 1983.
70 J. Hu, V. V. Galvita, H. Poelman and G. B. Marin, *Materials*, 2018, **11**, 1187.
71 M. Qasim, M. Ayoub, N. A. Ghazali, A. Aqsha and M. Ameen, *Ind. Eng. Chem. Res.*, 2021, **60**, 8621–8641.
72 Z. Cheng, L. Qin, J. A. Fan and L.-S. Fan, *Engineering*, 2018, **4**, 343–351.
73 J. Dai and K. J. Whitty, *Chem. Eng. Process.*, 2022, **174**, 108902.
74 R. D. Solunke and G. t Veser, *Ind. Eng. Chem. Res.*, 2010, **49**, 11037–11044.
75 N. Ruthwik, D. Kavya, A. Shadab, N. Lingaiah and C. Sumana, *Chem. Eng. Process.*, 2020, **153**, 107959.
76 M. Erans, E. S. Sanz-Pérez, D. P. Hanak, Z. Clulow, D. M. Reiner and G. A. Mutch, *Energy Environ. Sci.*, 2022, **15**, 1360–1405.
77 C. Intervention, Committee on Geo engineering Climate: Technical Evaluation and Discussion of Impacts, 2015.
78 O. Al Yafiee, F. Mumtaz, P. Kumari, G. N. Karanikolos, A. Decarlis and L. F. Dumée, *Chem. Eng. J.*, 2024, 154421.
79 Z. Li, X. Qin, Y. Li, H. Su, W. Zhang, G. Xu, Q. Ma, L. Hua and Q. Xu, *Future Batteries*, 2024, 100020.
80 P. Yuan, Z. Qiu and J. Liu Recent enlightening strategies for CO_2 capture: a review, in *IOP Conference Series: Earth and Environmental Science*, IOP Publishing., 2017, vol. 64, no. 1, p. 012046.
81 X. Wang and C. Song, *Front. Energy Res.*, 2020, **8**, 560849.
82 W. Y. Hong, *Carbon Capture Sci. Technol.*, 2022, **3**, 100044.
83 Z. Abubakar, E. M. Mokheimer and M. M. Kamal, *Int. J. Energy Res.*, 2021, **45**, 17461–17479.
84 L. M. Romeo, S. Espatolero and I. Bolea, *Int. J. Greenhouse Gas Control*, 2008, **2**, 563–570.
85 B. Aghel, S. Sahraie and E. Heidaryan, *Energy*, 2020, **201**, 117618.
86 M. Sharif, T. Zhang, X. Wu, Y. Yu and Z. Zhang, *Int. J. Greenhouse Gas Control*, 2020, **97**, 103059.
87 B. Aghel, S. Janati, S. Wongwises and M. S. Shadloo, *Int. J. Greenhouse Gas Control*, 2022, **119**, 103715.
88 N. J. M. C. Penders-van Elk, E. S. Hamborg, P. J. G. Huttenhuis, S. Fradette, J. A. Carley and G. F. Versteeg, *Int. J. Greenhouse Gas Control*, 2013, **12**, 259–268.

89 F. A. Chowdhury, H. Okabe, S. Shimizu, M. Onoda and Y. Fujioka, *Energy Procedia*, 2009, **1**, 1241–1248.
90 F. A. Chowdhury, H. Okabe, H. Yamada, M. Onoda and Y. Fujioka, *Energy Procedia*, 2011, **4**, 201–208.
91 F. A. Chowdhury, H. Yamada, T. Higashii, K. Goto and M. Onoda, *Ind. Eng. Chem. Res.*, 2013, **52**, 8323–8331.
92 F. Porcheron, A. Gibert, M. Jacquin, P. Mougin, A. Faraj, A. Goulon, P.-A. Bouillon, B. Delfort, D. Le Pennec and L. Raynal, *Energy Procedia*, 2011, **4**, 15–22.
93 F. Porcheron, A. Gibert, P. Mougin and A. Wender, *Environ. Sci. Technol.*, 2011, **45**, 2486–2492.
94 G. Puxty, R. Rowland, A. Allport, Q. Yang, M. Bown, R. Burns, M. Maeder and M. Attalla, *Environ. Sci. Technol.*, 2009, **43**, 6427–6433.
95 P. Singh, J. P. M. Niederer and G. F. Versteeg, *Chem. Eng. Res. Des.*, 2009, **87**, 135–144.
96 S. Park, H.-J. Song, M.-G. Lee and J. Park, *Korean J. Chem. Eng.*, 2014, **31**, 125–131.
97 S.-Y. Oh, S. Yun and J.-K. Kim, *Appl. Energy*, 2018, **216**, 311–322.
98 J. D. Figueroa, T. Fout, S. Plasynski, H. McIlvried and R. D. Srivastava, *Int. J. Greenhouse Gas Control*, 2008, **2**, 9–20.
99 N. MacDowell, N. Florin, A. Buchard, J. Hallett, A. Galindo, G. Jackson, C. S. Adjiman, C. K. Williams, N. Shah and P. Fennell, *Energy Environ. Sci.*, 2010, **3**, 1645–1669.
100 H. Zhai and E. S. Rubin, *Environ. Sci. Technol.*, 2013, **47**, 3006–3014.
101 I. Iliuta and M. C. Iliuta, *AIChE J.*, 2017, **63**, 2996–3007.
102 P. Brandl, M. Bui, J. P. Hallett and N. Mac Dowell, *Int. J. Greenhouse Gas Control*, 2022, **120**, 103771.
103 C. C. Chatziasteriou, E. S. Kikkinides and M. C. Georgiadis, *Comput. Chem. Eng.*, 2022, 107938.
104 I. P. Koronaki, L. Prentza and V. Papaefthimiou, *Renewable Sustainable Energy Rev.*, 2015, **50**, 547–566.
105 F. de Meyer and S. Jouenne, *Curr. Opin. Chem. Eng.*, 2022, **38**, 100868.
106 R. Zhao, L. Liu, L. Zhao, S. Deng, S. Li and Y. Zhang, *Renewable Sustainable Energy Rev.*, 2019, **114**, 109285.
107 M. Songolzadeh, M. T. Ravanchi and M. Soleimani, *Int. J. Chem. Biomol. Eng.*, 2012, **6**, 906–913.
108 N. Hedin, L. Andersson, L. Bergström and J. Yan, *Appl. Energy*, 2013, **104**, 418–433.
109 M. K. Mondal, H. K. Balsora and P. Varshney, *Energy*, 2012, **46**, 431–441.
110 A. S. Holmes, B. C. Price, J. M. Ryan and R. E. Styring, *Oil Gas J.*, 1983, **81**(26), 85–86.
111 M. T. Besong, M. M. Maroto-Valer and A. J. Finn, *Int. J. Greenhouse Gas Control*, 2013, **12**, 441–449.
112 C. Font-Palma, O. Errey, C. Corden, H. Chalmers, M. Lucquiaud, M. S. del Rio, S. Jackson, D. Medcalf, B. Livesey and J. Gibbins, *Process Saf. Environ. Prot.*, 2016, **103**, 455–465.
113 A. Ali, K. Maqsood, N. Syahera, A. B. M. Shariff and S. Ganguly, *Chem. Eng. Technol.*, 2014, **37**, 1675–1685.
114 C. Font-Palma, D. Cann and C. Udemu, *C*, 2021, **7**, 58.
115 C. Song, Q. Liu, S. Deng, H. Li and Y. Kitamura, *Renewable Sustainable Energy Rev.*, 2019, **101**, 265–278.
116 C. Ampelli, S. Perathoner and G. Centi, *Philos. Trans. R. Soc., A*, 2015, **373**, 20140177.
117 A. Alaswad, M. Dassisti, T. Prescott and A. G. Olabi, *Renewable Sustainable Energy Rev.*, 2015, **51**, 1446–1460.
118 W. Y. Cheah, P. L. Show, J.-S. Chang, T. C. Ling and J. C. Juan, *Bioresour. Technol.*, 2015, **184**, 190–201.
119 S.-H. Ho, W.-M. Chen and J.-S. Chang, *Bioresour. Technol.*, 2010, **101**, 8725–8730.
120 S.-H. Ho, C.-Y. Chen, D.-J. Lee and J.-S. Chang, *Biotechnol. Adv.*, 2011, **29**, 189–198.
121 G. Hu, N. J. Nicholas, K. H. Smith, K. A. Mumford, S. E. Kentish and G. W. Stevens, *Int. J. Greenhouse Gas Control*, 2016, **53**, 28–40.
122 X. Xu, X. Gu, Z. Wang, W. Shatner and Z. Wang, *Renewable Sustainable Energy Rev.*, 2019, **110**, 65–82.
123 S. S. Warudkar, K. R. Cox, M. S. Wong and G. J. Hirasaki, *Int. J. Greenhouse Gas Control*, 2013, **16**, 342–350.
124 J. Liu, D. S.-H. Wong, S.-S. Jang and Y.-T. Shen, *J. Taiwan Inst. Chem. Eng.*, 2017, **73**, 12–19.
125 J. Pirklbauer, G. Schöny, F. Zerobin, T. Pröll and H. Hofbauer, *Energy Procedia*, 2017, **114**, 2173–2181.
126 D. Bahamón García, A. Díaz-Márquez, P. Gamallo Belmonte and L. F. Vega, *Chem. Eng. J.*, 2018, **342**, 458–473.
127 R. Haghpanah, R. Nilam, A. Rajendran, S. Farooq and I. A. Karimi, *AIChE J.*, 2013, **59**, 4735–4748.
128 B. Wu, X. Zhang, Y. Xu, D. Bao and S. Zhang, *J. Cleaner Prod.*, 2015, **101**, 251–261.
129 M. Shen, L. Tong, S. Yin, C. Liu, L. Wang, W. Feng and Y. Ding, *Sep. Purif. Technol.*, 2022, **299**, 121734.
130 K. Nguyen, I. Iliuta, L.-C. Pasquier, F. Bougie and M. C. Iliuta, *Appl. Energy*, 2024, **376**, 124207.
131 J. Pires, M. Alvim-Ferraz, F. Martins and M. Simões, *Renewable Sustainable Energy Rev.*, 2012, **16**, 3043–3053.
132 J. Fu, N. R. Ahmad, C. P. Leo, J. M. Aberilla, I. D. Cruz, B. Alamani and S. P. Koh, *Gas Sci. Eng.*, 2024, 205401.
133 T. Graham, *London, Edinburgh Dublin Philos. Mag. J. Sci.*, 1866, **32**, 401–420.
134 S. Sourirajan, *Nature*, 1964, **203**, 1348–1349.
135 N. Du, H. B. Park, M. M. Dal-Cin and M. D. Guiver, *Energy Environ. Sci.*, 2012, **5**, 7306–7322.
136 I. Sreedhar, R. Vaidhiswaran, B. M. Kamani and A. Venugopal, *Renewable Sustainable Energy Rev.*, 2017, **68**, 659–684.
137 P. Bernardo, E. Drioli and G. Golemme, *Ind. Eng. Chem. Res.*, 2009, **48**, 4638–4663.
138 M. Kanniche, R. Gros-Bonnivard, P. Jaud, J. Valle-Marcos, J.-M. Amann and C. Bouallou, *Appl. Therm. Eng.*, 2010, **30**, 53–62.
139 A. S. Bhown and B. C. Freeman, *Environ. Sci. Technol.*, 2011, **45**, 8624–8632.
140 V. Kulshrestha, K. Awasthi, N. K. Acharya, M. Singh, D. K. Avasthi and Y. K. Vijay, *Desalination*, 2006, **195**, 273–280.
141 M. Pera-Titus, *Chem. Rev.*, 2014, **114**, 1413–1492.
142 K. Keizer, A. F. M. Leenaars and A. J. Burggraaf.
143 N. Abdullah, M. A. Rahman, M. H. D. Othman, J. Jaafar and A. F. Ismail, *Current Trends and Future Developments on (Bio-) Membranes*, Elsevier, 2018, pp. 45–70.

144 M. R. Rahimpour, F. Samimi, A. Babapoor, T. Tohidian and S. Mohebi, *Chem. Eng. Process.*, 2017, **121**, 24–49.
145 S. Yun and S. T. Oyama, *J. Membr. Sci.*, 2011, **375**, 28–45.
146 H. Hanley, *Trans. Faraday Soc.*, 1966, **62**, 2395–2402.
147 T. Finnigan and P. Skudder, *Filtr. Sep.*, 1989, **26**, 198–200.
148 S. Maley, Development of Ion Transport Membrane (ITM) Oxygen Technology for Integration in IGCC and Other Advanced Power Generation Systems, 2013.
149 S. Smart, C. X. C. Lin, L. Ding, K. Thambimuthu and J. C. D. Da Costa, *Energy Environ. Sci.*, 2010, **3**, 268–278.
150 V. Gitis and G. Rothenberg, *Ceramic membranes: new opportunities and practical applications*, John Wiley & Sons, 2016.
151 V. Singh, N. Meena, A. Golder and C. Das, *Int. J. Coal Sci. Technol.*, 2016, **3**, 226–234.
152 W. J. Koros and R. Mahajan, *J. Membr. Sci.*, 2000, **175**, 181–196.
153 B. Bhide and S. Stern, *J. Membr. Sci.*, 1991, **62**, 13–35.
154 S. Jana, M. Purkait and K. Mohanty, *Appl. Clay Sci.*, 2010, **47**, 317–324.
155 B. Nandi, R. Uppaluri and M. Purkait, *Appl. Clay Sci.*, 2008, **42**, 102–110.
156 N. Norahim, P. Yaisanga, K. Faungnawakij, T. Charinpanitkul and C. Klaysom, *Chem. Eng. Technol.*, 2018, **41**, 211–223.
157 J. Sánchez-Laínez, B. Zornoza, S. Friebe, J. Caro, S. Cao, A. Sabetghadam, B. Seoane, J. Gascon, F. Kapteijn and C. Le Guillouzer, *J. Membr. Sci.*, 2016, **515**, 45–53.
158 K. Scott, *Handbook of industrial membranes*, Elsevier, 1995.
159 S. M. Samaei, S. Gato-Trinidad and A. Altaee, *Sep. Purif. Technol.*, 2018, **200**, 198–220.
160 R. Rautenbach and W. Dahm, *J. Membr. Sci.*, 1986, **28**, 319–327.
161 D. F. Sanders, Z. P. Smith, R. Guo, L. M. Robeson, J. E. McGrath, D. R. Paul and B. D. Freeman, *Polymer*, 2013, **54**, 4729–4761.
162 L. M. Robeson, Q. Liu, B. D. Freeman and D. R. Paul, *J. Membr. Sci.*, 2015, **476**, 421–431.
163 J. C.-Y. Chen, University of Waterloo, 2002.
164 M. Farnam, H. Mukhtar and A. Mohd Shariff, *Appl. Mech. Mater.*, 2014, **625**, 701–703.
165 B. Freeman and I. Pinnau, *Trends Polym. Sci.*, 1997, **5**, 167–173.
166 X. Kong and J. Liu, *J. Phys. Chem. C*, 2019, **123**, 15113–15121.
167 S. R. Wickramasinghe, M. J. Semmens and E. L. Cussler, Hollow fiber modules made with hollow fiber fabric, *J. Membr. Sci.*, 1993, **84**(1–2), 1–14.
168 Y. Han and W. W. Ho, *J. Polym. Eng.*, 2020, **40**, 529–542.
169 H. B. Park, J. Kamcev, L. M. Robeson, M. Elimelech and B. D. Freeman, *Science*, 2017, **356**, eaab0530.
170 M. G. Buonomenna, W. Yave and G. Golemme, *RSC Adv.*, 2012, **2**, 10745–10773.
171 Z. Yang, W. Guo, S. M. Mahurin, S. Wang, H. Chen, L. Cheng, K. Jie, H. M. Meyer, D.-E. Jiang and G. Liu, *Chem*, 2020, **6**, 631–645.
172 P. M. Budd, N. B. McKeown and D. Fritsch, *J. Mater. Chem.*, 2005, **15**, 1977–1986.
173 H. B. Park, C. H. Jung, Y. M. Lee, A. J. Hill, S. J. Pas, S. T. Mudie, E. Van Wagner, B. D. Freeman and D. J. Cookson, *Science*, 2007, **318**, 254–258.
174 S. Sridhar, B. Smitha and T. Aminabhavi, *Sep. Purif. Rev.*, 2007, **36**, 113–174.
175 H. Lin, E. Van Wagner, B. D. Freeman, L. G. Toy and R. P. Gupta, *Science*, 2006, **311**, 639–642.
176 A. Javaid, *Chem. Eng. J.*, 2005, **112**, 219–226.
177 J. Y. Park and D. R. Paul, *J. Membr. Sci.*, 1997, **125**, 23–39.
178 W. M. Lee, *Polym. Eng. Sci.*, 1980, **20**, 65–69.
179 A. v Bondi, *J. Phys. Chem.*, 1964, **68**, 441–451.
180 D. W. Van Krevelen and K. Te Nijenhuis, *Properties of polymers: their correlation with chemical structure; their numerical estimation and prediction from additive group contributions*, Elsevier, 2009.
181 A. Singh, B. D. Freeman and I. Pinnau, *J. Polym. Sci., Part B: Polym. Phys.*, 1998, **36**, 289–301.
182 S. Deveci, Y. Oksuz, T. Birtane and M. Oner, *Polym. Test.*, 2016, **55**, 287–296.
183 R. Abedini, A. Mosayebi and M. Mokhtari, *Process Saf. Environ. Prot.*, 2018, **114**, 229–239.
184 P. J. Roman, F. Detlev, K. Thomas and P. Klaus-Viktor, *J. Membr. Sci.*, 2012, **389**, 343–348.
185 R. Wang, C. Cao and T.-S. Chung, *J. Membr. Sci.*, 2002, **198**, 259–271.
186 M. Wang, Z. Wang, S. Zhao, J. Wang and S. Wang, *Chin. J. Chem. Eng.*, 2017, **25**, 1581–1597.
187 C. Yeom, S. Lee and J. Lee, *J. Appl. Polym. Sci.*, 2000, **78**, 179–189.
188 S. Maghami, A. Mehrabani-Zeinabad, M. Sadeghi, J. Sánchez-Laínez, B. Zornoza, C. Téllez and J. Coronas, *Chem. Eng. Sci.*, 2019, **205**, 58–73.
189 S. R. Reijerkerk, K. Nijmeijer, C. P. Ribeiro Jr, B. D. Freeman and M. Wessling, *J. Membr. Sci.*, 2011, **367**, 33–44.
190 A. E. Gemeda, M. G. De Angelis, N. Du, N. Li, M. D. Guiver and G. C. Sarti, *J. Membr. Sci.*, 2017, **524**, 746–757.
191 G. Zhang and H. Lin, *Green Energy Environ.*, 2023, **9**(8), 1220–1238.
192 A. T. Bridge, B. J. Pedretti, J. F. Brennecke and B. D. Freeman, *J. Membr. Sci.*, 2022, **644**, 120173.
193 Z. Dai, L. Ansaloni and L. Deng, *Green Energy Environ.*, 2016, **1**, 102–128.
194 D. Wu, L. Zhao, V. K. Vakharia, W. Salim and W. W. Ho, *J. Membr. Sci.*, 2016, **510**, 58–71.
195 V. Vakharia, W. Salim, D. Wu, Y. Han, Y. Chen, L. Zhao and W. W. Ho, *J. Membr. Sci.*, 2018, **555**, 379–387.
196 A. Van Der Pluijm, N. Miyagishima, E. Van Der Burg and Y. Itami, *US Pat.*, 9962660, 2018.
197 Y. Han, W. Salim, K. K. Chen, D. Wu and W. W. Ho, *J. Membr. Sci.*, 2019, **575**, 242–251.
198 W. Salim, V. Vakharia, Y. Chen, D. Wu, Y. Han and W. W. Ho, *J. Membr. Sci.*, 2018, **556**, 126–137.
199 P. Li, H. Z. Chen and T.-S. Chung, *J. Membr. Sci.*, 2013, **434**, 18–25.
200 J.-J. Shieh and T. S. Chung, *J. Membr. Sci.*, 2000, **166**, 259–269.

201 M. Sadrzadeh, E. Saljoughi, K. Shahidi and T. Mohammadi, *Polym. Adv. Technol.*, 2010, **21**, 568–577.
202 M. Sadrzadeh, M. Amirilargani, K. Shahidi and T. Mohammadi, *J. Membr. Sci.*, 2009, **342**, 236–250.
203 M. Liu, K. Xie, M. D. Nothling, P. A. Gurr, S. S. L. Tan, Q. Fu, P. A. Webley and G. G. Qiao, *ACS Nano*, 2018, **12**, 11591–11599.
204 J. Zhao, G. He, G. Liu, F. Pan, H. Wu, W. Jin and Z. Jiang, *Prog. Polym. Sci.*, 2018, **80**, 125–152.
205 S. Dong, Z. Wang, M. Sheng, Z. Qiao and J. Wang, *J. Membr. Sci.*, 2020, **610**, 118221.
206 W. Yave, H. Huth, A. Car and C. Schick, *Energy Environ. Sci.*, 2011, **4**, 4656–4661.
207 W. Yave, A. Car, S. S. Funari, S. P. Nunes and K.-V. Peinemann, *Macromolecules*, 2010, **43**, 326–333.
208 Y. Chen, B. Wang, L. Zhao, P. Dutta and W. W. Ho, *J. Membr. Sci.*, 2015, **495**, 415–423.
209 Y. Chen, L. Zhao, B. Wang, P. Dutta and W. W. Ho, *J. Membr. Sci.*, 2016, **497**, 21–28.
210 M. J. Yoo, K. H. Kim, J. H. Lee, T. W. Kim, C. W. Chung, Y. H. Cho and H. B. Park, *J. Membr. Sci.*, 2018, **566**, 336–345.
211 P. Li, Z. Wang, W. Li, Y. Liu, J. Wang and S. Wang, *ACS Appl. Mater. Interfaces*, 2015, **7**, 15481–15493.
212 Y. Ying, Z. Yang, D. Shi, S. B. Peh, Y. Wang, X. Yu, H. Yang, K. Chai and D. Zhao, *J. Membr. Sci.*, 2021, **632**, 119384.
213 T. Li, Y. Pan, K.-V. Peinemann and Z. Lai, *J. Membr. Sci.*, 2013, **425**, 235–242.
214 H. Lin and B. D. Freeman, *J. Mol. Struct.*, 2005, **739**, 57–74.
215 M. Liu, M. D. Nothling, S. Zhang, Q. Fu and G. G. Qiao, *Prog. Polym. Sci.*, 2022, **126**, 101504.
216 C. Gu, Y. Liu, W. Wang, J. Liu and J. Hu, *Front. Chem. Sci. Eng.*, 2021, **15**, 437–449.
217 B. Chen, H. Xie, L. Shen, Y. Xu, M. Zhang, M. Zhou, B. Li, R. Li and H. Lin, *Small*, 2023, **19**, 2207313.
218 C. Wu, T. Yamagishi, Y. Nakamoto, S. Ishida, K. Nitta and S. Kubota, *J. Polym. Sci., Part B:Polym. Phys.*, 2000, **38**(17), 2285–2295.
219 H. W. Kim and H. B. Park, *J. Membr. Sci.*, 2011, **372**, 116–124.
220 P. Bernardo, J. C. Jansen, F. Bazzarelli, F. Tasselli, A. Fuoco, K. Friess, P. Izák, V. Jarmarová, M. Kačírková and G. Clarizia, *Sep. Purif. Technol.*, 2012, **97**, 73–82.
221 Y. Han, W. Salim, K. K. Chen, D. Wu and W. S. W. Ho, *J. Membr. Sci.*, 2019, **575**, 242–251.
222 H. Sanaeepur, S. Mashhadikhan, G. Mardassi, A. Ebadi Amooghin, B. Van der Bruggen and A. Moghadassi, *Korean J. Chem. Eng.*, 2019, **36**, 1339–1349.
223 V. Vakharia, W. Salim, D. Wu, Y. Han, Y. Chen, L. Zhao and W. S. W. Ho, *J. Membr. Sci.*, 2018, **555**, 379–387.
224 M. Liu, M. D. Nothling, S. Zhang, Q. Fu and G. G. Qiao, *Prog. Polym. Sci.*, 2022, 101504.
225 M. Etxeberria-Benavides, O. David, T. Johnson, M. M. Łozińska, A. Orsi, P. A. Wright, S. Mastel, R. Hillenbrand, F. Kapteijn and J. Gascon, *J. Membr. Sci.*, 2018, **550**, 198–207.
226 B. Chen, H. Xie, L. Shen, Y. Xu, M. Zhang, M. Zhou, B. Li, R. Li and H. Lin, *Small*, 2023, 2207313.
227 T. Wang, C. Cheng, L.-G. Wu, J.-N. Shen, B. Van der Bruggen, Q. Chen, D. Chen and C.-Y. Dong, *Environ. Sci. Technol.*, 2017, **51**, 6202–6210.
228 H. W. Yoon, T. H. Lee, C. M. Doherty, T. H. Choi, J. S. Roh, H. W. Kim, Y. H. Cho, S.-H. Do, B. D. Freeman and H. B. Park, *J. Phys. Chem. Lett.*, 2020, **11**, 2356–2362.
229 N. Nidamanuri, Y. Li, Q. Li and M. Dong, *Eng. Sci.*, 2020, **9**, 3–16.
230 A. D. Kiadehi, A. Rahimpour, M. Jahanshahi and A. A. Ghoreyshi, *J. Ind. Eng. Chem.*, 2015, **22**, 199–207.
231 A. D. Kiadehi, M. Jahanshahi, A. Rahimpour and S. A. A. Ghoreyshi, *Chem. Eng. Process.*, 2015, **90**, 41–48.
232 H. Lin and B. D. Freeman, *Macromolecules*, 2006, **39**, 3568–3580.
233 H. Lin, PhD dissertation, University of Texas, Austin, 2005.
234 S. L. Liu, L. Shao, M. L. Chua, C. H. Lau, H. Wang and S. Quan, *Prog. Polym. Sci.*, 2013, **38**, 1089–1120.
235 W. K. Setiawan and K.-Y. Chiang, *Chemosphere*, 2023, 139478.
236 G. Clarizia and P. Bernardo, *Polymers*, 2021, **14**, 10.
237 M. Isanejad, N. Azizi and T. Mohammadi, *J. Appl. Polym. Sci.*, 2017, **134**(9), DOI: **10.1002/app.44531**.
238 R. Kesting, *J. Polym. Sci., Part C: Polym. Lett.*, 1989, **27**, 187–190.
239 F. Karamouz, H. Maghsoudi and R. Yegani, *J. Nat. Gas Sci. Eng.*, 2016, **35**, 980–985.
240 S. Wang, Y. Liu, S. Huang, H. Wu, Y. Li, Z. Tian and Z. Jiang, *J. Membr. Sci.*, 2014, **460**, 62–70.
241 M. M. Rahman, S. Shishatskiy, C. Abetz, P. Georgopanos, S. Neumann, M. M. Khan, V. Filiz and V. Abetz, *J. Membr. Sci.*, 2014, **469**, 344–354.
242 M. A. Wahab and A. Sunarti, *Int. J. Membr. Sci. Technol.*, 2015, **2**, 78–84.
243 S. Sridhar, R. Suryamurali, B. Smitha and T. Aminabhavi, *Colloids Surf., A*, 2007, **297**, 267–274.
244 L. Wang, Y. Li, S. Li, P. Ji and C. Jiang, *J. Energy Chem.*, 2014, **23**, 717–725.
245 P. Taheri, M. S. Maleh and A. Raisi, *J. Environ. Chem. Eng.*, 2021, **9**, 105877.
246 Y. Liu, S. Yu, H. Wu, Y. Li, S. Wang, Z. Tian and Z. Jiang, *J. Membr. Sci.*, 2014, **469**, 198–208.
247 W. K. Setiawan and K.-Y. Chiang, *Chemosphere*, 2023, **338**, 139478.
248 W. Zhu, F. Liu, M. Gou, R. Guo and X. Li, *Green Chem. Eng.*, 2021, **2**, 132–143.
249 Y. Zheng, Y. Wu, B. Zhang and Z. Wang, *J. Appl. Polym. Sci.*, 2020, **137**, 48398.
250 S. Metz, M. Mulder and M. Wessling, *Macromolecules*, 2004, **37**, 4590–4597.
251 A. Car, C. Stropnik, W. Yave and K. V. Peinemann, *Adv. Funct. Mater.*, 2008, **18**, 2815–2823.
252 B. Zhu, X. Jiang, S. He, X. Yang, J. Long, Y. Zhang and L. Shao, *J. Mater. Chem. A*, 2020, **8**, 24233–24252.
253 T. C. Merkel, H. Lin, X. Wei and R. Baker, *J. Membr. Sci.*, 2010, **359**, 126–139.
254 X. He, A. Lindbråthen, T.-J. Kim and M.-B. Hägg, *Int. J. Greenhouse Gas Control*, 2017, **64**, 323–332.
255 Y. Han and W. W. Ho, *Chin. J. Chem. Eng.*, 2018, **26**, 2238–2254.

256 Y. Han, D. Wu and W. W. Ho, *J. Membr. Sci.*, 2019, **573**, 476–484.
257 P. V. Kortunov, M. Siskin, L. S. Baugh and D. C. Calabro, *Energy Fuels*, 2015, **29**, 5919–5939.
258 Y. Chen and W. W. Ho, *J. Membr. Sci.*, 2016, **514**, 376–384.
259 Y. Zhao and W. W. Ho, *J. Membr. Sci.*, 2012, **415**, 132–138.
260 R. Pelton, *Langmuir*, 2014, **30**, 15373–15382.
261 D. Wu, Y. Han, W. Salim, K. K. Chen, J. Li and W. W. Ho, *J. Membr. Sci.*, 2018, **565**, 439–449.
262 R. Pang, K. K. Chen, Y. Han and W. W. Ho, *J. Membr. Sci.*, 2020, **612**, 118443.
263 K. K. Chen, Y. Han, Z. Zhang and W. W. Ho, *J. Membr. Sci.*, 2021, **628**, 119215.
264 T. J. Kim, B. Li and M. B. Hägg, *J. Polym. Sci., Part B: Polym. Phys.*, 2004, **42**, 4326–4336.
265 T.-Y. Chen, X. Deng, L.-C. Lin and W. W. Ho, *J. Membr. Sci.*, 2022, **645**, 120195.
266 S. Yuan, Z. Wang, Z. Qiao, M. Wang, J. Wang and S. Wang, *J. Membr. Sci.*, 2011, **378**, 425–437.
267 L. Deng and M.-B. Hagg, *Ind. Eng. Chem. Res.*, 2015, **54**, 11139–11150.
268 Z. Qiao, Z. Wang, C. Zhang, S. Yuan, Y. Zhu, J. Wang and S. Wang, *AIChE J.*, 2013, **59**, 215–228.
269 C. Dong, Z. Wang, C. Yi and S. Wang, *J. Appl. Polym. Sci.*, 2006, **101**, 1885–1891.
270 J. Zhao, Z. Wang, J. Wang and S. Wang, *J. Membr. Sci.*, 2006, **283**, 346–356.
271 D. Venturi, D. Grupkovic, L. Sisti and M. G. Baschetti, *J. Membr. Sci.*, 2018, **548**, 263–274.
272 R. Casadei, E. Firouznia and M. G. Baschetti, *Membranes*, 2021, **11**, 442.
273 Y. Han, D. Wu and W. W. Ho, *J. Membr. Sci.*, 2018, **567**, 261–271.
274 R. Casadei, D. Venturi, M. Giacinti Baschetti, L. Giorgini, E. Maccaferri and S. Ligi, *Membranes*, 2019, **9**, 119.
275 T.-J. Kim, H. Vrålstad, M. Sandru and M.-B. Hägg, *Energy Procedia*, 2013, **37**, 986–992.
276 C. Zhang, Z. Wang, Y. Cai, C. Yi, D. Yang and S. Yuan, *Chem. Eng. J.*, 2013, **225**, 744–751.
277 N. B. McKeown, *Int. Scholarly Res. Not.*, 2012, **2012**(1), 513986.
278 U. Scherf, *J. Mater. Chem.*, 1999, **9**, 1853–1864.
279 A. A. Shamsabadi, M. Rezakazemi, F. Seidi, H. Riazi, T. Aminabhavi and M. Soroush, *Prog. Energy Combust. Sci.*, 2021, **84**, 100903.
280 M. Z. Ahmad, R. Castro-Muñoz and P. M. Budd, *Nanoscale*, 2020, **12**, 23333–23370.
281 Y. Wang, B. S. Ghanem, Z. Ali, K. Hazazi, Y. Han and I. Pinnau, *Small Struct.*, 2021, **2**, 2100049.
282 B. Comesaña-Gándara, J. Chen, C. G. Bezzu, M. Carta, I. Rose, M.-C. Ferrari, E. Esposito, A. Fuoco, J. C. Jansen and N. B. McKeown, *Energy Environ. Sci.*, 2019, **12**, 2733–2740.
283 N. B. McKeown, *Polymer*, 2020, **202**, 122736.
284 H. Zhou and W. Jin, *Membranes*, 2018, **9**, 3.
285 S. Sepahvand, M. Bahmani, A. Ashori, H. Pirayesh, Q. Yu and M. N. Dafchahi, *Int. J. Biol. Macromol.*, 2021, **182**, 1392–1398.
286 M. Nikkhah Dafchahi, H. Resalati, A. R. Saraeyan, A. Ghasemian and A. R. Shakeri, *Cellulose*, 2018, **25**, 4783–4790.
287 Z. Dai, V. Ottesen, J. Deng, R. M. L. Helberg and L. Deng, *Fibers*, 2019, **7**, 40.
288 M. Zhang, T. Xu, Q. Zhao, K. Liu, D. Liang and C. Si, *Carbon Capture Sci. Technol.*, 2024, **10**, 100157.
289 X.-L. Wei, S. Liang, Y.-Y. Xu, Y.-L. Sun, J.-F. An and Z.-S. Chao, *J. Membr. Sci.*, 2017, **530**, 240–249.
290 J. Chen, J. Xu, K. Wang, X. Cao and R. Sun, *Carbohydr. Polym.*, 2016, **137**, 685–692.
291 Y. Liu, H. Huang, P. Huo and J. Gu, *Carbohydr. Polym.*, 2017, **165**, 266–275.
292 V. Vatanpour, A. Dehqan, S. Paziresh, S. Zinadini, A. A. Zinatizadeh and I. Koyuncu, *Sep. Purif. Technol.*, 2022, **296**, 121433.
293 H. Nguyen, M. Wang, M.-Y. Hsiao, K. Nagai, Y. Ding and H. Lin, *J. Membr. Sci.*, 2019, **586**, 7–14.
294 A. F. Ismail, K. Chandra Khulbe, T. Matsuura, A. F. Ismail, K. C. Khulbe and T. Matsuura, *Gas Separation Membranes: Polymeric and Inorganic*, 2015, pp. 37–192.
295 A. Puleo, D. R. Paul and S. Kelley, *J. Membr. Sci.*, 1989, **47**, 301–332.
296 D. Nikolaeva, K. Verachtert, I. Azcune, J. C. Jansen and I. F. Vankelecom, *Carbohydr. Polym.*, 2021, **255**, 117375.
297 A. Rehman, Z. Jahan, F. Sher, T. Noor, M. B. K. Niazi, M. A. Akram and E. K. Sher, *Chemosphere*, 2022, **307**, 135736.
298 M. A. Silva, E. Belmonte-Reche and M. P. de Amorim, *Carbohydr. Polym.*, 2021, **254**, 117407.
299 A. Nagendran, S. Vidya and D. Mohan, *Soft Mater.*, 2008, **6**, 45–64.
300 L. Liu, C. M. Doherty, E. Ricci, G. Q. Chen, M. G. De Angelis and S. E. Kentish, *J. Membr. Sci.*, 2021, **638**, 119677.
301 Z. Dai, V. Ottesen, J. Deng, R. M. L. Helberg and L. Deng, *Fibers*, 2019, **7**(5), 40.
302 M. N. Dafchahi and B. Acharya, *Biomass Convers. Biorefin.*, 2023, 1–15.
303 D. Pawcenis, E. Twardowska, M. Leśniak, R. J. Jędrzejczyk, M. Sitarz and J. Profic-Paczkowska, *Int. J. Biol. Macromol.*, 2022, **213**, 738–750.
304 T. Yi, H. Zhao, Q. Mo, D. Pan, Y. Liu, L. Huang, H. Xu, B. Hu and H. Song, *Materials*, 2020, **13**, 5062.
305 N. A. D. Ho and C. Leo, *Environ. Res.*, 2021, **197**, 111100.
306 A. Pokharel, K. J. Falua, A. Babaei-Ghazvini, M. Nikkhah Dafchahi, L. G. Tabil, V. Meda and B. Acharya, *Polymers*, 2024, **16**, 996.
307 Y. Li, P. Jia, J. Xu, Y. Wu, H. Jiang and Z. Li, *Ind. Eng. Chem. Res.*, 2020, **59**, 2874–2882.
308 J. Ø. Torstensen, R. M. Helberg, L. Deng, Ø. W. Gregersen and K. Syverud, *Int. J. Greenhouse Gas Control*, 2019, **81**, 93–102.
309 S. N. Mithra and S. Ahankari, *Mater. Today Sustainability*, 2022, **19**, 100191.
310 R. Borgohain, U. Pattnaik, B. Prasad and B. Mandal, *Carbohydr. Polym.*, 2021, **267**, 118178.
311 F. Russo, F. Galiano, A. Iulianelli, A. Basile and A. Figoli, *Fuel Process. Technol.*, 2021, **213**, 106643.

312 A. Iulianelli, F. Russo, F. Galiano, M. Manisco and A. Figoli, *Int. J. Greenhouse Gas Control*, 2022, **117**, 103657.
313 A. Tena, L. Fernández, M. Sánchez, L. Palacio, A. Lozano, A. Hernández and P. Prádanos, *Chem. Eng. Sci.*, 2010, **65**, 2227–2235.
314 T.-S. Chung, S. S. Chan, R. Wang, Z. Lu and C. He, *J. Membr. Sci.*, 2003, **211**, 91–99.
315 C. M. Zimmerman, A. Singh and W. J. Koros, *J. Membr. Sci.*, 1997, **137**, 145–154.
316 M. Mozafari, S. Khoshhal Salestan, A. Arabi Shamsabadi, K. Jha, M. Tanwar, H. Kim, Z. Fakhraai and M. Soroush, *ACS Appl. Mater. Interfaces*, 2025, **17**(2), 3897–3910.
317 Y. Cheng, S. J. Datta, S. Zhou, J. Jia, O. Shekhah and M. Eddaoudi, *Chem. Soc. Rev.*, 2022, **51**, 8300–8350.
318 M. L. Jue and R. P. Lively, *React. Funct. Polym.*, 2015, **86**, 88–110.
319 B. Seoane, V. Sebastián, C. Téllez and J. Coronas, *CrystEngComm*, 2013, **15**, 9483–9490.
320 Y. H. Deng, J. T. Chen, C. H. Chang, K. S. Liao, K. L. Tung, W. E. Price, Y. Yamauchi and K. C. W. Wu, *Angew. Chem.*, 2016, **128**, 12985–12988.
321 K. C. Wong, P. S. Goh, A. F. Ismail, H. S. Kang, Q. Guo, X. Jiang and J. Ma, *Membranes*, 2022, **12**, 186.
322 O. Shekhah, L. Fu, R. Sougrat, Y. Belmabkhout, A. J. Cairns, E. P. Giannelis and M. Eddaoudi, *Chem. Commun.*, 2012, **48**, 11434–11436.
323 M. C. So, S. Jin, H.-J. Son, G. P. Wiederrecht, O. K. Farha and J. T. Hupp, *J. Am. Chem. Soc.*, 2013, **135**, 15698–15701.
324 O. Shekhah, J. Liu, R. Fischer and C. Wöll, *Chem. Soc. Rev.*, 2011, **40**, 1081–1106.
325 S. Khoshhal, A. A. Ghoreyshi, M. Jahanshahi and M. Mohammadi, *RSC Adv.*, 2015, **5**, 24758–24768.
326 X. Q. Cheng, Z. X. Wang, X. Jiang, T. Li, C. H. Lau, Z. Guo, J. Ma and L. Shao, *Prog. Mater. Sci.*, 2018, **92**, 258–283.
327 G. Wyszogrodzka, B. Marszałek, B. Gil and P. Dorożyński, *Drug Discovery Today*, 2016, **21**, 1009–1018.
328 V. I. Isaeva, K. E. Papathanasiou and L. M. Kustov, *Crystals*, 2020, **10**, 617.
329 S. Tai, W. Zhang, J. Zhang, G. Luo, Y. Jia, M. Deng and Y. Ling, *Microporous Mesoporous Mater.*, 2016, **220**, 148–154.
330 Z. Hu, Y. Peng, Z. Kang, Y. Qian and D. Zhao, *Inorg. Chem.*, 2015, **54**, 4862–4868.
331 R. Lin, L. Ge, S. Liu, V. Rudolph and Z. Zhu, *ACS Appl. Mater. Interfaces*, 2015, **7**, 14750–14757.
332 S. Anastasiou, N. Bhoria, J. Pokhrel, K. S. K. Reddy, C. Srinivasakannan, K. Wang and G. N. Karanikolos, *Mater. Chem. Phys.*, 2018, **212**, 513–522.
333 L. Dong, M. Chen, J. Li, D. Shi, W. Dong, X. Li and Y. Bai, *J. Membr. Sci.*, 2016, **520**, 801–811.
334 W. Li, Y. Zhang, P. Su, Z. Xu, G. Zhang, C. Shen and Q. Meng, *J. Mater. Chem. A*, 2016, **4**, 18747–18752.
335 K. Cho, L. J. Andrew and M. J. MacLachlan, *Angew. Chem., Int. Ed.*, 2023, **62**, e202300960.
336 F. Guo, B. Li, R. Ding, D. Li, X. Jiang, G. He and W. Xiao, *Membranes*, 2021, **11**, 693.
337 V. T. Do, C. Y. Tang, M. Reinhard and J. O. Leckie, *Environ. Sci. Technol.*, 2012, **46**, 13184–13192.
338 W. Sun, J. Shi, C. Chen, N. Li, Z. Xu, J. Li, H. Lv, X. Qian and L. Zhao, *RSC Adv.*, 2018, **8**, 10040–10056.
339 M. Hu and B. Mi, *Environ. Sci. Technol.*, 2013, **47**, 3715–3723.
340 Z. Xu, Y. Zhang, X. Qian, J. Shi, L. Chen, B. Li, J. Niu and L. Liu, *Appl. Surf. Sci.*, 2014, **316**, 308–314.
341 C. Petit and T. J. Bandosz, *Adv. Mater.*, 2009, **21**, 4753–4757.
342 Q.-L. Zhu and Q. Xu, *Chem. Soc. Rev.*, 2014, **43**, 5468–5512.
343 M. Tanhaei, A. R. Mahjoub and V. Safarifard, *Ultrason. Sonochem.*, 2018, **41**, 189–195.
344 K.-Y. A. Lin, F.-K. Hsu and W.-D. Lee, *J. Mater. Chem. A*, 2015, **3**, 9480–9490.
345 M. Ghadiri, A. Aroujalian, F. Pazani and P. Salimi, *Sep. Purif. Technol.*, 2024, **330**, 125315.
346 Q. Yang and B. Mi, *Adv. Chronic Kidney Dis.*, 2013, **20**, 536–555.
347 S. Iijima, *Nature*, 1991, **354**, 56.
348 S. Xiong, L. Li, L. Dong, J. Tang, G. Yu and C. Pan, *J. CO2 Util.*, 2020, **41**, 101224.
349 X. Cao, Z. Wang, Z. Qiao, S. Zhao and J. Wang, *ACS Appl. Mater. Interfaces*, 2019, **11**, 5306–5315.
350 K. Duan, J. Wang, Y. Zhang and J. Liu, *J. Membr. Sci.*, 2019, **572**, 588–595.
351 H. Fan, A. Mundstock, A. Feldhoff, A. Knebel, J. Gu, H. Meng and J. R. Caro, *J. Am. Chem. Soc.*, 2018, **140**, 10094–10098.
352 J. Fu, S. Das, G. Xing, T. Ben, V. Valtchev and S. Qiu, *J. Am. Chem. Soc.*, 2016, **138**, 7673–7680.
353 Y. Cheng, Y. Ying, L. Zhai, G. Liu, J. Dong, Y. Wang, M. P. Christopher, S. Long, Y. Wang and D. Zhao, *J. Membr. Sci.*, 2019, **573**, 97–106.
354 H. Fan, M. Peng, I. Strauss, A. Mundstock, H. Meng and J. Caro, *Nat. Commun.*, 2021, **12**, 38.
355 A. Knebel and J. Caro, *Nat. Nanotechnol.*, 2022, **17**, 911–923.
356 G. Liu, W. Jin and N. Xu, *Angew. Chem., Int. Ed.*, 2016, **55**, 13384–13397.
357 H. E. Karahan, K. Goh, C. Zhang, E. Yang, C. Yıldırım, C. Y. Chuah, M. G. Ahunbay, J. Lee, Ş. B. Tantekin-Ersolmaz and Y. Chen, *Adv. Mater.*, 2020, **32**, 1906697.
358 N. Hemanth and B. Kandasubramanian, *Chem. Eng. J.*, 2020, **392**, 123678.
359 A. P. Isfahani, A. Arabi Shamsabadi and M. Soroush, *Ind. Eng. Chem. Res.*, 2022, **62**, 2309–2328.
360 J. Shen, G. Liu, Y. Ji, Q. Liu, L. Cheng, K. Guan, M. Zhang, G. Liu, J. Xiong and J. Yang, *Adv. Funct. Mater.*, 2018, **28**, 1801511.
361 C. Y. Chuah, K. Goh, Y. Yang, H. Gong, W. Li, H. E. Karahan, M. D. Guiver, R. Wang and T.-H. Bae, *Chem. Rev.*, 2018, **118**, 8655–8769.
362 J. G. Wijmans and R. W. Baker, *J. Membr. Sci.*, 1995, **107**, 1–21.
363 A. A. Shamsabadi, A. P. Isfahani, S. K. Salestan, A. Rahimpour, B. Ghalei, E. Sivaniah and M. Soroush, *ACS Appl. Mater. Interfaces*, 2019, **12**, 3984–3992.
364 G. Liu, L. Cheng, G. Chen, F. Liang, G. Liu and W. Jin, *Chem. – Asian J.*, 2020, **15**, 2364–2370.
365 Z. Hu, Y. Yang, X.-F. Zhang, C. Xu and J. Yao, *Sep. Purif. Technol.*, 2023, **326**, 124704.

366 F. Shi, J. Sun, J. Wang, M. Liu, Z. Yan, B. Zhu, Y. Li and X. Cao, *J. Membr. Sci.*, 2021, **620**, 118850.
367 H. W. Kim, H. W. Yoon, S.-M. Yoon, B. M. Yoo, B. K. Ahn, Y. H. Cho, H. J. Shin, H. Yang, U. Paik and S. Kwon, *Science*, 2013, **342**, 91–95.
368 K. Wang, D. Chen, J. Tang, Z. Hong, Z. Zhu, Z. Yuan, Z. Lin, Y. Liu, R. Semiat and X. He, *Chem. Eng. J.*, 2024, **483**, 149305.
369 Z.-X. Low, P. M. Budd, N. B. McKeown and D. A. Patterson, *Chem. Rev.*, 2018, **118**, 5871–5911.
370 S. Kim and Y. M. Lee, *Prog. Polym. Sci.*, 2015, **43**, 1–32.
371 L. S. White, X. Wei, S. Pande, T. Wu and T. C. Merkel, *J. Membr. Sci.*, 2015, **496**, 48–57.
372 Y. Hua, S. Park and H. K. Jeong, *J. Environ. Chem. Eng.*, 2024, 113753.
373 C. Astorino, E. De Nardo, S. Lettieri, G. Ferraro, C. F. Pirri and S. Bocchini, *Membranes*, 2023, **13**(12), 903.
374 M. Sandru, T.-J. Kim, W. Capala, M. Huijbers and M.-B. Hägg, *Energy Procedia*, 2013, **37**, 6473–6480.
375 J. Pohlmann, M. Bram, K. Wilkner and T. Brinkmann, *Int. J. Greenhouse Gas Control*, 2016, **53**, 56–64.
376 S. Fu, D. Hasse and S. Kulkarni, *Bench Scale Testing of Next Generation Hollow Fiber Membrane Modules*, American Air Liquide Inc., Newark, DE (United States), 2020.
377 Y. Ding, *Ind. Eng. Chem. Res.*, 2019, **59**, 556–568.
378 Y. Hua, S. Park and H.-K. Jeong, *J. Environ. Chem. Eng.*, 2024, 113753.
379 C. Astorino, E. De Nardo, S. Lettieri, G. Ferraro, C. F. Pirri and S. Bocchini, *Membranes*, 2023, **13**, 903.
380 H. An, S. Park, H. T. Kwon, H.-K. Jeong and J. S. Lee, *J. Membr. Sci.*, 2017, **526**, 367–376.
381 N. Prasetya, N. F. Himma, P. D. Sutrisna, I. G. Wenten and B. P. Ladewig, *Chem. Eng. J.*, 2020, **391**, 123575.
382 A. Y. Ku, P. Kulkarni, R. Shisler and W. Wei, *J. Membr. Sci.*, 2011, **367**, 233–239.
383 O. C. David, D. Gorri, A. Urtiaga and I. Ortiz, *J. Membr. Sci.*, 2011, **378**, 359–368.
384 R. W. Baker, *Ind. Eng. Chem. Res.*, 2002, **41**, 1393–1411.
385 R. Mahajan and W. J. Koros, *Ind. Eng. Chem. Res.*, 2000, **39**, 2692–2696.
386 T. Bui, Y. Wong, M. Islam and K. Chua, *J. Membr. Sci.*, 2017, **539**, 76–87.
387 L. Li, R. Xu, C. Song, B. Zhang, Q. Liu and T. Wang, *Membranes*, 2018, **8**, 134.
388 A. W. Thornton, D. Dubbeldam, M. S. Liu, B. P. Ladewig, A. J. Hill and M. R. Hill, *Energy Environ. Sci.*, 2012, **5**, 7637–7646.
389 R. J. Gardner, R. A. Crane and J. F. Hannan, *Chem. Eng. Prog.*, 1977, **73**, 76–78.
390 R. Spillman, *in Membrane science and technology*, Elsevier, 1995, vol. 2, pp. 589–667.
391 C. W. Colling, G. A. Huff Jr and J. V. Bartels, *US Pat.*, 6830691, 2004.
392 C. H. Lau, P. T. Nguyen, M. R. Hill, A. W. Thornton, K. Konstas, C. M. Doherty, R. J. Mulder, L. Bourgeois, A. C. Y. Liu and D. J. Sprouster, *Angew. Chem., Int. Ed.*, 2014, **53**, 5322–5326.
393 Y. Huang and D. R. Paul, *Polymer*, 2004, **45**, 8377–8393.
394 M. Yavari, S. Maruf, Y. Ding and H. Lin, *J. Membr. Sci.*, 2017, **525**, 399–408.
395 A. F. Ismail and W. Lorna, *Sep. Purif. Technol.*, 2002, **27**, 173–194.
396 A. Bos, I. Pünt, M. Wessling and H. Strathmann, *J. Membr. Sci.*, 1999, **155**, 67–78.
397 C. Zhou, T.-S. Chung, R. Wang, Y. Liu and S. H. Goh, *J. Membr. Sci.*, 2003, **225**, 125–134.
398 Y. Kamiya, K. Mizoguchi and Y. Naito, *J. Polym. Sci., Part B:Polym. Phys.*, 1992, **30**, 1177–1181.
399 F. Moghadam and H. B. Park, *Curr. Opin. Chem. Eng.*, 2018, **20**, 28–38.
400 S. Kanehashi, A. Aguiar, H. T. Lu, G. Q. Chen and S. E. Kentish, *J. Membr. Sci.*, 2018, **549**, 686–692.
401 C. A. Scholes, S. E. Kentish and G. W. Stevens, *Sep. Purif. Rev.*, 2009, **38**, 1–44.
402 C. A. Scholes, G. W. Stevens and S. E. Kentish, *J. Membr. Sci.*, 2010, **350**, 189–199.
403 H. Demir and S. Keskin, *Macromol. Mater. Eng.*, 2024, **309**, 2300225.
404 O. Vopička, M. G. De Angelis and G. C. Sarti, *J. Membr. Sci.*, 2014, **449**, 97–108.
405 O. Vopička, M. G. De Angelis, N. Du, N. Li, M. D. Guiver and G. C. Sarti, *J. Membr. Sci.*, 2014, **459**, 264–276.
406 E. Ricci, A. E. Gemeda, N. Du, N. Li, M. G. De Angelis, M. D. Guiver and G. C. Sarti, *J. Membr. Sci.*, 2019, **585**, 136–149.
407 E. Ricci, E. Di Maio, M. Degli Esposti, L. Liu, G. Mensitieri, P. Fabbri, S. E. Kentish and M. G. De Angelis, *J. Membr. Sci.*, 2021, **628**, 119226.
408 W. Koros, *J. Polym. Sci., Polym. Phys. Ed.*, 1980, **18**, 981–992.
409 O. Vopička and K. Friess, *J. Polym. Sci., Part B: Polym. Phys.*, 2014, **52**, 1490–1495.
410 M. Saberi, A. Dadkhah and S. Hashemifard, *J. Membr. Sci.*, 2016, **499**, 164–171.
411 S. Khoshhal Salestan, A. Rahimpour, R. Abedini, M. A. Soleimanzade and M. Sadrzadeh, *J. Polym. Sci.*, 2022, **60**, 1392–1406.
412 M. Minelli and G. C. Sarti, *J. Membr. Sci.*, 2013, **435**, 176–185.
413 M. Minelli, S. Campagnoli, M. G. De Angelis, F. Doghieri and G. C. Sarti, *Macromolecules*, 2011, **44**, 4852–4862.
414 P. K. Roy, K. Kumar, F. M. Thakkar, A. D. Pathak, K. G. Ayappa and P. K. Maiti, *J. Membr. Sci.*, 2020, **613**, 118377.
415 E. Tocci, A. Gugliuzza, L. De Lorenzo, M. Macchione, G. De Luca and E. Drioli, *J. Membr. Sci.*, 2008, **323**, 316–327.
416 H. Daglar, I. Erucar and S. Keskin, *Mater. Adv.*, 2021, **2**, 5300–5317.
417 I. Erucar, G. Yilmaz and S. Keskin, *Chem. – Asian J.*, 2013, **8**, 1692–1704.
418 J. G. Wijmans and R. W. Baker, *J. Membr. Sci.*, 1995, **107**, 1–21.
419 S. Sadeghi and J. D. Howe, *J. Phys. Chem. C*, 2023, **127**, 3715–3725.
420 E. Ghasemnejad-Afshar, S. Amjad-Iranagh, M. Zarif and H. Modarress, *Polym. Test.*, 2020, **83**, 106339.

421 K. q Yu, Z. s Li and J. Sun, *Macromol. Theory Simul.*, 2001, **10**, 624–633.
422 Q. Xu, J. Gao, F. Feng, T.-S. Chung and J. Jiang, *J. Membr. Sci.*, 2023, **678**, 121678.
423 J. C. Maxwell, *A Treatise on Electricity and Magnetism*, Oxford, Clarendon Press, 1873.
424 V. D. Bruggeman, *Ann. Phys.*, 1935, **416**, 636–791.
425 J. Felske, *Int. J. Heat Mass Transfer*, 2004, **47**, 3453–3461.
426 S. Keskin and S. Alsoy Altinkaya, *Computation*, 2019, **7**, 36.
427 H. Daglar and S. Keskin, *Coord. Chem. Rev.*, 2020, **422**, 213470.
428 O. F. Altundal, C. Altintas and S. Keskin, *J. Mater. Chem. A*, 2020, **8**, 14609–14623.
429 Y. J. Colón and R. Q. Snurr, *Chem. Soc. Rev.*, 2014, **43**, 5735–5749.
430 C. Altintas, I. Erucar and S. Keskin, *ACS Appl. Mater. Interfaces*, 2018, **10**, 3668–3679.
431 Z. Qiao, C. Peng, J. Zhou and J. Jiang, *J. Mater. Chem. A*, 2016, **4**, 15904–15912.
432 D. Torelli, H. Moustafa, K. W. Jacobsen and T. Olsen, *npj Comput. Mater.*, 2020, **6**, 158.
433 E. Ren, P. Guilbaud and F.-X. Coudert, *Digital Discovery*, 2022, **1**, 355–374.
434 M. Li, W. Cai, C. Wang and X. Wu, *Phys. Chem. Chem. Phys.*, 2022, **24**, 18764–18776.
435 S. Budhathoki, O. Ajayi, J. A. Steckel and C. E. Wilmer, *Energy Environ. Sci.*, 2019, **12**, 1255–1264.
436 C. Altintas and S. Keskin, *ACS Sustainable Chem. Eng.*, 2018, **7**, 2739–2750.
437 T. Yuan and L. Sarkisov, *Adv. Theory Simul.*, 2022, **5**, 2200159.
438 S. A. Abdollahi and S. F. Ranjbar, *Sci. Rep.*, 2023, **13**, 8812.
439 A. Priya, B. Devarajan, A. Alagumalai and H. Song, *Sci. Total Environ.*, 2023, 163913.
440 R. Giro, H. Hsu, A. Kishimoto, T. Hama, R. F. Neumann, B. Luan, S. Takeda, L. Hamada and M. B. Steiner, *npj Comput. Mater.*, 2023, **9**, 133.
441 Z. Zhang, X. Cao, C. Geng, Y. Sun, Y. He, Z. Qiao and C. Zhong, *J. Membr. Sci.*, 2022, **650**, 120399.
442 E. Ren and F.-X. Coudert, *Chem. Sci.*, 2023, **14**, 1797–1807.
443 K. M. Jablonka, D. Ongari, S. M. Moosavi and B. Smit, *Chem. Rev.*, 2020, **120**, 8066–8129.
444 Y. G. Chung, E. Haldoupis, B. J. Bucior, M. Haranczyk, S. Lee, H. Zhang, K. D. Vogiatzis, M. Milisavljevic, S. Ling and J. S. Camp, *J. Chem. Eng. Data*, 2019, **64**, 5985–5998.
445 F. Kadirkhan, P. S. Goh, A. F. Ismail, W. N. F. Wan Mustapa, M. H. M. Halim, W. K. Soh and S. Y. Yeo, *Membranes*, 2022, **12**, 71.
446 A. Wypych, *Databook of plasticizers*, Elsevier, 2023.
447 M. Zhang, L. Deng, D. Xiang, B. Cao, S. S. Hosseini and P. Li, *Processes*, 2019, **7**, 51.
448 S. Sridhar, S. Bee and S. Bhargava, *Chem. Eng. Dig.*, 2014, **1**, 1–25.
449 D. S. Bakhtin, S. E. Sokolov, I. L. Borisov, V. V. Volkov, A. V. Volkov and V. O. Samoilov, *Membranes*, 2023, **13**, 519.
450 A. Nandy, G. Terrones, N. Arunachalam, C. Duan, D. W. Kastner and H. J. Kulik, *Sci. Data*, 2022, **9**, 74.
451 A. Nandy, C. Duan and H. J. Kulik, *J. Am. Chem. Soc.*, 2021, **143**, 17535–17547.
452 G. G. Terrones, S.-P. Huang, M. P. Rivera, S. Yue, A. Hernandez and H. J. Kulik, *J. Am. Chem. Soc.*, 2024, **146**, 20333–20348.
453 A. Nandy, S. Yue, C. Oh, C. Duan, G. G. Terrones, Y. G. Chung and H. J. Kulik, *Matter*, 2023, **6**, 1585–1603.
454 Y. Duan, L. Li, Z. Shen, J. Cheng and K. He, *Membranes*, 2023, **13**, 480.
455 Q. Qian, P. A. Asinger, M. J. Lee, G. Han, K. Mizrahi Rodriguez, S. Lin, F. M. Benedetti, A. X. Wu, W. S. Chi and Z. P. Smith, *Chem. Rev.*, 2020, **120**, 8161–8266.
456 N. A. O. Sciences, D. E. Earth, L. Studies, B. O. C. Sciences and C. O. A. R. A. F. A. N. E. I. S. Science, 2019.
457 Z. Dai and L. Deng, *Sep. Purif. Technol.*, 2023, 126022.
458 E. Favre, *Membranes*, 2022, **12**, 884.
459 M. Pfister, B. Belaissaoui and E. Favre, *Ind. Eng. Chem. Res.*, 2017, **56**, 591–602.
460 R. Bounaceur, E. Berger, M. Pfister, A. A. R. Santos and E. Favre, *J. Membr. Sci.*, 2017, **523**, 77–91.
461 A. Jomekian and R. M. Behbahani, *J. Membr. Sci. Res.*, 2021, **7**, 209–223.
462 M. Yuan, H. Teichgraeber, J. Wilcox and A. R. Brandt, *Int. J. Greenhouse Gas Control*, 2019, **84**, 154–163.
463 C. J. Geankoplis, *Separation Process Principles*, 2003.
464 R. Bounaceur, N. Lape, D. Roizard, C. Vallieres and E. Favre, *Energy*, 2006, **31**, 2556–2570.
465 B. Belaissaoui, D. Willson and E. Favre, *Chem. Eng. J.*, 2012, **211**, 122–132.
466 P. Shao, M. M. Dal-Cin, M. D. Guiver and A. Kumar, *J. Membr. Sci.*, 2013, **427**, 451–459.
467 H. Zhai, E. S. Rubin and P. L. Versteeg, *Environ. Sci. Technol.*, 2011, **45**(6), 2479–2485.
468 J. Kotowicz and Ł. Bartela, *Energy*, 2012, **38**, 118–127.
469 L. Zhao, E. Riensche, L. Blum and D. Stolten, *J. Membr. Sci.*, 2010, **359**, 160–172.
470 A. M. Arias, M. C. Mussati, P. L. Mores, N. J. Scenna, J. A. Caballero and S. F. Mussati, *Int. J. Greenhouse Gas Control*, 2016, **53**, 371–390.
471 N. Mac Dowell, P. S. Fennell, N. Shah and G. C. Maitland, *Nat. Clim. Change*, 2017, **7**, 243–249.
472 L. Rizzo, W. Gernjak, P. Krzeminski, S. Malato, C. S. McArdell, J. A. S. Perez, H. Schaar and D. Fatta-Kassinos, *Sci. Total Environ.*, 2020, **710**, 136312.
473 N. Lu and D. Xie, *Int. J. Chem. React. Eng.*, 2016, **14**, 1–31.
474 T. Westermann and T. Melin, *Chem. Eng. Process.*, 2009, **48**, 17–28.
475 B. Kumar, B. Muchharla, M. Dikshit, S. Dongare, K. Kumar, B. Gurkan and J. M. Spurgeon, *Environ. Sci. Technol. Lett.*, 2024, **11**, 1161–1174.
476 M. Namdari, Y. Kim, D. J. Pimlott, A. M. Jewlal and C. P. Berlinguette, *Chem. Soc. Rev.*, 2025, **54**, 590–600.
477 D. Segets, C. Andronescu and U.-P. Apfel, *Nat. Commun.*, 2023, **14**, 7950.
478 Z. Liu, J. Qian, G. Zhang, B. Zhang and Y. He, *Sep. Purif. Technol.*, 2024, **330**, 125177.

479 J. Kampen and M. S. Annaland, *J. Mater. Chem. A*, 2021, **9**, 14627–14629.
480 Z.-Y. Zhang, H. Tian, L. Bian, S.-Z. Liu, Y. Liu and Z.-L. Wang, *J. Energy Chem.*, 2023, **83**, 90–97.
481 R. P. W. J. Struis, S. Stucki and M. Wiedorn, *J. Membr. Sci.*, 1996, **113**, 93–100.
482 W.-L. Tan, H.-F. Tan, A. Ahmad and C. Leo, *J. CO2 Util.*, 2021, **48**, 101533.
483 S. Escorihuela, C. Cerdá-Moreno, F. Weigelt, S. Remiro-Buenamañana, S. Escolástico, A. Tena, S. Shishatskiy, T. Brinkmann, A. Chica and J. M. Serra, *J. CO2 Util.*, 2022, **55**, 101813.
484 J. Zou, J. Huang and W. W. Ho, *Ind. Eng. Chem. Res.*, 2007, **46**, 2272–2279.
485 H. Wang, L. Shan, W. Shi, M. Wang, G. Quan, Z. Wang, L. Cui and J. Yan, *J. Environ. Chem. Eng.*, 2023, **11**, 110218.
486 Q. Zhao, M. Fu, Z. Xu, L. Deng, Y. Li, X. Meng, Q. Su and W. Cheng, *Mol. Catal.*, 2023, **551**, 113651.
487 H. Xu, R. Jin and C. P. O'Brien, *ACS Appl. Mater. Interfaces*, 2023, **15**, 56305–56313.
488 Q. H. Pham, E. Goudeli and C. A. Scholes, *Chem. Eng. J.*, 2024, **489**, 151442.
489 J. Lee, H.-G. Park, M.-H. Hyeon, B.-G. Kim, S. K. Kim and S.-Y. Moon, *Chem. Eng. J.*, 2021, **403**, 126457.
490 T. Wang, K. Ge, K. Chen, C. Hou and M. Fang, *Phys. Chem. Chem. Phys.*, 2016, **18**, 13084–13091.
491 S. Shishatskiy, J. R. Pauls, S. P. Nunes and K.-V. Peinemann, *J. Membr. Sci.*, 2010, **359**, 44–53.
492 L. E. Hatch, J. M. Creamean, A. P. Ault, J. D. Surratt, M. N. Chan, J. H. Seinfeld, E. S. Edgerton, Y. Su and K. A. Prather, *Environ. Sci. Technol.*, 2011, **45**, 5105–5111.
493 Y. Y. Birdja, R. l E. Vos, T. A. Wezendonk, L. Jiang, F. Kapteijn and M. T. Koper, *ACS Catal.*, 2018, **8**, 4420–4428.
494 T. L. Soucy, Y. Liu, J. B. Eisenberg and C. C. McCrory, *ACS Appl. Energy Mater.*, 2021, **5**, 159–169.
495 G. K. Dutta and N. Karak, *J. Cleaner Prod.*, 2021, **285**, 124906.
496 S. Kundu and N. Karak, *Chem. Eng. J.*, 2022, **438**, 135575.
497 A. H. Behroozi and R. Xu, *Chem. Catal.*, 2023, **3**(3), 100550.
498 J. J. Chen, P. C. Oh and S. B. M. Saleh, *Korean J. Chem. Eng.*, 2024, **41**, 609–637.
499 F. R. Pomilla, A. Brunetti, G. Marcì, E. I. García-López, E. Fontananova, L. Palmisano and G. Barbieri, *ACS Sustainable Chem. Eng.*, 2018, **6**, 8743–8753.
500 A. Brunetti, F. R. Pomilla, G. Marcì, E. I. Garcia-Lopez, E. Fontananova, L. Palmisano and G. Barbieri, *Appl. Catal., B*, 2019, **255**, 117779.
501 W. Chen, G.-B. Huang, H. Song and J. Zhang, *J. Mater. Chem. A*, 2020, **8**, 20963–20969.
502 A. Nishimura, Y. Okano, M. Hirota and E. Hu, *Int. J. Photoenergy*, 2011, **2011**, 305650.
503 S. K. Movahed, P. Jafari and S. Mallakpour, *J. Environ. Chem. Eng.*, 2023, **11**, 110426.
504 C.-C. Hu, C.-Y. Wang, M.-C. Tsai, R. L. G. Lecaros, W.-S. Hung, H.-A. Tsai, K.-R. Lee and J.-Y. Lai, *Chem. Eng. J.*, 2022, **450**, 138008.
505 I. Díaz, C. Pérez, N. Alfaro and F. Fdz-Polanco, *Bioresour. Technol.*, 2015, **185**, 246–253.
506 J. Luo, A. S. Meyer, R. V. Mateiu and M. Pinelo, *New Biotechnol.*, 2015, **32**, 319–327.
507 R. Cazelles, J. Drone, F. Fajula, O. Ersen, S. Moldovan and A. Galarneau, *New J. Chem.*, 2013, **37**, 3721–3730.
508 M. Z. do Valle Gomes, G. Masdeu, P. Eiring, A. Kuhlemann, M. Sauer, B. Åkerman and A. E. Palmqvist, *Catal. Sci. Technol.*, 2021, **11**, 6952–6959.
509 J. J. Sheng, *J. Nat. Gas Sci. Eng.*, 2015, **22**, 252–259.
510 N. Kumar, M. A. Sampaio, K. Ojha, H. Hoteit and A. Mandal, *Fuel*, 2022, **330**, 125633.
511 B. Jia, J.-S. Tsau and R. Barati, *Fuel*, 2019, **236**, 404–427.
512 A. Abedini, F. Torabi and N. Mosavat, *Int. J. Oil, Gas Coal Technol.*, 2015, **9**, 265–279.
513 N. Zhang, M. Wei and B. Bai, *Fuel*, 2018, **220**, 89–100.
514 B. F. Snyder, M. Layne and D. E. Dismukes, *Int. J. Greenhouse Gas Control*, 2020, **93**, 102885.
515 A. Midttun, E. Enger, A. Lind, M. Lia, J. Meyer, M. V. Storaas, J. Lereim and P. Nygaard, Carbon capture–-from waste to energy: a stylized case from a pioneering initiative at Klemetsrud, Oslo. Report to the CLIMIT–demo project 618215: Potential for financing and pricing Carbon Capture in Waste-to Energy Installations in cities, 2019.
516 E. N. Kalogirou, *in Waste-to-Energy Technologies and Global Applications*, CRC Press, 2024, pp. 80–138.
517 C. Preston, The carbon capture project at air products' port Arthur hydrogen production facility, in *14th greenhouse gas control technologies conference Melbourne*, 2018, pp. 21–26.
518 T. A. Meckel, A. P. Bump, S. D. Hovorka and R. H. Trevino, *Greenhouse Gases: Sci. Technol.*, 2021, **11**, 619–632.
519 Y. Shiyi, M. Desheng, L. Junshi, Z. Tiyao, J. Zemin and H. Haishui, *Pet. Explor. Dev.*, 2022, **49**, 955–962.
520 X. Zhang, Q. Liao, Q. Wang, L. Wang, R. Qiu, Y. Liang and H. Zhang, *Energy*, 2021, **225**, 120297.
521 E. Adu, Y. Zhang and D. Liu, *Can. J. Chem. Eng.*, 2019, **97**, 1048–1076.
522 D. Lirong, S. Longde, L. Weifeng, W. Mingyuan, G. Feng, G. Ming and H. Jiang, *Pet. Explor. Dev.*, 2023, **50**, 1246–1260.
523 A. Peltz, S. Anderson, N. Saunders, J. Koka, J. Graham and B. Portela, Strategies for attaining CO_2 sequestration with environmental integrity, in *Abu Dhabi International Petroleum Exhibition and Conference* (p. D021S035R002), SPE, 2022.
524 R. J. Pawar, G. S. Bromhal, J. W. Carey, W. Foxall, A. Korre, P. S. Ringrose, O. Tucker, M. N. Watson and J. A. White, *Int. J. Greenhouse Gas Control*, 2015, **40**, 292–311.
525 M. J. Regufe, A. Pereira, A. F. Ferreira, A. M. Ribeiro and A. E. Rodrigues, *Energies*, 2021, **14**, 2406.
526 A. Hastings and P. Smith, *Front. Clim.*, 2020, **2**, 601778.
527 G. Thakur, S. Bose and A. Selveindran, Carbon Storage Focused Reservoir Management: A Practical Example to Respond to Climate Change, in *Proceedings of the Future Technologies Conference*, Springer Nature Switzerland, Cham, 2023, pp. 578–592.
528 V. Nuñez-Lopez, R. Gil-Egui, P. Hosseininoosheri, S. D. Hovorka and L. W. Lake, *Carbon life cycle analysis of CO2-*

EOR for net carbon negative oil (NCNO) classification, Univ. of Texas, Austin, TX (United States), 2019.
529 A. Kamolov, Z. Turakulov, S. Rejabov, G. Díaz-Sainz, L. Gómez-Coma, A. Norkobilov, M. Fallanza and A. Irabien, *Membranes*, 2023, **13**, 130.
530 D. Kearns, H. Liu and C. Consoli, Technology readiness and costs of CCS, Global CCS institute, 2021, vol. 3.
531 D. V. D. A. John Zhou, R. Chalaturnyk, G. Meikle, M. Gray and B. W. Sanah Dar, Bonnie Drozdowski, and Heather Campbell, Carbon Capture, Utilization, and Storage (CCUS) Technology Innovation to Accelerate Broad Deployment in Alberta, Alberta Innovates, Albertainnovates.ca, 2022.
532 R. M. Cuéllar-Franca and A. Azapagic, *J. CO2 Util.*, 2015, **9**, 82–102.
533 H. H. Khoo and R. B. Tan, *Environ. Sci. Technol.*, 2006, **40**, 4016–4024.
534 J. Koornneef, T. van Keulen, A. Faaij and W. Turkenburg, *Int. J. Greenhouse Gas Control*, 2008, **2**, 448–467.
535 B. Singh, A. H. Strømman and E. G. Hertwich, *Int. J. Greenhouse Gas Control*, 2011, **5**, 911–921.
536 Z. Nie, A. Korre and S. Durucan, *Energy Procedia*, 2011, **4**, 2510–2517.
537 C. A. Scholes, K. H. Smith, S. E. Kentish and G. W. Stevens, *Int. J. Greenhouse Gas Control*, 2010, **4**, 739–755.
538 S. C. Kumbharkar, P. B. Karadkar and U. K. Kharul, *J. Membr. Sci.*, 2006, **286**, 161–169.
539 M. A. Carreon and S. R. Venna, *Metal-Organic Framework Membranes for Molecular Gas Separations*, World Scientific, 2020.

